Characterization of cellular functions of the deubiquitinating enzyme OTUD4

– Dissertation –

zur
Erlangung des Doktorgrades (Dr. rer. nat.)
der
Mathematisch-Naturwissenschaftlichen Fakultät
der
Rheinischen Friedrich-Wilhelms-Universität Bonn

vorgelegt von
Richa Das
aus
Bhubaneswar, Indien

Bonn, Juli 2019

Angefertigt mit Genehmigung der Mathematisch-Naturwissenschaftlichen Fakultät der Rheinischen Friedrich-Wilhelms-Universität Bonn

1. Gutachter: Prof. Dr. Ina Vorberg
2. Gutachter: Prof. Dr. Waldemar Kolanus

Tag der Promotion: 18.11.2019

Erscheinungsjahr: 2020

Declaration

I hereby declare that I have written this dissertation without sources unless otherwise indicated in this thesis. This has been written without any third party assistance.

Parts of the data shown in the Results chapter 3 of this thesis have been published in the following publication with me as the first author.

- **New roles for the de-ubiquitylating enzyme OTUD4 in an RNA-protein network and RNA granules.**
  Richa Das, Lukas Schwintzer, Stanislav Vinopal, Eva Aguado Roca, Ana-Maria Oprisoreanu, Susanne Schoch, Frank Bradke, Meike Broemer
  Journal of Cell Science, 2019; 132(12). pii: jcs229252.

Contents

Summary

Post-translational modification of proteins with ubiquitin influences myriad of cellular processes by affecting protein stability, degradation, localization and protein-protein interactions. Ubiquitin gets transferred to target proteins via an E1-E2-E3 enzymatic cascade. Deubiquitinating enzymes (DUBs) are ubiquitin-specific proteases that counterbalance this process.

The deubiquitinating enzyme OTUD4 was found mutated in the rare Gordon Holmes syndrome associated with hypogonadotropic hypogonadism, ataxia and dementia in humans. OTUD4 is important for embryonic development and structural integrity of cerebellum in zebrafish. However, the molecular function of OTUD4 in neuronal context has remained elusive. To explore this, I performed pull-down experiments from mouse brain lysates to identify new interaction partners. Mass spectrometry analysis revealed that OTUD4 is part of a large network of RNA-binding proteins. Many of its interactions with these RNA-binding proteins are RNA-dependent. This study characterizes OTUD4 as an intrinsically disordered protein that interacts with RNA itself, despite lacking a canonical RNA-binding domain. I propose that OTUD4 engages in unconventional RNA-binding mediated by its intrinsically disordered regions.
Eukaryotic cells contain RNA-protein assemblies known as RNP granules. I show that OTUD4 associates with higher order ribonucleoprotein assemblies: neuronal RNA transport granules and stress granules. Under physiological conditions, OTUD4 colocalizes with RNA transport granules in rat hippocampal neurons. Live cell-imaging reveals trafficking behavior along the neurites, implicating OTUD4 function in the transport of untranslated mRNA and local protein synthesis. Furthermore, upon heat and oxidative stress, OTUD4 colocalizes with stress granules (SG) in mammalian cells. SGs represent sites of stalled translation containing untranslated mRNAs and proteins under stress conditions. Taking into account the impaired SG formation in OTUD4 deficient cells, our findings conclude it as a critical regulator of SG assembly. However, its catalytic activity did not seem to be essential for the process. Its role in integrated stress response is underscored by the observation that cells lacking OTUD4 exhibit impaired SG formation, increased sensitivity and apoptosis, both under basal and post-stress conditions. Taken together, this study reveals important aspects of OTUD4 functionality that might further the understanding of RNA-protein networks and mRNA translation in cells and cellular stress response.

List of Abbreviations

A	Alanine
aa	Amino acid
ACN	Acetonitrile
ALS	Amyotrophic lateral sclerosis
APS	Ammonium persulfate
ATP	Adenosine triphosphate
bp	Base pair
BSA	Bovine serum albumin
C	Cysteine
cDNA	Complementary deoxyribonucleic acid
cm	Centimeter
CMV	Human cytomegalovirus
CO_2	Carbon dioxide
CRISPR	Clustered Regularly Interspaced Short Palindromic Repeats
Da	Dalton
DNA	Deoxyribonucleic acid
DAPI	4',6-diamidino-2-phenylindole
Dcp1a	mRNA Decapping enzyme 1a
ddH_2O	Double-distilled water
DEPC	Diethyl pyrocarbonate
DIV	Days in vitro
DMEM	Dulbecco's modified Eagle medium
DMSO	Dimethyl Sulfoxide
dNTP	Deoxyribonucleoside triphosphate
DTT	Dithiothreitol
DUB	Deubiquitinating enzyme
E. coli	*Escherichia coli*, bacterium
ECL	Enhanced chemiluminescent
EGFP	Enhanced green fluorescent protein
eIF	Eukaryotic translation initiation factor
et al.	et alia; and others
FBS	Fetal Bovine Serum
FISH	Fluorescence In Situ Hybridization
FMRP	Fragile X mental retardation protein
FRAP	Fluorescence recovery after photobleaching
FTLD	Frontotemporal lobar degeneration
FUS	Fused in sarcoma

fwd	Forward
x g	Relative centrifugal force (rcf)
G	Glycine (Gly)
G3BP1	Ras GTPase activating SH3 domain-binding protein1
GCN2	General control nonderepressible 2
GFP	Green fluorescent protein
h	Hour (s)
HA	Human influenza hemagglutinin
HBSS	Hank's Balance Salt Solution
HECT	Homologous To E6-AP Carboxyl Terminus
HEK	Human embryonic kidney
HEPES	4-(2-hydroxyethyl)-1-piperazineethanesulfonic acid
hnRNP	Heterogeneous nuclear ribonucleoproteins
HRI	Heme-regulated eIF2α kinase
HRP	Horseradish peroxidase
HuB	Hu antigen B
IAA	Iodoacetamide
IBM	Inclusion body myopathy
ICC	Immunocytochemistry
IDR	Intrinsically disordered region
IF	Immunofluorescence
IGF2BP	Insulin-like growth factor 2 mRNA-binding protein
IP	Immunoprecipitation
JAMMs	JAB1/MPN/Mov34 metalloenzyme
K	Lysine (Lys)
Kb	Kilo base pair
kDa	Kilo Dalton
KO	Knockout
LB	Luria-Bertani
LCD	Low complexity domain
LC-MS/MS	Liquid chromatography-mass spectrometry/mass spectrometry
lncRNA	Long non-coding RNAs
LLPS	Liquid-liquid phase separation
M	Molar
MAP1b	Microtubule-associated protein 1B
MEM-HS	Minimal Essential Medium- Horse Serum
min	Minute (s)
mJ	Millijoules
MJD	Machado-Josephin domain
ml	Milliliter
mm	Millimeter
mM	Millimolar
mRNA	Messenger ribonucleic acid

MS	Mass spectrometry
ms	Millisecond
N2a	Neuro-2a
Neg. Ctrl.	Negative Control
NF-κB	Nuclear factor 'κ-light chain-enhancer' of activated B cells
ng	Nanogram
nm	Nanometer
OTU	Ovarian tumor
OTUD4	Ovarian tumor - domain containing protein 4
PAGE	Polyacrylamide gel electrophoresis
PARP	Poly (ADP-ribose) polymerase
PBS	Phosphate Buffered Saline
PCR	Polymerase chain reaction
PERK	PKR-like endoplasmic reticulum kinase
PFA	Paraformaldehyde
PKR	Protein kinase R
poly(A)	Polyadenylated RNA
PVDF	Polyvinylidene difluoride
R	Arginine
RACK1	Receptor of activated protein kinase C 1
RBD	RNA-binding domain
RBP	RNA-binding protein
RBR	RING-Inbetween-RING
rev	Reverse
RING	Really Interesting New Gene
RNA	Ribonucleic acid
RNP	Ribonucleoprotein
rpm	Rounds per minute
RSK2	Ribosomal S6 Kinase 2
RT	Room temperature
RT-PCR	Reverse transcription polymerase chain reaction
s	Second (s)
S	Serine
SA	Sodium arsenite
SDS	Sodium Dodecyl Sulfate
SG	Stress granule
sgRNA	Single guide RNA
siRNA	Small interfering ribonucleic acid
SMA	Spinal muscular atrophy
smFISH	Single Molecule Fluorescence In Situ Hybridization
SMN	Survival motor neuron protein
SSC	Saline-Sodium Citrate
TAE	Tris-Acetate-EDTA

TBS	Tris-buffered saline
TDP-43	TAR DNA-binding protein 43
TEMED	N, N, N′, N′-Tetramethylethylenediamine
TFA	Trifluoroacetic acid
TIA-1	T-Cell-Restricted Intracellular Antigen-1
TIAR	TIA1-related protein/ TIA1-like protein (also TIAL1)
TRAF2	Tumor necrosis factor receptor-associated factor-2
TTP	Tristetraprolin
U	Unit
Ub	Ubiquitin
UCH	Ubiquitin C-terminal hydrolases
UPS	Ubiquitin-proteasome system
USP	Ubiquitin-specific proteases
UV	Ultraviolet
V	Valine
V	Volt
VCP	Valosin-containing protein
w/v	Weight per volume
WB	Western blot
WT	Wildtype
YB1	Y-box binding protein 1
ZBP1	Zipcode binding protein 1
ZFAND1	Zinc finger AN1-type-containing protein 1
µg	Microgram
µl	Microlitre
µm	Micrometer
%	Percent
°C	Degree Celsius

1 Introduction

1.1 The Ubiquitin-Proteasome System

The ubiquitin-proteasome system (UPS) is a major pathway, classically known to degrade ubiquitin-conjugated proteins by targeting them to the 26S proteasome (Gallastegui & Groll, 2010). Ubiquitination is implicated in regulating an uncounted number of biological processes including DNA damage signaling, transcription, endocytosis and several others (Hicke, 2001; Jackson & Durocher, 2013; Muratani & Tansey, 2003). It influences protein interactions, protein stability, subcellular localization, enzymatic activity and protein degradation. The fundamentals of the ubiquitin system are outlined here.

1.1.1 Ubiquitin conjugation

Ubiquitin (Ub) is a highly conserved, 76-amino acid polypeptide. Single ubiquitin moieties or polymeric ubiquitin chains are attached to substrate proteins, which is referred to as ubiquitination (Hershko & Ciechanover, 1998). The assembly of ubiquitin chains initiates with the addition of a first ubiquitin molecule to a lysine residue of a substrate, referred to as monoubiquitination. Ubiquitin itself has eight ubiquitination sites- seven lysine residues (K6, K11, K27, K29, K33, K48 and K63) and an N-terminal methionine residue (M1) (Kirisako et al., 2006; Peng et al., 2003; Xu et al., 2009). Polyubiquitin chains are formed when at least one of these residues gets ubiquitinated.

Ubiquitin conjugation to proteins is achieved by a series of enzymes (E1, E2 and E3) in a three-step sequential reaction (Pickart, 2001). At first, an E1 activating enzyme activates ubiquitin in an ATP-dependent reaction. The activation takes place by the formation of a thiol ester bond between the C-terminus of ubiquitin and a cysteine residue in the active site of E1 (Schulman & Harper, 2009). The activated ubiquitin is then transferred to a cysteine residue in an E2 conjugating enzyme (Olsen & Lima, 2013). Lastly, E3 ligases execute the final step by binding to the E2-Ub complex and the

substrate and bringing both into close proximity. E3 transfers the activated Ub to the substrate, thus forming an isopeptide bond between the C-terminal carboxyl group of ubiquitin (Gly76) of ubiquitin and the ε-amino group of a lysine residue of the substrate (Deshaies & Joazeiro, 2009). The human genome encodes two E1s for ubiquitin, approximately 40 E2s and more than 600 E3 enzymes (Husnjak & Dikic, 2012).

E3 ligases are classified into three groups depending on the presence of characteristic domains: Homologous To E6-AP Carboxyl Terminus (HECT) domain, Really Interesting New Gene (RING) domain or RING-Inbetween-RING (RBR) domain. The RING-type E3s are the largest family of ubiquitin ligases. All three classes possess different strategies to transfer the ubiquitin to the target protein (Deshaies & Joazeiro, 2009; Rotin & Kumar, 2009; Smit & Sixma, 2014).

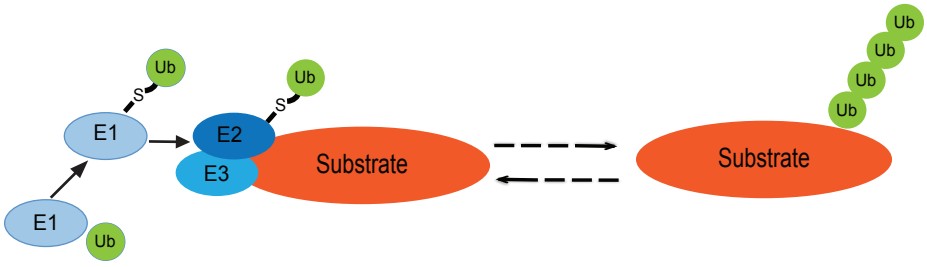

Figure 1: Three-step cascade of ubiquitin conjugation. Ubiquitin is attached to a substrate protein by E1 activating enzyme, E2 conjugating enzyme and an E3 ligase.

Different types of polyubiquitin chains are associated with diverse cellular consequences (Wagner et al., 2011; Xu et al., 2009). Other than the most commonly described consequence of proteasomal degradation, non-degradative consequences of ubiquitination also exist in cells. The classical K48- and K63-linked polyubiquitin chains are predominantly found in cells (Xu et al., 2009). K48 linkages efficiently recruit the substrate proteins to the 26S proteasome for degradation (Chau et al., 1989). In contrast, K63 linkages are involved in cellular signaling (Chen & Sun, 2009). They reportedly function as regulators of the NF-κB transcription factor (Deng et al., 2000; Wang et al., 2001), DNA repair (Doil et al., 2009; Stewart et al., 2009), oxidative stress response and translation (Silva et al., 2015; Spence et al., 2000). Other atypical linkages such as K11-linked polyubiquitin chains or M1-linked linear chains have also been studied in diverse cellular contexts (Aalto et al., 2019; Kulathu & Komander, 2012; Wu et al., 2010).

Several layers of complexity exist in the regulation of ubiquitination events making it a versatile and sophisticated system (Yau & Rape, 2016). Altogether, the tremendous amount of roles of ubiquitin in various biological contexts makes it a post-translational modification of high importance.

1.2 Deubiquitinating enzymes (DUBs)

Ubiquitination is a reversible post-translational modification. Deubiquitinating enzymes (also called deubiquitinases) are proteases that hydrolyze peptide bonds between two ubiquitin molecules and in some cases between ubiquitin and substrate in order to remove ubiquitin from substrates or edit ubiquitin chains (Komander, 2009). There are currently 99 DUBs identified in the human genome that are classified into five families according to their catalytic domain: ubiquitin-specific proteases (USPs), ubiquitin C-terminal hydrolases (UCHs), ovarian tumor proteases (OTUs), JAB1/MPN/Mov34 metalloenzymes (JAMMs) and Machado-Josephin domain proteases (MJDs) (Clague et al., 2013). Additionally, MINDY- and ZUP1-family DUBs have only recently been added to the DUB classes (Abdul Rehman et al., 2016; Kwasna et al., 2018). Most of the DUBs are cysteine proteases, with a catalytic triad of cysteine, histidine and aspartate responsible for their enzymatic activity. DUBs deubiquitinate proteins either by binding directly to the protein substrate to be deubiquitinated or by binding the ubiquitin chains to be cleaved.

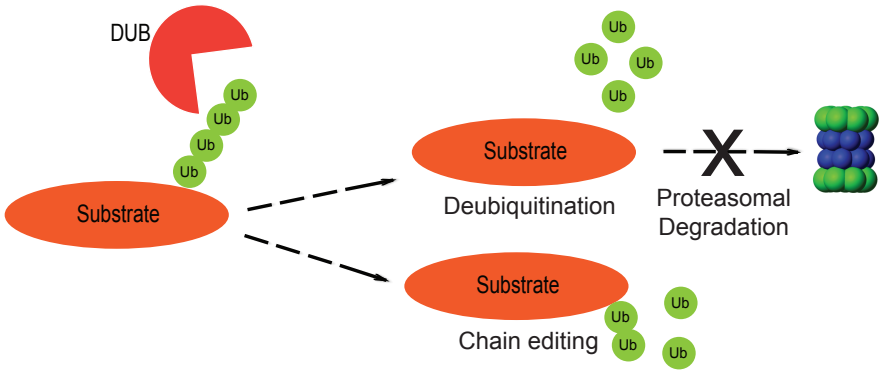

Figure 2: Schematics illustrating the activity of DUB proteases cleaving ubiquitin chains. DUBs can either deubiquitinate substrates or edit ubiquitin chains with diverse cellular consequences.

Owing to the extensive role of ubiquitination in various cellular places, it is not surprising that DUBs have emerged as key regulators of cellular processes. In cells, DUBs that cleave Lys48-linked polyubiquitin chains can rescue the proteins from proteasomal degradation. By disassembly of ubiquitin chains, for example, prior to proteasomal degradation, DUBs maintain the free ubiquitin pool. DUBs are also implicated in other housekeeping functions such as DNA repair and damage response, innate immune signaling and endocytosis (Clague et al., 2019).
Many DUBs function as part of protein complexes, which possibly imparts the functional diversity to each of them (Sowa et al., 2009; Ventii & Wilkinson, 2008). Additionally, post-translational modifications and specific intracellular localization of DUBs also impact their cellular functions.

1.2.1 DUBs in human diseases

Deregulation of DUBs has been linked to several diseases such as autoimmune disorders, cancer and neurodegeneration (Harrigan et al., 2018). For example, missense mutations in one of the highly conserved DUBs i.e. USP9X cause intellectual disability and its increased expression (Homan et al., 2014) is associated with several human cancers such as prostate cancer (Murtaza et al., 2015). Furthermore, identification of selective DUB inhibitors has placed DUBs as attractive therapeutic targets in diseases such as multiple myeloma and solid tumors (D'Arcy et al., 2015; Harrigan et al., 2018; Wang et al., 2016).

1.3 OTU domain-containing protein 4 (OTUD4)

OTU domain-containing protein 4 (OTUD4) is a DUB belonging to the OTU family of deubiquitinases. Only limited knowledge exists regarding its physiological functions. OTUD4 regulates dorsoventral patterning in zebrafish (Tse et al., 2013) and contributes to alkylation damage response (Zhao et al., 2015). Interestingly, it exerts its role in alkylation damage response with the help of two other DUBs, USP7 and USP9X, and relies on their catalytic activity. OTUD4's own catalytic activity seems dispensable in this context (Zhao et al., 2015). In contrast, the functional significance of its DUB activity has been implicated in NF-κB signaling and antiviral response (Liuyu et al., 2019; Zhao et al., 2018). It has been shown that OTUD4 suppresses IL1-β-dependent NF-κB signaling by K63-specific deubiquitination of MYD88 (Zhao et al., 2018). A recent publication identified mitochondrial antiviral signaling protein (MAVS) as K48-specific substrate of OTUD4 (Liuyu et al., 2019). MAVS is an adaptor protein required for defense against RNA viruses. OTUD4 deubiquitinates MAVS, prevents it from

proteasomal degradation and thereby enhances the innate immune response upon viral infection (Liuyu et al., 2019).
Recently, homozygous mutations in OTUD4 were found in a familial form of Gordon Holmes syndrome. Gordon Holmes syndrome is characterized by hypogonadotropic hypogonadism and ataxia. Interestingly, patients with mutations in OTUD4 and the ubiquitin ligase RNF216 in addition also developed dementia (Margolin et al., 2013). The physiological relevance of OTUD4 in this context is still poorly studied. In the same study, knockdown of OTUD4 in zebrafish led to a reduced size of optic tectum and cerebellum and eye defects. Injection of wild type human OTUD4 could rescue this phenotype. The DUB activity of OTUD4 did not seem to be essential in this case as the rescue construct used, lacked the OTU-domain responsible for its catalytic activity.

DUBs can recognize and cleave polyubiquitin chains selectively, depending on their linkage types. The linkage specificity varies between the different DUB families. The largest class of DUBs, USPs displays no linkage preferences while many members of the OTU-family DUBs show preferences for certain chain types (Mevissen et al., 2013; Ritorto et al., 2014). For example, OTUB1, one of the most abundant DUBs, displays specificity for Lys48-linked chains (Clague et al., 2015; Mevissen et al., 2013) while OTULIN exclusively hydrolyzes M1-linked chains (Keusekotten et al., 2013). OTUD4 is able to cleave ubiquitin chains of two different linkage types. OTUD4 purified from bacteria preferentially cleaves K48-linked polyubiquitin chains *in vitro* (Mevissen et al., 2013; Zhao et al., 2015). Mutation of the catalytic cysteine to alanine (C45A) completely abrogates its DUB activity (Mevissen et al., 2013; Zhao et al., 2015). In contrast, OTUD4 purified from HEK293T cellular extracts displayed a K63-specific DUB activity. This switch in linkage-specificity occurs due to phosphorylation near the catalytic domain of OTUD4 in HEK293T cells (Zhao et al., 2018). In Drosophila, CG3251 (fly homolog of OTUD4) contains a serine residue instead of cysteine in the OTU-domain and has lost its DUB-activity (Louis et al., 2015).

1.4 Ribonucleoprotein complexes (RNPs)

The regulation of gene expression determines the cellular proteome and fate of an individual cell under basal and stressful conditions. RNA-binding proteins (RBPs) interact with specific RNAs to form ribonucleoprotein complexes (RNPs) that determine the fate and function of RNA and regulate gene expression (Schwanhausser et al., 2011). The development of proteome-wide approaches has revolutionized the annotation of RNA binding proteins in yeast and mammalian cells (Baltz et al., 2012;

Beckmann et al., 2015; Castello et al., 2012; Mitchell et al., 2013). Recently, a total of 1,914 RBPs were annotated in humans (Hentze et al., 2018).

A classical RBP can interact with RNA transcripts through well-defined RNA-binding domains (RBDs). Several canonical RBDs are structurally very well studied such as RNA recognition motifs (RRM), hnRNP K homology domain (KH), DEAD box helicase domain, zinc-finger domain (Clemens et al., 1993; Daubner et al., 2013; Del Campo & Lambowitz, 2009; Lewis et al., 2000). Individual RBPs contain multiple repeats of individual RBDs, arranged structurally conferring RNA-binding affinity and functional diversity to the RBPs (Lunde et al., 2007; Oberstrass et al., 2005). Interestingly, many of the newly identified RBPs lack a classical RNA-binding domain indicating towards unconventional ways of interaction with RNA. For instance, more than half of 529 RBPs characterized in Hela cells did not possess a canonical domain reported for RNA-binding specificity. In fact, most of the non-canonical binding sites included enzymatic cores, DNA binding domains or sites responsible for protein-interactions. Proteins harboring intrinsically disordered regions (IDRs) have been prevalent in unconventional RNA binding (Castello et al., 2012; Castello et al., 2016). IDRs are stretches of low hydrophobic amino acid residues that lack a defined 3D structure. They consist of low complexity, repetitive amino acid sequences of arginine-glycine (RGG), arginine-serine (RS), tyrosine-glycine-serine (G/S(Y)G/S) motifs that have been reported to be found in proteins lacking a classical RBDs and yet interacting with RNA bases with variable binding specificities (Jarvelin et al., 2016). For example, an RGG box motif in Fragile X mental retardation protein (FMRP) selectively recognizes sc1 RNA by intermolecular hydrogen bonding between base pairs (Phan et al., 2011).
RBPs affect all stages of mRNA metabolism such as splicing, polyadenylation, transport, translation and degradation (Gerstberger et al., 2014). Unconventional RBPs enriched in the RNA interactome capture are metabolic enzymes, kinases, ubiquitin proteases and ligases (Castello et al., 2012; Kwon et al., 2013; Mitchell et al., 2013).

RNP complexes appear as microscopically visible units, lacking an enclosed membrane structure, termed as ‘RNA/RNP granules’. Distinct classes of RNP granules are widespread throughout the cell serving different functions (Figure 3). These include germ cell granules (P-granules) found in the peripheral poles of germ cells in *C. elegans* or *D. melanogaster*. Neuronal transport granules are found in neurons under physiological conditions (Kohrmann et al., 1999; Zhang et al., 2001). In contrast, stress granules (SGs) and P-bodies, both are formed by stress-induced translational arrest in the cytoplasm of somatic cells (Kedersha et al., 1999; Sheth & Parker, 2003). Also, RNP

granules in the nucleus are found in the form of Cajal bodies or paraspeckles (Fox et al., 2002; Gall et al., 1999).

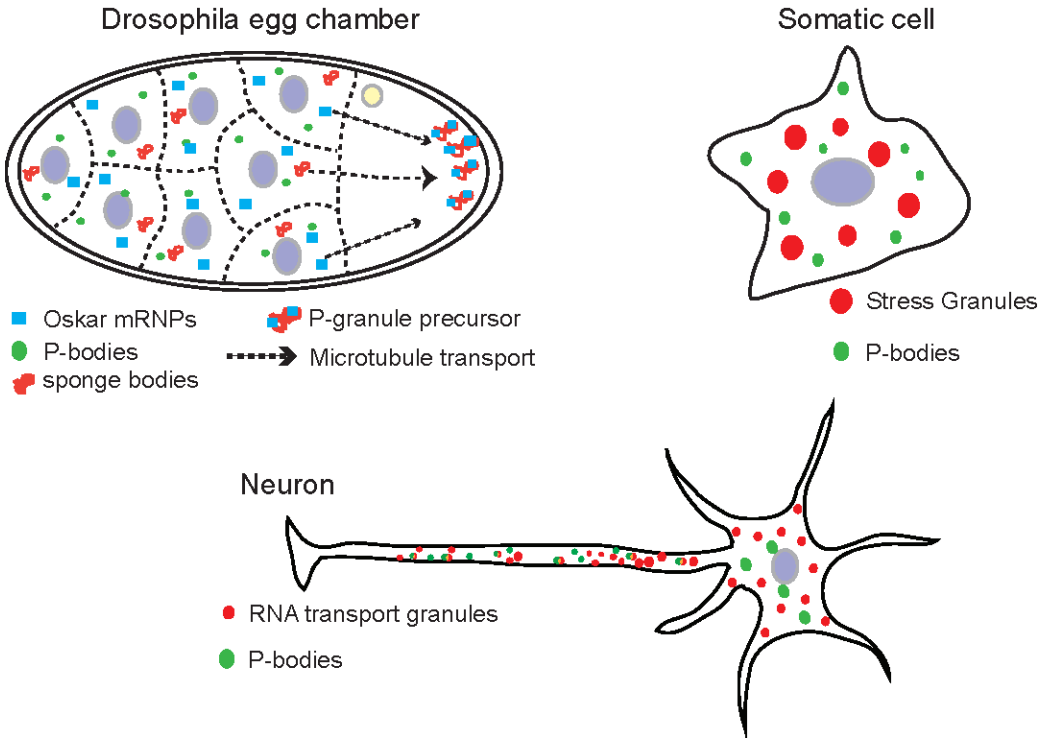

Figure 3: Distinct classes of mRNP granules across diverse cell types. Figure adapted from (Buchan, 2014).

The mRNP complexes are very dynamic, with constant changes in the numerous RNA-protein interactions dictated by functional requirements. Although the composition of each type of RNP granule is distinct in terms of mRNA selectivity, some conserved set of RBPs is associated with more than one type of RNP granule. These include RNA-binding proteins such as Staufen, survival motor neuron protein (SMN), Fragile X mental retardation protein (FMRP) and TAR DNA-binding protein 43 (TDP-43) among others (Anderson & Kedersha, 2006). Together, RNA-protein granules are spatially arranged in different locations in cells to regulate mRNA storage, transport, localization, translation or degradation. In this study, I have mainly focused on SGs and neuronal transport granules that are introduced in depth in the following sections.

1.5 Neuronal RNA Granules

Activity-dependent translation contributes to synaptic plasticity, axon guidance, long-term learning and memory (Costa-Mattioli et al., 2009; Hirokawa, 2006; Wang et al., 2010). Translation of messenger RNA occurs at the sites where protein activity is required upon physiological signals from the environment (Kohrmann et al., 1999; Zhang et al., 2001). Due to the asymmetric structure of neurons, nascent transcripts from the nucleus are transported as neuronal RNA granules or transport granules along the neurites, to be localized at particular sites of function (synapse). In response to activity-dependent stimulation, the dendritic mRNAs are released from the neuronal granules to initiate their translation locally at the synapses (Figure 4).
Neuronal transport granules consist of mRNAs and RNA-binding proteins and components of translational machinery, small and large ribosomal subunits. mRNA transcripts that have been identified in these granules include for example ß-actin, CaMKIIα, Arc; typical RNA-binding proteins in transport granules are Staufen, hnRNPA2, FMRP, Dead box-3, Purα, etc. Additionally, a set of microtubule-associated proteins like KIF5 was also identified (Elvira et al., 2006; Kanai et al., 2004).

Neuronal granules display a microtubule-dependent, active movement in anterograde and retrograde directions (Tubing et al., 2010). One of the first characterizations of the movement of mRNA in transport granules was done by observing the movement of RNA stained with fluorescent SYTO14, which stained endogenous RNA in the dendrites of cultured cortical neurons (Knowles et al., 1996). The movements of RNA-binding proteins such as Staufen and Zipcode binding protein 1 (ZBP1/IMP1/IGF2BP1) as part of RNA transport granules are also very well demonstrated in living neurons (Kohrmann et al., 1999; Zhang et al., 2001). The transport of the mRNAs along the long neurite trajectories depends on motor proteins: kinesins and dyneins (Hirokawa, 2006; Kanai et al., 2004; Villace et al., 2004).
It is generally observed that mRNA and ribosomes are present in a translationally repressed state in transport granules. In response to appropriate stimulation, the synaptic activity increases and the translation of mRNAs is initiated locally, at the site of function (Graber et al., 2013; Krichevsky & Kosik, 2001). For example, FMRP has been demonstrated to be a translational repressor regulating the local translation of MAP1b and CamKIIα transcripts at dendritic spines upon metabotropic glutamate receptor stimulation (Kao et al., 2010; Lu et al., 2004; Zalfa et al., 2003).

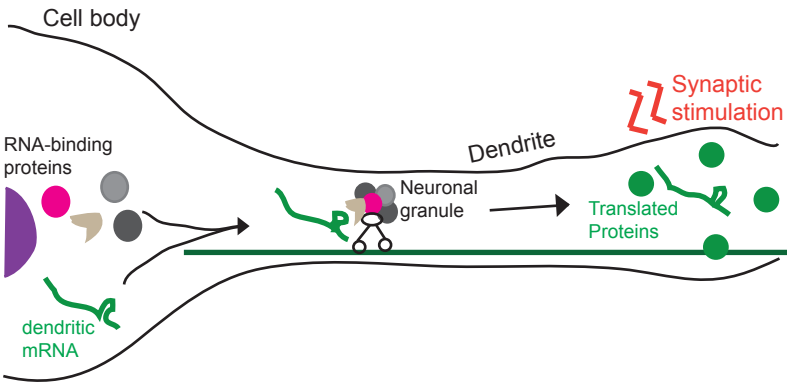

Figure 4: Model of RNA transport in neurons. mRNAs bind to RBPs and are transported as neuronal granules for local translation at synapses. The figure is modified from (Hirano et al., 2017).

1.5.1 Functional significance

Neuronal RNA granules are essential for the transport and local translation of certain mRNAs. They are required to maintain synaptic plasticity and long-term memory formation in neurons (Bakthavachalu et al., 2018). The local translation of certain mRNAs, for example, dendritic ß-actin mRNA at the postsynapse leads to synaptic growth and arborization of neurons (Eom et al., 2003; Yoon et al., 2016; Zhang et al., 2001). Local protein synthesis plays a role in axonal repair after nerve injury in mice (Perry et al., 2012). And also ataxin-mediated neuronal RNP assembly is required in long-term memory formation in olfactory neurons of *Drosophila* (Bakthavachalu et al., 2018).
RNA-binding protein SMN1 has been implicated in the motor neuron disease spinal muscular atrophy (SMA) (Lorson et al., 1999). Loss of SMN1 in SMA models has been associated with defects in axonal localization and translation of transcripts such as Gap43 and ß-actin, subsequently affecting the axonal outgrowth and growth cone stability (Donnelly et al., 2013; Fallini et al., 2016; Fallini et al., 2011). Additionally, SMN1 also functions as a chaperone for the mRNP assembly of IMP1 (ZBP1) protein and ß-actin mRNA (Donlin-Asp et al., 2017). Fragile-X mental retardation protein (FMRP) has also been shown to associate with multiple mRNAs in neurons regulating local translation and synaptic growth (Brown et al., 2001; Darnell et al., 2001).

Recent RNA deep sequencing studies have identified 1000-4500 different mRNAs in growing axons and >2500 different mRNAs in dendrites (Cajigas et al., 2012; Zivraj et

al., 2010). By combining biochemistry and genome-wide techniques, a large body of work has revealed that an individual mRNA can interact with multiple RBPs and a single RBP can have multiple target mRNAs (Ascano et al., 2012; Keene, 2007).

1.6 Cellular Stress Response

When cells encounter stressful conditions, they activate an integrated stress response (ISR) to maintain cellular homeostasis. Depending on the severity of the stress, the cells adapt by shutting down protein synthesis and simultaneously expressing stress response genes. Alternatively, they undergo apoptosis upon chronic stress (Pakos-Zebrucka et al., 2016). A key step in ISR is phosphorylation of eukaryotic initiation factor 2 alpha (eIF2α) by four stress sensing kinases: protein kinase R (PKR), PKR-like endoplasmic reticulum kinase (PERK), general control nonderepressible 2 (GCN2), and Heme-regulated eIF2α kinase (HRI) (Dever et al., 1992; Garcia et al., 2007; Han et al., 2001; Harding et al., 1999). Phosphorylation of eIF2α at serine 51 inhibits eIF2B activity; thereby causing a depletion of eIF2-GTP-Met-tRNA$_i^{Met}$ ternary preinitiation complex that blocks translation initiation (Jackson et al., 2010; Sudhakar et al., 2000). As a part of the stress response program, cells form stress granules (contain translationally dormant mRNAs) and P-bodies (contain mRNA degradation machinery).

1.7 Stress Granules (SGs)

In eukaryotic cells, stress granules are higher order RNA-protein assemblies formed under several types of stress insults such as reactive oxygen species (oxidative stress), unfolded protein response (endoplasmic reticulum stress), heat shock, inhibition of the 26S proteasome, ultraviolet light and viral infections. SGs are typically formed when translation initiation is inhibited by phosphorylation of eIF2α resulting in polysome disassembly (Kedersha et al., 1999). Ribosomes already engaged in translation elongation ''run-off' from the polysomes forming translationally stalled non-canonical 48S pre-initiation complexes lacking eIF2 initiation factor. These non-translating mRNPs are core constituents of SGs (Kedersha & Anderson, 2002). Upon recovery from stress, stalled mRNAs in SGs can bind to ribosomes to resume translation (Buchan & Parker, 2009) (Figure 5).
In the past decade, there has been an elaborate body of work on SGs, their biological significance and connection to human diseases, making them one of the most studied

RNP granules. Here I outline the basics of SG composition, dynamics and their biological functions.

1.7.1 Composition

Diverse systematic approaches have been employed to identify the proteome of SGs. In one study, the stable 'core' of the SGs was purified and subjected to mass spectrometry (MS) analysis (Jain et al., 2016). Recently, other proximity-labeling based methods such as APEX and Bio-ID have been employed to identify novel SG-associated proteins (Markmiller et al., 2018; Youn et al., 2018).
Messenger ribonucleoprotein complexes (mRNPs) consist of untranslated mRNAs together with a vast spectrum of RBPs, translation initiation factors (eIF4E, eIF4G, eIF4A, eIF4), 40S ribosomal subunits, chaperones and helicases (Jain et al., 2016; Kedersha & Anderson, 2002; Kimball et al., 2003). Approximately 50% of the SG proteome are RNA-binding proteins. The non-RNA binding proteins include metabolic enzymes, post-translational modification enzymes and components of signaling pathways (Buchan, 2014; Jain et al., 2016). Such non-RBPs are presumably recruited to SGs through protein-protein interactions. Although some of the core SG-associated proteins are conserved across eukaryotes, SG composition is largely heterogeneous and varies depending on the type of stress and cell (Aulas et al., 2017; Buchan et al., 2011; Markmiller et al., 2018). For instance, in mammalian cells, ZFAND1 is present only in arsenite-induced SGs and excluded in granules induced by heat stress (Turakhiya et al., 2018).

SGs are highly enriched in poly(A) RNA (Kedersha et al., 1999; Mollet et al., 2008). The identification of individual mRNA transcripts is rather scarce (Damgaard & Lykke-Andersen, 2011; Zurla et al., 2011). Unlike the proteome, the transcriptome of SGs was not elaborately identified. Only recently, Khong and co-workers undertook a comprehensive approach to identify the core SG transcriptome by RNA-sequencing and single-molecule fluorescence in situ hybridization (smFISH) in yeast and mammalian cells. It revealed that diverse populations of essentially every type of RNA including few long non-coding RNAs (lncRNA) are accumulated in SGs (Khong et al., 2017).

1.7.2 Assembly and Disassembly of SGs

Many RNA-binding proteins found in SGs contain intrinsically disordered regions (IDRs) or low complexity domains (LCDs). These proteins undergo concentration dependent liquid-liquid phase separation (LLPS) to form reversible SG foci (Hyman et

al., 2014; Kato et al., 2012). The prion-like domain of human T cell intracellular antigen-1 (TIA-1) protein promotes SG formation (Gilks et al., 2004). The LLPS is driven by multivalent dynamic RNA-protein, protein-protein interactions between proteins possessing IDRs (Lin et al., 2015; Molliex et al., 2015). This model is widely accepted for SG assembly. Many of the SG-associated RBPs such as hnRNPA1, Ataxin2, FUS undergo phase separation *in vitro* (Bakthavachalu et al., 2018; Lin et al., 2015; Patel et al., 2015).

SGs are composed of dense core structures surrounded by regions of lower density referred to as 'shell' (Jain et al., 2016). Different FRAP-based approaches show fast exchange rates of proteins in and out of SGs indicating a dynamic behavior of these granules (Kedersha et al., 2005; Ohshima et al., 2015). The exchange rate of mRNAs in and out of SGs is significantly lower compared to the proteins (Zhang et al., 2011).
SGs follow distinct stages of assembly and disassembly. The translationally stalled mRNPs complexes coalesce through specific protein-protein, RNA-protein and RNA-RNA interactions. They grow into stable core assemblies as more RNP complexes join, subsequently forming mature SGs. Once the stress is released, SGs start to disassemble by dispersing of the shell followed by the core proteins, allowing mRNPs re-enter translation (Jain et al., 2016; Wheeler et al., 2016).
RNA-binding proteins such as Ras GTPase activating SH3 domain-binding protein1 (G3BP1), T cell intracellular antigen-1 (TIA-1), Tristetraprolin (TTP), FMRP and TDP-43 nucleate the core of SGs, promoting their assembly (Kedersha & Anderson, 2007).

Several SG core proteins, post-translational modifications and protein-protein interactions affect the assembly and clearance of SGs (Buchan et al., 2013; Ohn et al., 2008; Yang et al., 2014). In yeast and mammalian cells, numerous helicases and chaperones affect the rate of SG disassembly during the recovery phase (Cherkasov et al., 2013; Jain et al., 2016; Walters et al., 2015). Also, evidence indicates that SG clearance is hampered by inhibition of autophagy (Buchan et al., 2013). The dynamics of SGs depend on ATP-dependent remodeling complexes (Jain et al., 2016). SG assembly and clearance is highly context-specific depending on the type of stress.

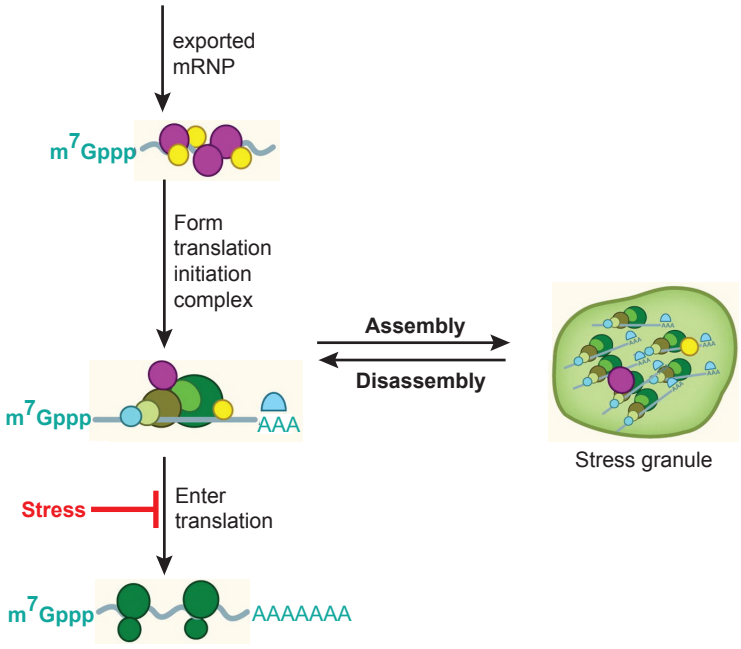

Figure 5: Schematic of mRNPs accumulating as stress granules upon stalled translation. Under steady state, mRNAs are actively engaged in translation by interacting with ribosomes and translation initiation factors. Under exogenous stress, translation is arrested to form SGs. mRNPs in SGs can re-enter translation initiation upon stress release. The figure is adapted from (Ramaswami et al., 2013).

1.7.3 Functional significance

Formation of SGs correlates with decreased translation and many SG-associated proteins are known translational repressors. SGs contain several constituents belonging to signaling pathways indicating that the formation of SGs can modulate these signaling pathways (Buchan, 2014; Kedersha et al., 2013).

Formation of SGs has been associated with cell survival. Under extreme stress conditions, SG formation decides whether a cell survives or enters apoptosis. Impairment of SG assembly has been linked with poor cell survival rates, demonstrating the protective effects of SG formation following stress exposure (Eisinger-Mathason et al., 2008). Sequestration of apoptosis-promoting factors into SGs such as RACK1, TRAF2 and RSK2 promotes resistance to apoptosis (Arimoto et al., 2008; Eisinger-Mathason et al., 2008; Kim et al., 2005).

Previous studies have indicated that viruses inhibit SG formation by cleavage of critical SG-associated proteins such as G3BP. This suggests an antiviral function of SGs during infections. SGs sequester key translational components, thus reducing the availability of ribosomes and translation factors required for viral replication (Carpenter et al., 2006; Onomoto et al., 2012; Onomoto et al., 2014; Reineke & Lloyd, 2013).
As SGs include numerous proteins involved in RNA metabolism, they have broad effects on mRNA function and the physiology of cells.

1.8 RNA granules in diseases

RNA granules regulate RNA metabolism such as transport, translation, storage and decay. They have been implicated both in health and disease. To date, mutations in intrinsically disordered regions of mRNP associated proteins like Staufen, TIA1, ataxin2, FMRP, TDP-43, hnRNPA2B1/hnRNPA1 and FUS have been implicated in various neurodegenerative disorders including amyotrophic lateral sclerosis (ALS), frontotemporal lobar degeneration (FTLD), spinal muscular atrophy (SMA) and others (Elden et al., 2010; Kim et al., 2013; Mackenzie et al., 2017; Ramaswami et al., 2013; Sreedharan et al., 2008; Vance et al., 2009). Accumulation of pathological TDP-43 inclusions is a major characteristic in the familial forms of ALS/FTLD and also part of other neurodegenerative diseases (Chen-Plotkin et al., 2010; Neumann et al., 2006).
Apart from defects in processes of RNA metabolism such as splicing defects, ALS-associated mutations in TDP-43 have been shown to affect the dynamics of RNA transport granules trafficking in living neurons. It was speculated that larger and slowly traveling granules due to mutations in TDP-43 contribute to the disease pathology. This could be due to an impaired translation of particular target mRNAs (Alami et al., 2014; Liu-Yesucevitz et al., 2014). In Fragile X mental retardation syndrome, loss of FMRP reportedly alters local mRNA translation leading to defective synaptic maturation and plasticity (Banerjee et al., 2018).
Reports linking SGs with disorders such as ALS/FTLD, Fragile X syndrome, spinocerebellar ataxia-2 and inclusion body myopathy (IBM) have increased in the recent years (Didiot et al., 2009; Vanderweyde et al., 2013; Wolozin, 2012, 2014). RNA-binding proteins with IDRs phase separate into liquid droplets *in vitro*, and this might contribute to some aspects of SG properties in cells (Brangwynne, 2013; Kato et al., 2012). Mutations in the low complexity domains of RBPs result in impaired SG dynamics. The pathogenic mutated proteins reportedly form constitutive granules by promoting self-aggregation in the absence of stress (Guo et al., 2011; Kim et al., 2013; Mackenzie et al., 2017). One current hypothesis is that persistent SGs mature into

stable beta-amyloid like fibers, enriched with IDR-containing proteins. These structures might act as 'crucibles' for the formation of pathological aggregates eventually triggering defects in RNA biogenesis and translation (Kim et al., 2013; Lin et al., 2015; Ling et al., 2013; Molliex et al., 2015). Examples of other SG-associated proteins displaying pathogenic assembly when mutated include TIA1, valosin-containing protein (VCP) and ubiquilin-2 (Alexander et al., 2018; Buchan et al., 2013; Mackenzie et al., 2017). In line with this, inhibition of SG assembly by knockdown of ataxin-2, an RNP-granule protein, suppresses toxicity and progression of neurodegeneration in different animal models (Becker et al., 2017; Scoles et al., 2017; Zhang et al., 2018).

Well-characterized SG-associated proteins have also been implicated in the pathogenesis of other diseases including cancer, viral infections and inflammatory diseases (Anderson et al., 2015; Lloyd, 2013). As SGs are pro-survival and anti-apoptotic, their formation is associated with tumor progression and contributes to cancer cell survival as a part of the cellular stress response (Anderson et al., 2015). Diminishing SG formation by decreasing levels of SG-nucleating protein G3BP1 also diminishes tumor progression and metastasis (Somasekharan et al., 2015). Similarly, chemotherapeutic treatments induce SG formation that can cause resistance to cancer treatments (Adjibade et al., 2015; Szaflarski et al., 2016). Hence, preventing SG formation may be a valuable therapeutic option.

1.9 Aim of the study

Whole exome sequencing identified mutations in the deubiquitinating enzyme OTUD4 in autosomal hereditary Gordon Holmes syndrome, characterized by endocrine dysfunction, ataxia and dementia. Patients bearing OTUD4 mutation showed disorganized cerebellum phenotype and neuronal loss in the hippocampal region. Also knockdown of OTUD4 in zebrafish displayed similar phenotypes (Margolin et al., 2013). However, apart from these phenotypic observations, very few mechanistic insights existed regarding the function of OTUD4. Recent reports describe functions of OTUD4 in diverse processes such as DNA damage repair, NF-κB signaling and antiviral response. Despite its abundant expression in the nervous system, the functional relevance of OTUD4 in this context is completely unknown.

This work aims to identify new interaction partners and potential substrates of OTUD4 in mouse brain tissues systematically, by performing pull-down experiments followed by mass spectrometry analysis. Enrichment analysis of the candidate proteins will assign novel molecular functions to OTUD4.

To investigate the localization and behavior of OTUD4 and its interacting proteins in different cellular systems, importantly in primary neurons, I utilized different imaging techniques. OTUD4-deficient cell lines should be analyzed for differences in this context and associated downstream effects. Further, the goal is to address how the disease mutation affects the catalytic activity and function of OTUD4.
Eventually, these findings might lead to a better understanding of the functional roles of OTUD4 in the nervous system, which will be a prerequisite to further understand its catalytic activity and disease relevance in this context.

2 Materials and Methods

2.1 Materials

2.1.1 Technical Devices and Consumables

Table 1. Technical Devices

Device Name	**Company**
Amaxa Nucleofector system	Lonza
Centrifuge (falcon tubes)	5804, Eppendorf
Centrifuge (eppendorf tubes)	5424, Eppendorf
ChemiDoc MP Imaging System	Bio-Rad
CL-1000® Ultraviolett Crosslinker	UVP®, Fischer Scientific
CO_2 incubator	ICO 240, Memmert
CO_2 incubator	MIDI 40, Thermo Fisher Scientific
Cooling Centrifuge (eppendorf tubes)	5417R, Eppendorf
Cooling Centrifuge (falcon tubes)	Megafuge 40R, Thermo Fisher Scientific
Countess™ Automated Cell Counter	Invitrogen
Electrophoresis Chamber (agarose gels)	Mini-Sub® Cell GT Systems, Bio-Rad
Electrophoresis Chamber (agarose gels)	Wide Mini-Sub®Cell GT Systems, Bio-Rad
Electrophoresis Chamber (SDS-PAGE)	XCell SureLockTM Mini-Cell, Invitrogen
Heat block	VWR
Heating Incubator	IN30, Memmert
Homogenizer	Potter S, B. Braun
Incubator Shaker	New Brunswick™ Innova® 40, New Brunswick Scientific
Incubator Shaker	New Brunswick™ Excella® E24, New Brunswick Scientific
Magnetic Separator	BioTools

Microwave	Bosch
NanoDrop™ One	Thermo Fisher Scientific
Orbital Shaker	PS4-10T, Biosan
PCR Cycler	Bio-Rad Tetrad2
pH Meter SevenEasy™	Mettler Toledo
Plate Reader	Tecan Infinite F200 pro
Power Supply	VWR™ Power source™ 300V, VWR
Roller Mixer	SRT6D, Stuart
Semi dry Transfer Unit	TE77 Amersham Biosciences
Spinning Wheel/Rotator	SB2, Stuart
Sterile Bench	Scanlaf Mars 1200 Safety Class II
TapeStation 4200	Agilent Technologies
Thermomixer	ThermoMixer C, Eppendorf
Ultracentrifuge	WX ULTRA Series, Thermo Scientific
Vaccum Pump	Vacusafe, Integra
Vaccum concentrator	Concentrator plus, Eppendorf
Vortex	IKA®Vortex Genius
Waterbath	WNB, Memmert

Table 2. Microscopes

Device Name	**Company**
Confocal Laser Scanning Microscope	LSM 780, Zeiss
CellVoyager CV6000	Yokogawa, Tokyo, Japan
DeltaVision Elite high (live cell imaging)	GE Healthcare Life Sciences
Inverted Fluorescence Microscope	Leica DM IL LED, Leica Microsystems
Inverted Routine Microscope	Nikon Eclipse Ts2, Nikon

Table 3. Consumables

Name	**Company**
Cell Culture flasks (T-12.5, T-25, T-75)	Sarstedt
Cell Culture petri-dishes (6 cm, 10 cm, 15 cm)	Sarstedt
Cell Culture plates (6-well, 12-well, 24-well, 96-well)	Sarstedt

Countess™ cell counting chambers slides	Invitrogen
Coverslips (0-13-0.16 mm thickness)	R. Langenbrinck GmbH
Cryogenic Vials	VWR
'Eppendorf' tubes (0.5 ml, 1.5 ml, 2 ml)	Sarstedt
Falcon tubes (15 ml and 50 ml)	Sarstedt
Freezing Container	Nalgene® Mr. Frosty, VWR
Inoculation spreader	Sarstedt
LoBind eppendorf tubes	Eppendorf
Microscope slides	Thermo Scientific Menzel (Gläser 76x26 mm)
Nucleofection cuvettes	Lonza
Pasteur Pipettes	Sarstedt
Pipettes	Gilson
Syringe filter 0.22 µm	Roth
21-gauge needle syringe	B. Braun
4-12% Bis-Tris gradient gels	NuPAGE, Life Technologies
96-well glass bottom Microplates	Greiner Bio-One, Sigma-Aldrich
µ-Slide 8-Well Chamber	Ibidi

2.1.2 Chemicals and Reagents

Table 4. Chemicals

Name	**Company**
2-Mercaptoethanol	Roth
4',6-diamidino-2-phenylindole (DAPI)	Sigma-Aldrich
Acetic Acid	Roth
Acetonitrile LC-MS Grade	Roth
Acrylamide/Bis solution 40%	Bio-Rad
Agar Agar	Roth
Agarose, low melt	Peqlab
Albumin Fraction V (BSA)	Roth
Ammonium Persulfate (APS)	Roth
Ampicillin	Roth

Bromophenol blue	Sigma-Aldrich
Calcium Chloride ($CaCl_2$)	Roth
ChemiBLOCKER	Merck-Millipore
DEPC-Treated Water	Invitrogen
Dextran Sulfate 50%	Sigma-Aldrich
Dimethyl Sulfoxide (DMSO)	Sigma-Aldrich
Dithiothreitol (DTT)	Roth
DNA ladder (1 Kb)	NEB
DNA ladder (100bp)	NEB
dNTP Mix	Promega
Dulbecco's Modified Eagle Medium (DMEM)+ L-GlutaMAX™-I	Gibco
Dynabeads Oligo(dT)25	Life Technologies
Enhanced chemiluminescent substrate (ECL) WesterBright™ Advansta	Biozyme
Ethanol	Roth
Ethanol (denatured)	Roth
Ethylenediaminetetraacetic Acid (EDTA)	Roth
Fetal Bovine Serum (FBS)	Gibco
Fish Gelatin	Sigma-Aldrich
FlexiTube siRNAs	Qiagen
Formamide	Sigma-Aldrich
Glucose	Roth
Glycerol	Roth
Glycine	Roth
Hank's Balanced Salt Solution (HBSS)	Gibco
HEPES	Roth
Horse Serum	Gibco
Iodoacetamide (IAA)	Sigma-Aldrich
Isopropanol	Roth
Kanamycin	Roth
L-glutamine (for MEM-HS)	Gibco
L-glutamine (for N2 medium)	Invitrogen
LB Medium	Roth

Lithium Chloride (LiCl)	Sigma-Aldrich
Lithium Dodecylsulfate (LiDS)	Sigma-Aldrich
MEM amino acids	Gibco
MEM non-essential amino acids	Gibco
Methanol	Roth
Milk powder	Roth
Minimal Essential Medium (MEM)	Gibco
N, N, N′, N′-Tetramethylethylenediamine (TEMED)	Sigma-Aldrich
Neuropan-2	PAN-Biotech
NP-40 Igepal	Sigma-Aldrich
Opti-MEM I reduced serum medium	Gibco
Paraformaldehyde (PFA) (16% w/v)	Thermo Fisher Scientific
Penicillin-Streptomycin	Invitrogen
Phenol/Chloroform/Isoamylalcohol	Roth
Phosphate Buffered Saline (PBS)	Gibco
Poly-L-lysine hydrobromide MW >300	Sigma-Aldrich
Potassium Acetate (CH_3COOK)	Roth
Potassium Chloride (KCl)	Roth
Prehybridization Solution 2X	Sigma-Aldrich
ProLong Gold Antifade Reagent	Thermo Fisher Scientific
Protease Inhibitor (Complete-EDTA-free)	Roche
Proteasome Inhibitor (MG132)	Merck
Protein Ladder (10-250 kDa)	Life Technologies
Puromycin dihydrochloride	Sigma
Saline-Sodium Citrate (SSC)	Sigma-Aldrich
SimplyBlue Coomassie G-250 SafeStain	Invitrogen
Sodium Arsenite	Fischer Scientific
Sodium Chloride (NaCl)	Roth
Sodium Dodecyl Sulfate (SDS)	Roth
Sodium Hydrogen Phosphate (Na_2HPO4)	Roth
Sodium Hydroxide (NaOH)	Roth
Sodium Pyruvate	Invitrogen
Sucrose	Roth

SuperSignal West Femto reagent ECL	Thermo Fisher Scientific
Sybr® Green	Invitrogen
ThermoPol® Reaction Buffer (10X)	NEB
Trifluoroacetic acid, MS-grade (TFA)	Sigma-Aldrich
Tris (Base)	Roth
Tris HCl	Roth
Triton X-100	Roth
Trypan Blue Stain	Invitrogen
Trypsin, sequencing grade, MS	Promega
Trypsin/EDTA	PAN-Biotech
Tween-20	Roth

Table 5. Enzymes

Alkaline Phosphatase (1000 U)	Roche
Deep-Vent Polymerase	NEB
DNase I, RNase free	Roche
PfuTurbo® DNA polymerase	Agilent Technologies
Proteinase K	NEB
Restriction Enzymes	NEB
RNase A	Thermo Fisher Scientific
RNaseOUT™	Invitrogen
T4 DNA Ligase	NEB

Table 6. Beads

Anti-FLAG M2 agarose	Sigma-Aldrich
Anti-HA agarose affinity gel	Sigma-Aldrich
GFP-TRAP	Chromotek
Magnetic-anti-HA	Life Technologies
Mouse-IgG-agarose	Sigma-Aldrich

2.1.3 Commercial Kits

Table 7. Kits

Kit	Company
Bradford Protein Quantification Reagent	Bio-Rad
Effectene transfection reagent	Qiagen
EndoFree Plasmid Maxi kit	Qiagen
Fugene HD transfection kit	Promega
In Fusion® HD EcoDry™ Cloning Kit	Clontech
Lipofectamine RNAiMAX Transfection Kit	Invitrogen
Minipreparation Kit	Peqlab
One-Step RT-PCR Kit	Qiagen
Qiafilter Maxi Kit	Qiagen
Qiafilter Midi Kit	Qiagen
Qiaquick Gel Extraction Kit	Qiagen
Qiaquick PCR Purification Kit	Qiagen
Rat Neuron Nucleofector Kit	Lonza

2.1.4 Antibodies

Table 8. Primary Antibodies

Target Protein	Host species	Application	Supplier
α- ß-actin	mouse	WB (1:5000)	Abcam, #ab8224
α- c-myc (9E10)	mouse	WB (1:1500)	Life Technologies, #132500
α- cleaved caspase3 (Asp175)	rabbit	WB (1:1000)	Cell Signaling, #9661
α- cleaved PARP (4B5BD2)	mouse	WB (1:1000)	Abcam, #ab110315
α- Dcp1a	mouse	IF (1:100)	Novus Biologicals # H00055802-M06
α- Flag M2	mouse	WB (1:5000) IF (1:500)	Sigma-Aldrich, #F1804

α- FMRP	rabbit	WB (1:1500) IF (1:200)	Abcam, #ab17722
α- GFP	chicken	WB (1:5000)	Abcam, #ab13970
α- G3BP1	rabbit	WB (1:1500) IF (1:250)	Abcam, #ab181150
α- HA (3f10)	rat	WB (1:2000)	Roche, #11867423001
α- OTUD4 (HPA036623)	rabbit	WB (1:1500) IF (1:100)	Sigma-Aldrich
α- OTUD4	mouse	WB (1:1500) IF (1:200)	Bethyl Labs (A304-605A)
α-P-eIF2α	rabbit	WB (1:1000)	Cell Signaling, #9721
α-TIA1 (C-20)	goat	IF (1:500)	Santa Cruz, #sc1751
α-TIAR	mouse	WB (1:1000) IF (1:100)	BD Bioscience, #610352
α-SMN1	mouse	IF (1:200)	BD Bioscience, #610646

Table 9. Secondary Antibodies

Target Species	Conjugation	Host Species	Application	Supplier
Chicken	HRP	goat	WB (1:4000)	Biozol
Goat	HRP	donkey	WB (1:4000)	Santa Cruz
Mouse	HRP	goat	WB (1:4000)	Biozol
Rabbit	HRP	goat	WB (1:4000)	Biozol
Rat	HRP	goat	WB (1:4000)	Biozol

Goat	AlexaFluor® 488	donkey	IF (1:500)	Life Technologies
Mouse	AlexaFluor® 488	donkey	IF (1:500)	Life Technologies
Mouse	AlexaFluor® 568	donkey	IF (1:500)	Life Technologies
Rabbit	AlexaFluor® 488	donkey	IF (1:500)	Life Technologies
Rabbit	AlexaFluor® 568	donkey	IF (1:500)	Life Technologies
Rabbit	AlexaFluor® 568	goat	IF (1:500)	Life Technologies

2.1.5 Cell lines and properties

Table 10. Cell lines

Cell line	Characteristics
HEK293T	Human embryonic kidney cells, expressing simian virus 40 large T antigen
Hela	Human adenocarcinoma cell line
SH-SY5Y	Human neuroblastoma cell line
Neuro-2a (N2a)	Murine neuroblastoma cell line

2.1.6 Expression Constructs

All expression constructs were cloned from human cDNA as template unless otherwise stated.

Table 11. Plasmids generated in this study

Construct	Tag	Vector Backbone
pN3x-HA-OTUD4	HA	pN3HA (provided by Christoph Thiele)
pEGFP-C3-OTUD4	GFP	pEGFP-C3(Clontech)
pEGFP-C3-OTUD4 $_{1-551}$	GFP	pEGFP-C3
pEGFP-C3-OTUD4 $_{1-900}$	GFP	pEGFP-C3
pEGFP-C3-OTUD4 $_{550-1113}$	GFP	pEGFP-C3
pCMV-3Tag6-OTUD4	Flag	pCMV-3Tag6 (Agilent Technologies)
pCMV-3Tag6-OTUD4 C45A	Flag	pCMV-3Tag6
pCMV-3Tag6-OTUD4 G398V	Flag	pCMV-3Tag6
pCMV-3Tag6-OTUD4 delTUD	Flag	pCMV-3Tag6
siRNA7 resistant pCMV-3Tag6-OTUD4	Flag	pCMV-3Tag6
siRNA7 resistant pCMV-3tag6-OTUD4 C45A	Flag	pCMV-3Tag6
siRNA7 resistant pCMV-3tag6-OTUD4 G398V	Flag	pCMV-3Tag6
p-β-actin-mOrange2-OTUD4	mOrange2	p-β-actin-mOrange2-C1[1]

[1]mOrange2 was amplified from mOrange2-EB3-7 (Addgene #57953 a gift from Michael Davidson).

p-β-actin-mNeon-SMN1[2]	mNeon	pmNeonGreen-C1 (Gentaur Europe BVBA) & p-βactin-vector (provided by Casper Hoogenraad, (Kapitein et al., 2010)

Table 12. Other plasmids

GFP-SMN1	Addgene ID: 37057, deposited by Greg Matera (Shpargel & Matera, 2005)
pFRT-TODestFLAGHA_HuB	Addgene ID: 65755, deposited by Thomas Tuschl (Landthaler et al., 2008)
pDESTmycIGF2BP3	Addgene ID: 19879, deposited by Thomas Tuschl (Landthaler et al., 2008)

2.1.7 Oligonucleotides

All oligonucleotides were purchased from Sigma-Aldrich unless otherwise stated.

Table 13. Primers for amplification of cDNAs

In-frame cloning

Expression Construct	Primer sequence
pN3HA-OTUD4_fwd	5'-atagatctaatggaggctgccgtc
pN3HA-OTUD4_rev	5'-tagtcgactcaagtgtgctgtcccctat
pEGFP-C3-OTUD4_fwd	5'-atagatctaatggaggctgccgtc
pEGFP-C3-OTUD4_rev	5'-tagtcgactcaagtgtgctgtcccctat
pEGFP-C3-OTUD4 $_{1\text{-}551}$_fwd	5'-atagatctaatggaggctgccgtc
pEGFP-C3-OTUD4 $_{1\text{-}551}$_rev	5'-tagtgtcgactcacttctttgactttgatggtga
pEGFP-C3-OTUD4 $_{1\text{-}900}$_fwd	5'-atagatctaatggaggctgccgtc
pEGFP-C3-OTUD4 $_{1\text{-}900}$_rev	5'-tagtgtcgactcaagacagatccagattttcca
pEGFP-C3-OTUD4 $_{550\text{-}1113}$_fwd	5'-gcagatctaaagaagttagagtgcccttctc
pEGFP-C3-OTUD4 $_{550\text{-}1113}$_rev	5'-tagtcgactcaagtgtgctgtcccctat
p-βactin-mOrange2-OTUD4_fwd	5'-cgcggatccgaggcagccgtc
p-βactin-mOrange2-OTUD4_rev	5'-gcgcggatcctcaagtgtgctgtcccct

[2] SMN1 was subcloned from GFP-SMN1 into pmNeonGreen-C1. Resulting mNeonGreen-SMN1 cassette was then excised and subcloned into a modified p-β-actin-vector.

Site-directed mutagenesis

Expression Construct	Primer sequence
pCMV-3Tag6-OTUD4 C45A_fwd	5'-gccaaggacgggtcggccctgttccgggccgtg
pCMV-3Tag6-OTUD4 C45A_rev	5'-cacggcccggaacagggccgacccgtccttggc
pCMV-3Tag6-OTUD4 G398V_fwd	5'-gcgttctctagtcattcttcagTgtcacagtctcag
pCMV-3Tag6-OTUD4 G398V_rev	5'-ctgagactgtgacActgaagaatgactagagaacgc
siRNA7 resistant flag-OTUD4_fwd	5'-gggaaccaaatgtctccccatcacaggtaacagaaaataattttc
siRNA7 resistant flag-OTUD4_rev	5'-gaaaattattttctgttacctgtgatggggagacatttggttccc
siRNA7 resistant flag-OTUD4 C45A_fwd	5'-gccaaggacgggtcggccctgttccgggccgtg
siRNA7 resistant flag-OTUD4 C45A_rev	5'-cacggcccggaacagggccgacccgtccttggc
siRNA7 resistant flag-OTUD4 G398V_fwd	5'-gcgttctctagtcattcttcagtgtcacagtctcag
siRNA7 resistant flag-OTUD4 G398V_rev	5'-ctgagactgtgacactgaagaatgactagagaacgc

In-fusion cloning

pCMV-3Tag6-OTUD4 delTUD_fwd1	5'-agcccgggcgggatccgaggctgccgtcggcgtc
pCMV-3Tag6-OTUD4 delTUD_rev1	5'-ccctgacactgtgttctgagcttgttttgacttcagc
pCMV-3Tag6-OTUD4 delTUD_fwd2	5'-aacacagtgtcagggaagaagatg
pCMV-3Tag6-OTUD4 delTUD_rev2	5'-cgggccccccctcgatcaagtgtgctgtcccctatgg

Table 14. Primers for sequencing

OTUD4 Sequencing Primer #1 Fwd	5'- AGCTCAGCAAAAACGTGATT
OTUD4 Sequencing Primer #2 Fwd	5'- TTCTCAGAGTAGCAATCCATG
OTUD4 Sequencing Primer #3 Fwd	5'- CTATCCTGGGTTTCCTTGTAA

Table 15. FlexiTube siRNA sequences (Qiagen)

Oligos	Target sequence
human OTUD4 siRNA #2	5'-CAGAGAGAAATTTGAAGCGTT
human OTUD4 siRNA #5	5'-CAGAATGGCCTGTATTCACTA
human OTUD4 siRNA #7	5'-ATGTTTCTCCTTCACAAGTAA

Table 16. CRISPR guide RNA sequences

Oligos	Target sequence	Position
mouse OTUD4 CRISPR seq#1_Fwd	5'- CACCGCATGCGGAGAGCAGACGCAG	Exon 11
mouse OTUD4 CRISPR seq#1_rev	5'- AAACCTGCGTCTGCTCTCCGCATGC	Exon 11
mouse OTUD4 CRISPR seq#2_Fwd	5'- CACCGGTTCACTCTGAGAATGGAC	Exon 15
mouse OTUD4 CRISPR seq#2_rev	5'- AAACGTCCATTCTCAGAGTGAACC	Exon 15

2.1.8 Softwares and Plugins

Table 17. Software

Software	Company
Adobe Illustrator	Adobe Systems, Inc.
Adobe Photoshop	Adobe Systems, Inc.
CellProfiler 3.0.0	https://cellprofiler.org/
EndNote X7.7.1	Thomson Reuters
Fiji	Image J, Wayne Rasband, National Institute of Health, USA
GraphPad Prism 5.0	GraphPad Software
Image Lab 5.1	Bio-Rad Laboratories
Microsoft Office	Microsoft Corporation
Proteome Discoverer software 2.1.0.81	Thermo Fisher Scientific
Serial Cloner 2.6.1	Serial Basics
SoftWoRx 7.00	GE Healthcare Life Sciences
ZEN 2010 software	Zeiss, black edition

Table 18. Fiji Plugins

Fiji Plugin	Application
MTrackJ	Live cell granule tracking
Straighten	Live cell granule tracking
KymoResliceWide	Generation of kymographs
Analyze particle	Quantification of FMRP/OTUD4 co-localization
Velocity Measurement Tool	Quantification of granule mobility

2.2 Methods

2.2.1 Molecular biology methods

2.2.1.1 PCR Amplification

In order to generate eukaryotic expression plasmids, DNA fragments were cloned into expression vectors. For this, cDNAs were amplified by polymerase chain reaction (PCR). For in-frame cloning strategy, unique restriction sites were inserted in the primers used to amplify a DNA fragment of interest. This allows enzymatic digestion of the amplified gene of interest, to position it in a eukaryotic expression vector of choice by subsequent ligation. A standard PCR reaction was set up as follows:

PCR reaction set up

200 ng	Template DNA
5 µl	ThermoPol Reaction Buffer (10X)
400 µM	dNTP Solution Mix (10 mM)
2 µM	Forward Primer (100 µM)
2 µM	Reverse Primer (100 µM)
1 unit	Deep Vent DNA Polymerase
Add ddH_2O up to 50 µl	

Cycling conditions for standard PCR

Step	Cycle Number	Temperature	Time
Initial Denaturation	1x	95°C	5 minutes
Denaturation	30x cycles	95°C	30 seconds
Annealing		55°C-65°C	30 seconds
Extension		72°C	1 minute per kbp
Final Extension	1x	72°C	5 minutes
Hold		4°C	

The amplified PCR product was cleaned up using the Qiafilter PCR purification kit (Qiagen) according to the manufacturer's instructions.

2.2.1.2 Agarose gel electrophoresis

In order to separate DNA samples, agarose gels (1% w/v agarose in TAE buffer) were cast and run in an electrophoretic chamber. 5 µl DNA loading dye and 1X concentrated Sybr® Green (for visualization of nucleic acids) were added to the samples and they were loaded on the gel. In order to determine the sizes of the DNA fragments, a standard DNA ladder was loaded. Electrophoresis was performed at 100 V. Bands were detected by exposing the gel to UV light of the ChemiDoc gel imaging system.

TAE Buffer

40 mM	Tris
20 mM	Acetic acid
1 mM	EDTA

2.2.1.3 Extraction of DNA from agarose gels

The DNA fragments of desired length were excised from the agarose gel using a clean scalpel under UV transilluminator. DNA was extracted from the gel pieces using Qiaquick Gel Extraction kit (Qiagen) according to manufacturer's instructions. The extracted DNA was reconstituted with 30 µl of buffer EB (10mM Tris-Cl, pH 8.5) provided with the kit.

2.2.1.4 Restriction digestion of DNA

In order to introduce restriction sites, DNA is subjected to enzymatic digestion by incubating with bacterial endonucleases (restriction enzymes) that recognize specific DNA sequences. Hydrolysation of DNA strands leads to 3' or 5' overhangs and digested DNA fragments can be introduced into expression vectors carrying the same restriction sites in their multiple cloning site. For digestion, the whole PCR product or 2 µg of plasmid DNA was incubated with 1 µl of each restriction enzyme and appropriate buffer optimal for the activity of the enzymes. Digestion was done at 37°C for 2 h. The reaction was stopped by analysis of samples on an agarose gel.

2.2.1.5 Dephosphorylation of DNA

Cut plasmid DNA needs to be dephosphorylated (removal of 5'-phosphate groups) at the ends to avoid vector religation and ensure ligation with the insert fragment. The DNA samples were dephosphorylated directly after digestion. For this purpose,

digested DNA was incubated with 1 U alkaline phosphatase and 1X dephosphorylation buffer and the reaction was carried out at 37°C for 1 h.

2.2.1.6 Ligation

After purification of DNA fragments via gel electrophoresis and extraction from gels, ligation of insert DNA and digested vector was performed in a 10 µl ligation reaction. DNA fragments were incubated with 1000 U T4 DNA ligase and ligation buffer (supplied with ligase). Usually, DNA fragments were added in 1:3 of vector to insert ratio. The ligation reaction was carried out for 1 h at room temperature (RT) or overnight at 16°C.

2.2.1.7 Transformation of chemically competent *E.coli* bacteria

Ligated DNA samples or plasmid DNA need to be transformed into competent cells in order to amplify the plasmid. The aliquots of cells were thawed on ice. When thawed, 10 µl of the ligation reaction was added to 100 µl aliquots of chemically competent XL10-Gold cells. For retransformation, 200 ng of plasmid DNA was used. The tubes were placed on the ice for 10 min. To ensure that the plasmid enters inside the bacteria, the cells were heat shocked at 42°C for 50 s in the thermomixer. Immediately the tubes were placed back on ice for 2 min. 1 ml of LB media (without antibiotics) was added to the cells and these were grown by shaking at 37°C for 1 h for expression of the antibiotic resistance gene. Afterward, the cells were collected by centrifugation at 500 x g for 5 min and the supernatant was discarded. The cell pellet was completely re-suspended using 100 µl of LB media and was streaked on LB agar plates containing appropriate antibiotic (100 µg/ml ampicillin or 25 µg/ml kanamycin) corresponding to the resistance gene carried by the vector backbone. The plates were incubated at 37°C overnight. The next day, colonies of bacteria were picked and plasmid DNA was purified by mini or midi preparation.

2.2.1.8 Plasmid purification (Mini preparation)

For minipreparation, the colonies were picked from the LB agar plate using a pipette tip and inoculated in 2 ml of LB medium with the appropriate antibiotic. The culture grew overnight with vigorous shaking (250 rpm) at 37°C. Next day the culture was spun down by centrifugation for 5 min at 3800 x g. The pellet was completely re-suspended using 200 µl of Buffer P1. Next, 200 µl of lysis buffer P2 was added and mixed gently by inverting the tubes several times to start the bacterial lysis. The lysate

was incubated for 5 min at RT. 200 µl of buffer P3 was added and mixed by inversion to facilitate the neutralization. After 10 min of incubation on ice, the bacterial protein debris was removed by centrifugation at 20,800 x g for 10 min. The supernatant was transferred to a fresh tube, 350 µl of isopropanol was added and the tube was inverted a few times for proper mixing. This was followed by centrifugation at top speed for 10 min to precipitate the plasmid DNA from the supernatant. The DNA pellet was washed once with 1 ml of 70% ethanol by spinning at 20,800 x g for 3 min to remove the residual salt. The ethanol was poured out completely and the DNA pellet was air-dried for approximately 10 min at RT. Finally, the pellet was re-suspended with 50 µl of Tris/EDTA buffer or water. The concentration was measured using a Nanodrop. A typical yield from a mini preparation was between 150 ng – 500 ng. The DNA was stored at -20°C for future applications.

Buffer P1	**Buffer P2**	**Buffer P3**
50 mM Tris-HCl, pH 8 10 mM EDTA 100 µg/ml RNase A 1 mM DTT Stored at 4°C	200 mM NaOH 1% SDS	3M CH_3COOK pH 5.5

2.2.1.9 Plasmid purification (Midi / Maxi preparation)

For large-scale plasmid purification, midi or maxi preparations were performed using kits from Qiagen according to manufacturer's instructions. In brief, for midi preparation, a single colony was picked and inoculated in 50 ml of LB medium containing an appropriate selective antibiotic. For maxi preparation, 100 ml of LB medium was used. The bacterial culture was grown overnight and harvested by centrifugation at 6000 x g at 4°C. Alkaline lysis of the bacterial pellet was performed by re-suspending the pellet in buffer P1 (provided with the kit), incubating the mixture with NaOH-SDS containing buffer P2 in the presence of RNase A. The lysate was neutralized by addition of buffer P3 containing acidic potassium acetate. The precipitated debris such as chromosomal DNA, proteins and salt was filtered by the QIAfilter cartridge resulting in a cleared lysate. This was further loaded on to the equilibrated QIAGEN-tip. The plasmid DNA binds to the resin of the tip, followed by washing to remove traces of contaminants further enhancing the purity of the bound DNA. The DNA was eluted using high salt buffer, followed by isopropanol precipitation and washing with 70% ethanol. The purified plasmid DNA was air-dried and reconstituted with appropriate amount of Tris/EDTA Buffer for future applications.

High purity yield of plasmid DNA is required for efficient transfections. To transfect the primary neurons in this study, we have used EndoFree Plasmid Maxi Kit from Qiagen, which ensures efficient removal of bacterial endotoxins.

2.2.1.10 Site-Directed Mutagenesis

In vitro site-directed mutagenesis is used to introduce point mutations in DNA plasmids. The protocol was carried out according to the QuickChange II Site-Directed Mutagenesis kit (Agilent Technologies). For this, oligonucleotide primers for amplification of the gene of interest are designed to carry the desired mutation according to the instructions. The PCR reaction set up and the cycling conditions are described below using the high fidelity *PfuTurbo*® DNA polymerase. The PCR product is treated with *Dpn I* for 1 h at 37°C to digest the parental DNA template and to select the newly synthesized DNA with the mutations (Nelson & McClelland, 1992). The PCR product was transformed into competent cells using standard procedures and the mutated plasmid DNA was purified as described above.

PCR Reaction set up

25 ng	Template DNA
5 µl	Polymerase Buffer (10X))
200 µM	dNTP Solution Mix (10 mM)
12.5 µM	Forward Primer (100 µM)
12.5 µM	Reverse Primer (100 µM)
1 unit	*PfuTurbo*® DNA polymerase
Add ddH_2O up to 50 µl	

Cycling conditions for site-directed mutagenesis PCR

Step	Cycle Number	Temperature	Time
Initial Denaturation	1x	95°C	1 minute
Denaturation	12x cycles	95°C	30 seconds
Annealing		55°C	1 minute
Extension		68°C	1 minute per kbp
Hold		4°C	

2.2.1.11 DNA sequence analysis

In order to confirm the presence of the desired insert in the plasmid and to check for errors in the sequence, the Sanger sequencing service from Microsynth was used. For this purpose, 1.2 µg DNA and 3 µl sequencing primer (10 µM) was constituted in 12 µl aqua bidest and sent for sequencing. Sequence information was analyzed using Serial Cloner 2.6.1 software.

2.2.2 Eukaryotic cell culture methods

2.2.2.1 Maintenance of cell lines

HEK293T and Hela cells along with the neuroblastoma cell lines N2a and SH-SY5Y have been used to perform experiments in this project. All the cell lines were usually cultured in T-75 flasks containing Dulbecco's Modified Eagle's Medium (DMEM) supplemented with 10% fetal bovine serum (FBS) and 50 units/ml penicillin and 50 µg/ml streptomycin. The cells were maintained in an incubator set to 37°C in a humidified 5% CO2 atmosphere. To maintain the viability and the phenotypic stability of these cell lines, they were sub-cultured twice a week in 1:10 ratio. Only the SH-SY5Y cells were sub-cultured in 1:5 ratio twice per week.

For sub-culturing the adherent cells, the medium was aspirated and the cells were washed with PBS. This was followed by trypsinization where the cells were treated with 0.05% Trypsin/EDTA and incubated for 5 min at 37°C. 9 ml of FBS-containing growth medium was added to the cells to inactivate the trypsin. The cells were triturated gently against the walls of the flask to dissociate them into single cell suspension. After, the cells were diluted to an appropriate ratio and transferred to new culture flasks containing fresh growth medium. If needed, the cell number and viability was determined by using Trypan Blue staining and an automated cell counter. Subsequently, cells were plated in dishes or multi-well plates for specific experiments and cultured in the CO_2 incubator.

2.2.2.2 Freezing of cells

For freezing of cells, cells were detached from the culture flasks by trypsinization as described above. Cells were pelleted by centrifugation at 1500 rpm for 5 min at RT. The supernatant was removed and the cell pellet was re-suspended in freezing medium (see below) and aliquoted in cryogenic vials. Vials were placed in the freezing

container with 100% isopropanol at -80°C overnight. This allows the cells to freeze slowly. Next day the vials were transferred to liquid nitrogen for long-term storage.

Freezing medium

50%	FBS
10%	DMSO
40%	DMEM

2.2.2.3 Thawing of cells

Frozen cells from liquid nitrogen were thawed at RT for 5 min. The cells were washed once by resuspending in 10 ml of PBS in a 15 ml falcon tube and centrifuged at 1500 rpm for 5 min at RT. The supernatant was aspirated and the cell pellet was re-suspended in appropriate growth medium. The cells were transferred to cell culture flasks. The following day the medium was changed to fresh culture medium and cells were cultured at 37°C until they reached 70% confluency to be ready for first passage.

2.2.2.4 Transfection of HEK293T cells with calcium phosphate

Transfection by calcium phosphate is a simple yet highly efficient technique to deliver DNA in cultured mammalian cells. This is based on the complex formation between calcium phosphate and DNA (Chen & Okayama, 1987). Exponentially growing HEK293T cells were trypsinized and seeded at 2 x 10^6 cells per 10-cm dish containing 10 ml media. This was done one day prior to transfections so that the cells would reach 20-30% confluency the following day. For a 10-cm dish, 10 µg of plasmid DNA was diluted to 300 µl of ddH_2O containing 30 µl of 2.5 M $CaCl_2$. After vortexing, 300 µl of HeBS solution (see below) was added. The mixture was then incubated for 10 min at RT before adding the complexes to the cells. The mixture was added in a drop-wise manner to the cells and cells were incubated at 37°C, 5% CO_2. Subsequently, the cells were harvested 24 or 48 hours post-transfection for further analysis.

2x HeBS Buffer (Hepes-Buffered Saline)

pH 7.05

0.28 M	NaCl
0.05 M	HEPES
1.5 mM	Na_2HPO_4

Add ddH_2O until 150 ml

2.2.2.5 Transfection of Hela cells with Effectene reagent

Transfections of Hela cells were done with expression plasmids using Effectene transfection reagent (Qiagen). One day before transfections, 1.2 x 10^5 cells were seeded per well of a 6-well plate in 1.5 ml growth medium. Immediately before transfections, the cells were washed once with PBS and fresh medium was added. For transfections, 0.4 µg of DNA was diluted with 100 µl of Buffer EC. 3.2 µl of Enhancer was added to the DNA (1:8 DNA-Enhancer ratio), mixed by short vortexing and incubated for 5 minutes at RT. To the DNA-Enhancer mixture, 10 µl of Effectene reagent was added and mixed by vortexing for 10 s. After an incubation of 10 min at RT, 600 µl of growth medium was added to the transfection complexes, which were immediately added drop-wise to the cells in the 6-well plates. After 4 h, the medium was changed and the cells were further incubated at 37°C, 5% CO_2 for 24 - 48 h to obtain appropriate expression levels.

2.2.2.6 Transfection of Hela cells with siRNA

To perform knockdown of OTUD4, siRNA transfections were done with Lipofectamine RNAiMAX. One day prior to transfections, 8 x 10^4 Hela cells were plated per well of a 6-well plate in 1.5 ml of growth medium. 2 tubes per well, each containing 150 µl OptiMEM I were prepared. In one of the tubes, 9 µl of Lipofectamine® RNAiMAX was diluted and in the second tube 30 pmol of siRNA was diluted. Both the solutions were combined and mixed by pipetting up and down. After 5 minutes incubation at RT, 250 µl of the transfection mix was added dropwise to the cells. The cells were incubated at 37°C, 5% CO_2 for 48 h to 72 h for an efficient knockdown. For controls cells were transfected with AllStars negative control (Qiagen).

2.2.2.7 Induction of stress granules by different stress stimuli

To induce stress granules, 3 x 10^5 cells were seeded per well of a 6-well plate, one day prior to stress treatment. For immunostaining of SGs, cells were seeded on poly-L-lysine-coated coverslips in 6-well plates. For induction of oxidative stress, cells were incubated with 0.5 mM sodium arsenite for 30 min - 1 h at 37°C. For heat shock experiments, SH-SY5Y cells were treated at 42°C for 1 h and Hela cells were exposed to 44°C for 1 h. Proteotoxic stress was induced by inhibiting the proteasome by treating the cells at 37°C with 100 µM MG132 for 90 min. For subsequent imaging experiments, the treatment was stopped at indicated time points by fixing the cells with paraformaldehyde. For detection of proteins by western blots, the treatment was

stopped by placing the cells on ice and harvesting immediately for lysis preparation as described above.

2.2.2.8 Primary neuronal culture

Primary hippocampal neurons were isolated and cultured from embryonic (E17) rats as described previously (De Hoop et al., 1998). In brief, embryos were removed from the uterus of the pregnant rodent and decapitated. Hippocampi were dissected from the brains and prepared in ice-cold Hank's Balanced Salt Solution (HBSS) supplemented with HEPES (HBSS+/+_HEPES solution). The hippocampi were pooled in a 15 ml falcon tube, HBSS+/+_HEPES solution was aspirated and the hippocampi were trypsinized with 0.05% Trypsin-EDTA at 37°C for 15 min. This was followed by three times washing: once with HBSS containing DNase and twice with HBSS+/+_HEPES solution. The cells were dissociated using fire-polished glass pipette to obtain single cell-suspension and the density of the cells was determined by counting with a cell counter. Subsequently, the neurons were plated at required density in a 6-cm dish in Minimum Essential Medium with 10% heat-inactivated horse serum (MEM-HS) on poly-L-lysine-coated coverslips and the dishes were placed in the incubator maintained at 36.5°C, 5% CO_2. The next day the coverslips with neurons were flipped to 6-cm dishes with glial feeder layer containing N2 medium.

For the culture of glial cells, the cell suspension corresponding to 4-5 brains was plated in T-75 culture flasks filled with 10 ml MEM-HS. The next day MEM-HS medium was changed to N2 medium. The culture was allowed to grow and then was passaged once a week in 1:3-1:2 ratios once they reached 80%-90% confluency. For the preparation of glial feeder layer in 6-cm dish, 85000 cells were plated in approximately 5 ml MEM-HS. The following day medium was changed to N2.

Minimum Essential Medium with horse serum (MEM-HS)
pH 7.3

100 ml	Minimal Essential Medium (10x)
40 ml	$NaHCO_3$ (5.5%)
30 ml	Glucose (20%)
10 ml	L-glutamine (200 mM)
20 ml	MEM amino acids (50x)
20 ml	MEM non-essential amino acids (100x)
100 ml	Horse serum (heat-inactivated)

Add ddH_2O until 1 L and sterile filter

N2 medium
pH 7.3

5 ml	Neuropan 2 (100x)
5 ml	Sodium pyruvate (100 mM)
15 ml	Glucose (20%)
20 ml	$NaHCO_3$ (5.5%)
5 ml	L-glutamine (200mM)
50 ml	MEM medium (10x)
Add ddH_2O up to 500 ml	

HBSS+/+_HEPES solution	500 ml	HBSS (1X)
	7 mM	HEPES (1M)

2.2.2.9 Transfection of primary neurons

For a single transfection reaction, cell suspension containing $3x10^5$ neurons was pipetted into 1.5 ml eppendorf tube and centrifuged at 76 x g for 5 min. The supernatant was aspirated and 100 µl of pre-warmed rat neuron nucleofector solution was added to the cells and gently re-suspended. For each reaction, 3-5 µg of highly purified DNA (EndoFree Plasmid Maxi Kit) was added and re-suspended well. Subsequently, this mixture was transferred to the nucleofection cuvettes and the cells were electroporated with the Amaxa Nucleofector system (Rat Neuron Nucleofector Kit, Lonza, program O-003). The cells were immediately re-suspended with pre-warmed MEM-HS. The resulting suspension of the transfected cells was plated onto poly-L-lysine-coated coverslips in 6-cm petri dishes in MEM-HS and swirled gently. The cells were maintained in 5% CO_2 at 36.5°C. After 4 h, the coverslips were flipped onto a 6-cm dish containing astrocytes in MEM with N2 supplements. The neurons were grown for 4 days *in vitro* (DIV 4) before fixation.
For live cell imaging experiments, $1.5x10^5$ neurons were transfected with 3 µg of purified DNA and plated onto poly-L-lysine-coated chamber slides. After 3 h, the medium was changed to N2-supplemented medium, which before had been incubated for three days on a glial feeder layer. Live cells imaging experiments were performed at DIV 4.

2.2.2.10 Generation of OTUD4 knockout cells by CRISPR/Cas9

OTUD4 knockout cells were generated using CRISPR/Cas9 mediated genome editing according to (Ran et al., 2013).

Design of targeting sequences: In brief, 20-bp targeting single guide RNA (sgRNA) was designed using the web-based tool E-CRISP (http://www.e-crisp.org/E-CRISP). Suitable sequences were generated based on the closest proximity to the target mutation and lowest number of off-target sites. 20-bp target sequence should be followed by 5'-NGG PAM motif in the genomic DNA of mouse *OTUD4* gene. Two guide sequences targeting exon 11 (KO1 & KO2) and exon 15 (KO3 & KO4) of *OTUD4* were designed.

Cloning of sgRNA into Cas9 expression vector: The complementary sequences corresponding to each guide RNA were designed and oligonucleotide annealing was performed according to the following reaction:

Reaction set up

1 µM Forward oligo
1 µM Reverse oligo
25 µl Hybridization buffer (2X)
Add ddH_2O up to 50 µl

Incubation profile

Step	Temperature	Time
Denaturation	90°C	4 minutes
Hybridization	70°C	10 minutes
Cool down	25°C	Gradually over 45 minutes

Hybridization buffer (2X)- 200 mM NaCl, 100 mM HEPES, pH 7.4

Each set of hybridized guide sequences were cloned separately into Cas9 expression plasmid pSpCas9(BB)-2A-Puro with U6-promoter (Addgene ID: PX459). The 5'-phosphorylated guide oligos contain overhangs to be ligated into the *BbsI* digested pSpCas9 vector according to the following reaction:

Ligation Reaction

7.5 µl Annealed oligos
1 µl Digested vector
1 µl T4-buffer
0.5 µl T4-DNA ligase
Incubate at 16°C overnight

The newly cloned plasmids were verified by DNA sequencing. This was followed by transformation and plasmid purification using a miniprep kit.

Transfections: The verified CRISPR plasmids were transfected into N2a cells using Fugene HD transfection kit according to manufacturer's instructions. 24 h after transfections, cells expressing CRISPR plasmid were selected using puromycin at 3 µg/ml concentration for one week.

Isolation of clonal cell lines: To isolate single cell clones, dilution cloning was performed. The cells were washed with PBS, trypsinized and cell density was determined by automated cell counter. The cells were diluted to a final concentration of 1 cell/100 µl and seeded (100 µl) on 96-well plates. Cells were cultured for approximately 2 weeks and single cell clones were selected. Single cell clones were subsequently expanded to 24-well plates and passaged every week.

Testing: To verify the knockout clones, cells were seeded on 96-well plates and were analyzed by Outknocker deep sequencing evaluation tool developed by the group of Prof. Veit Hornung (Schmid-Burgk et al., 2014). Each cell clone was frozen in liquid nitrogen as described above.

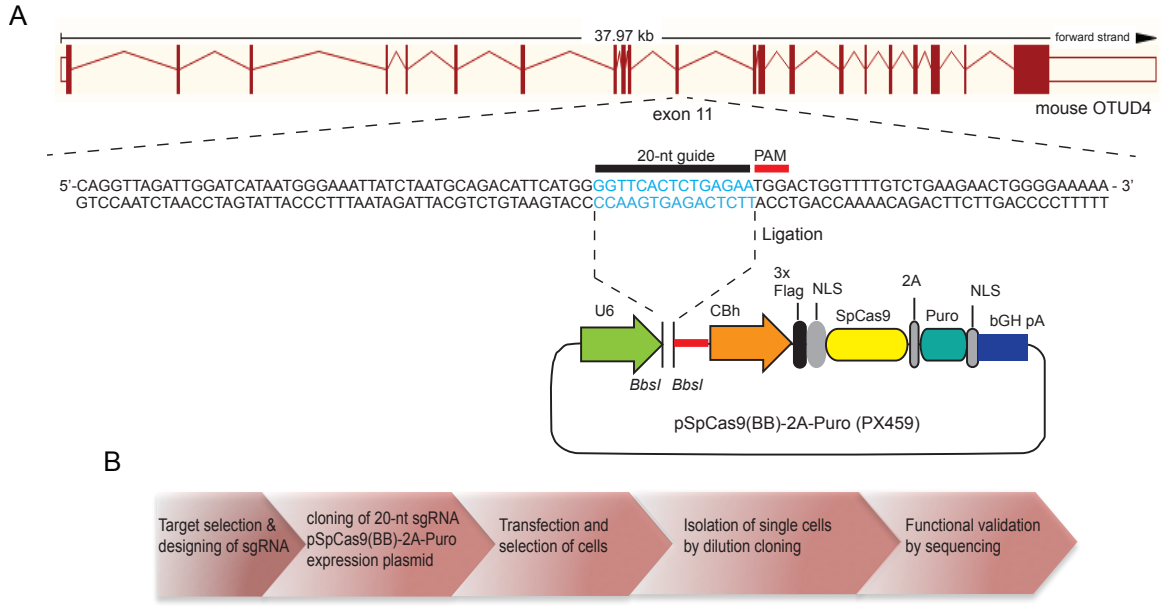

Figure 6: **Schematics for generation of OTUD4 knockout cells using CRISPR/Cas9 genome editing strategy** (A) Mouse *OTUD4* gene on chromosome 8 consists of 21 coding exons. 20-bp target sequence in exon 11 precedes the 5'-NGG PAM motif. Schematic for cloning of guide sequence oligos into BbSI Cas9 plasmid is shown. Modified from (Ran et al., 2013). (B) A general outline of different steps in the CRISPR gene editing technique.

2.2.3 Biochemical Methods

2.2.3.1 Preparation of cell lysates

To extract soluble proteins, the culture medium was removed and cells were washed once with PBS and then detached from the cell culture dish by scraping in 1 ml of cold PBS on ice. Cells were pelleted by centrifugation at 1000 x g for 5 min at 4°C. The supernatant was removed and the cell pellet was either frozen at -80°C for future usages or was immediately processed for lysis. For this, cells were re-suspended thoroughly in appropriate volume of lysis buffer (depending on the amount of cells) supplemented with DTT and protease inhibitors (see below). Cells harvested from a 70% confluent 10-cm dish, 500 µl of lysis buffer was used. The samples were incubated for 20 min at 4°C, gently rotating on a spinning wheel to ensure complete lysis. Then, the samples were centrifuged at 20,000 x g for 20 min, 4°C to separate the insoluble cellular debris. The clear lysate was transferred to fresh tubes and was used for further applications.

Cell Lysis Buffer

125 mM	Tris, pH 7.5
150 mM	NaCl
1 %	TritonX-100
10 %	Glycerol
1 mM	EDTA
1 mM	DTT

Complete protease inhibitor

2.2.3.2 Protein quantification

Protein concentrations of cell lysates were measured using Bradford reagent (Bradford, 1976). To determine the concentration, 1-20 µl of the cell lysate samples were diluted in 800 µl ddH_2O. For accurate measurements, two dilutions were taken per sample. To generate a standard curve, following concentrations of BSA were prepared: 0, 1, 2, 4, 8, 12 µg/ml in ddH_2O. 0 µg/ml of BSA indicated only ddH_2O as a blank sample. Then Bradford reagent was added to the tubes, which immediately changed color depending on the amount of protein in the tubes. These samples were vortexed and pipetted in duplicates in a 96-well plate. After 5 min of incubation, the absorbance was measured at 595 nm using TECAN infinite 200® PRO plate reader. The

protein concentrations were calculated in relation to measured sample absorbance against the standard curve of known protein content (BSA in this case).

2.2.3.3 Co-immunoprecipitation

In order to confirm interactions between OTUD4 and other proteins, co-immunoprecipitations (IPs) in HEK293T cells were performed.
For this, 10-cm dishes of HEK293T cells were transfected with overexpression plasmids as indicated in respective experiments. After 48 h, cells were harvested and lysates were prepared as described above. Approximately, 20 µl of lysate was reserved as an input sample. The remaining lysate was utilized for immunoprecipitation (IP). Approximately, 30 µl of beads slurry was used per 500 µg of cell extracts. IP was carried out by incubating the remaining lysate with anti-HA coupled agarose beads, anti-flag M2 affinity beads or GFP-trap beads to capture the respective fusion proteins. Beads were washed thrice with 1 ml of lysis buffer without protease inhibitors to remove the storage buffer (centrifugation at 1200 rpm, 1 min at RT). The lysate-bead mixture was incubated in low binding eppendorf tubes for 4 h at 4°C with gentle rotation on the spinning wheel. Immobilized protein was spun down and washed four times with 1 ml wash buffer (centrifugation at 1200 rpm, 1 min at RT). After the last wash, the pellet was centrifuged again and the supernatant was carefully removed completely.
For elution, immobilized protein was resuspended with 45 µl glycine (0.1 M, pH = 2.5) and agitated at 25°C for 20 min. After neutralization with 5 µl NH_4CO_3 (1 M, pH = 8.8), the eluate was centrifuged at 13000 rpm for 1 min at RT. The input sample and the eluate were denatured with Laemmli sample buffer at 95°C for 5 min before resolving them on an SDS-PAGE gel.
For RNase A treatment, the cleared lysates were additionally treated with 50 µg/ml RNase A at 37°C for 15 min.

IP Wash Buffer

10 mM	Tris, pH 7.5
150 mM	NaCl
0.1%	TritonX-100
5%	Glycerol

Laemmli sample buffer

125 mM	Tris pH 6.8
6%	SDS
20%	Glycerol
0.02%	Bromophenol blue
10%	ß-Mercaptoethanol

2.2.3.4 Sodium dodecyl sulfate - polyacrylamide gel electrophoresis (SDS-PAGE)

The protein extracts were resolved according to their molecular weight by SDS-PAGE. Depending on the size of the protein to be resolved, the acrylamide concentration of the separating gel varied from 8% - 12%. A higher percentage acrylamide gel with large pore size resolves relatively smaller molecular weight protein and vice versa. For separation of a wide range of molecular weight proteins, 4% - 12% gradient gels were used.

First separation gels were cast and overlaid with 70% ethanol to ensure a straight surface. After polymerization, the stacking gel was cast and combs with 10 or 12 wells were applied. Gels were polymerized for at least 1 h at RT or stored in the fridge overnight.

For standard purposes, the protein samples cooked with Laemmli buffer were loaded onto SDS-PAGE gel assembled in an electrophoretic chamber. The gel was run using running buffer (see below) at 200 V (constant voltage) for roughly 1 h before the samples ran out of the gel as visualized by observing the bromophenol blue present in the Laemmli buffer. Subsequently, the gel was stained with Coomassie to visualize proteins directly or was subjected to immunoblotting.

	Stacking Gel	**Resolving Gel**	
	4%	8%	10%
ddH_2O	6.35 ml	3.8 ml	3.43 ml
1.5 M Tris HCl (pH 8.8)	-	1.75 ml	1.75 ml
1.0 M Tris HCl (pH 6.8)	2.5 ml	-	-
Acrylamide Solution (40 %)	1.1 ml	1.4 ml	1.75 ml
SDS (20%)	50 µl	35 µl	35 µl
APS (20%)	60 µl	42 µl	42 µl
TEMED	6 µl	4.2 µl	4.2 µl

Running Buffer	25 mM	Tris
	0.5 M	Glycine
	7 mM	SDS

2.2.3.5 Western Blotting and detection

Semi-dry blotting system was used to transfer the size-separated proteins from the SDS polyacrylamide gels to polyvinylidene difluoride (PVDF) membranes for further analysis. Before the start of the transfer, the PVDF membrane was activated with 100% methanol for a few seconds and washed once in transfer buffer. Then the acrylamide gel and four pieces of filter papers were equilibrated with the transfer buffer. Subsequently, the 'sandwich' was assembled vertically on the semi-dry unit by stacking two soaked filter papers at the bottom, followed by the membrane and then the gel on its top. Finally, the gel was covered with two sheets of wet filter papers. The transfer was performed under constant voltage of 22 V for 2 h. For the transfer of smaller sized proteins, the transfer time was shortened.
For immunoblotting, the PVDF membranes were briefly rinsed with PBS-T or TBS-T and were blocked with 5% milk in PBS (w/v) or 5% milk in TBS-T for 1 h at RT. Afterward, the membrane was incubated with primary antibodies diluted with 2.5% milk in PBS-T (0.25% Tween-20) overnight at 4°C or 2 h at RT. The following day, the blot was washed three times 5 min with PBS-T or TBS-T and incubated with horseradish peroxidase (HRP)-conjugated secondary antibodies diluted in blocking buffer. The membrane was washed three times with PBS-T or TBS-T and proteins were detected using enhanced chemiluminescent substrate (ECL) or SuperSignal West Femto reagent, which is a more sensitive ECL to detect low levels of proteins. Images were acquired on a ChemiDoc MP Imaging System. For re-probing with other antibodies, the same membrane was incubated in stripping buffer for 2 h at RT and was extensively washed and blocked with milk.

1X Transfer Buffer	50 mM	Tris
	40 mM	Glycine
	1 mM	SDS
	20%	Ethanol
	Add ddH_2O until 1 L	

Stripping Buffer	0.2 M	Glycine, pH 2.5
	0.1%	SDS
	1%	Tween

2.2.4 Identification of OTUD4 interactors using HA-affinity purification

2.2.4.1 Preparation of mouse brain lysate

All animal experiments were performed in compliance with the guidelines for the welfare of experimental animals issued by the Federal Government of Germany. C57BL/6 mice were euthanized with Isoflurane, decapitated and the brains were isolated. The brains were dissected from four mice to separate the cortex and cerebellum, followed by lysis in ice-cold homogenizing buffer (see below) in a Teflon-Glass homogenizer (7 strokes). The cortex and cerebellum homogenates were supplemented with 2% Triton X-100 and incubated at 4°C for 2 h in the spinning wheel with gentle rotation. The lysates were cleared by ultracentrifugation with an F50L-24x1.5 Rotor (Thermo Fisher Scientific) at 20,000 rpm for 10 min. The protein concentration of the lysates was roughly estimated using a NanoDrop instrument.

Homogenizing Buffer	0.32 M	Sucrose
	50 M	EDTA
	2 mM	HEPES
	Complete protease inhibitor	
	pH 7.4	

2.2.4.2 HA-affinity purification

HEK293T cells were transfected with pN3HA-OTUD4 (18 x 10-cm dishes) or empty vector (15 x 10-cm dishes). 48 h post transfection, cells were lysed for 1 h in ice-cold lysis buffer. Lysates were incubated with HA-magnetic beads overnight at 4°C. Afterward, beads were washed twice with low salt buffer, twice with high salt buffer, and again twice with low salt buffer. HA-OTUD4 immobilized to beads was then incubated with approximately 5 mg of protein in mouse cortex or cerebellum lysate at 4°C for 5 h. Beads were washed 4x in PBS with 0.5% Triton X-100 and subsequently incubated in Laemmli sample buffer for 5 min at 95°C. The HA-IP eluates were separated on 4-12% Bis-Tris gradient gels and stained with Coomassie SafeStain. Gel slices were excised for analysis by LC-MS/MS.

Lysis Buffer	Low salt buffer	High salt buffer
20 mM Tris-HCl, pH 8 150 mM NaCl 1% Triton X-100 1 mM DTT Protease Inhibitor Phosphatase inhibitor	20 mM Tris-HCl, pH 8 100 mM NaCl 0.1% Triton X-100	20 mM Tris-HCl, pH 8 150 mM NaCl 0.1% Triton X-100

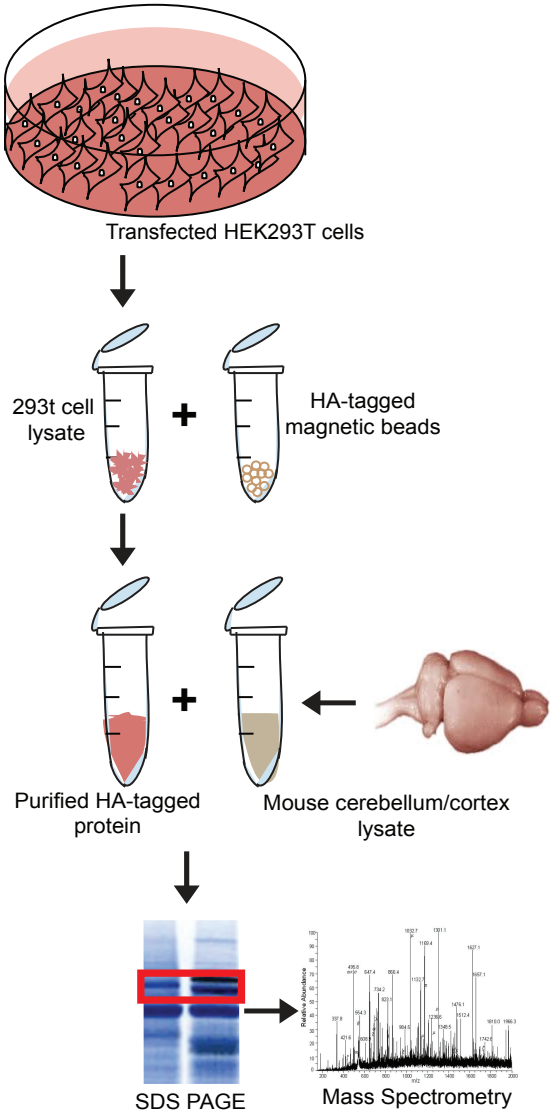

Figure 7: Workflow for the identification of OTUD4 interactors from mouse brain using HA-affinity purification

2.2.5 Mass spectrometric analysis

Mass spectrometry analysis was performed by the MS core facility in the Institute for Biochemistry and Molecular biology (IBMB), University of Bonn.

2.2.5.1 Peptide preparation

For protein identification, gel slices were subjected to in-gel digestion (Jeno et al., 1995; Rosenfeld et al., 1992). In brief, slices were extracted using a clean scalpel, placed in 0.5 ml LoBind Eppendorf tubes and washed consecutively with water, 50% acetonitrile (ACN), and 100% ACN. Proteins were reduced with 20 mM DTT in 50 mM ammonium bicarbonate and alkylated with 40 mM iodoacetamide (in 50 mM bicarbonate) in the dark for 30 min. The slices were washed again and dehydrated with ACN. Dried slices were incubated with 330 ng trypsin (sequencing grade, Promega) at 37°C overnight. The peptide extract was separated and remaining peptides extracted with 50% ACN. Peptides were dried in a vacuum concentrator and stored at -20°C.

2.2.5.2 LC-MS measurements

Peptides were dissolved in 0.1% TFA and 1/3 was injected onto a C18 trap column (20 mm length, 100 µm inner diameter, ReproSil-Pur 120 C18-AQ, 5 µm, Dr. Maisch GmbH) made in-house. Bound peptides were eluted onto a C18 analytical column (200 mm length, 75 µm inner diameter, ReproSil-Pur 120 C18-AQ, 3 µm, with 0.1% formic acid as solvent A). Peptides were separated during a linear gradient from 2% to 35% solvent B (90% acetonitrile, 0.1% FA) within 80 min at 350 nl/min. The Nano HPLC was coupled online to an LTQ Orbitrap Velos mass spectrometer (Thermo Fisher Scientific). Peptide ions between 330 and 1600 m/z were scanned in the Orbitrap detector with a resolution of 30,000 (maximum fill time 400 ms, AGC target 106). The 25 most intense precursor ions (threshold intensity 3000, isolation width 1.0 Da) were subjected to collision-induced dissociation (CID, normalized energy 35) and analyzed in the linear ion trap. Fragmented peptide ions were excluded from repeat analysis for 15 s.

2.2.5.3 Data analysis

Raw data processing and analysis of database searches were performed with Proteome Discoverer software 2.1.0.81 (Thermo Fisher Scientific). Peptide identification was done with an in-house Mascot server version 2.5 (Matrix Science Ltd). MS2 data were

searched against Mus musculus sequences in SwissProt (release 2016_02) and common contaminants. Precursor ion m/z tolerance was 8 ppm, fragment ion 0.5 Da. Tryptic peptides with up to two missed cleavages were searched. Carbamidomethylation of cysteines was set as static modification. Oxidation of methionine and N-terminal protein acetylation was allowed as dynamic modifications. Mascot results were assigned q-values by the percolator algorithm (Kall et al., 2008) version 2.05 as implemented in Proteome Discoverer. Spectra of peptide spectrum matches (PSMs) with q>0.01 were sent to a second round of database search with semitryptic enzyme specificity (one missed cleavage allowed) where carbamidomethylation was searched as a dynamic modification. Proteins were included if at least two peptides were identified with q≤0.01. False positive rates were estimated to be 0.8%, 1.2%, and 1.0% on PSM, peptide, and protein level respectively.
Proteins that were identified in at least 2 out of 3 experiments per tissue and were enriched ≥30 fold over control samples (based on peak area) were considered putative interactors.

2.2.6 Methods for detecting protein-RNA interactions

2.2.6.1 Oligo (dT) pulldown assay

To capture intact mRNA from crude cell extracts, oligo (dT)-coated Dynabeads were used. The method is based on the principle that the oligo (dT) on the surface of the resins binds to the poly(A) tails of mRNA by base pairing to capture the mRNA.
mRNA-isolation from HEK293T lysates was carried out using Dynabeads oligo(dT)25 according to manufacturer's instructions. In short, the beads were prepared by washing once with binding buffer. The HEK293T cell extracts were prepared by adding 1 ml lysis buffer to a cell pellet of 4 x 10^6 cells and passing the lysate three times through a 21 gauge needle syringe to ensure complete lysis. The crude lysate was mixed with the washed beads and gently rotated for 10 min at RT to anneal mRNA to the oligo (dT) sequence. mRNA immobilized to beads was washed once with 1 ml of each wash buffers A and B using a magnetic stand. In case of RNase A treatment, the beads were washed once with buffer A and then treated with or without RNase A (100 µg/ml) in wash buffer B for 15 min at 37°C. Dynabeads treated at 37°C were re-suspended once more in wash buffer B. Proteins bound to the immobilized mRNA were eluted by incubating the beads in Laemmli sample buffer for 5 min at 95°C.

Binding buffer	Lysis buffer	Wash Buffer A	Wash Buffer B
20 mM Tris-HCl, pH 7.5 1 M LiCl 2 mM EDTA	100mM Tris-HCl, pH 7.5 500 mM LiCl 10 mM EDTA 1% LiDS 5mM DTT 100 units/ml RNaseOUT	10mM Tris-HCl, pH 7.5 0.15 M LiCl 1 mM EDTA 0.1% LiDS 50 units/ml RNaseOUT	10mM Tris-HCl, pH 7.5 0.15 M LiCl 1 mM EDTA 50 units/ml RNaseOUT

2.2.6.2 RNA-Protein Immunoprecipitation

Two 10-cm dishes of HEK293T cells were transfected with Flag-tagged pCMV-3Tag-6-OTUD4 and empty pCMV-3Tag-6 vector. Cells were UV-crosslinked (200 mJ/cm^2) 48 h after transfection and re-suspended in lysis buffer. To improve lysis the cell suspension was snap frozen in liquid nitrogen and thawed at room temperature. Anti-flag M2 affinity gel beads were blocked with 2 mg/ml BSA for 30 min at RT prior to incubation, to prevent unspecific binding of proteins from the lysate. Cleared supernatant was incubated with blocked beads, overnight at 4°C. Then beads were washed 4x with lysis buffer and re-suspended in lysis buffer. Contaminating DNA was digested with RNase-free DNase I (100 units/ml) for 30 min at 37°C. To elute the RNA bound to immobilized flag-OTUD4, beads were treated with Proteinase K (0.7 mg/ml) for 30 min at 37°C. The RNA was then extracted with phenol/chloroform and precipitated with ethanol. After re-suspension in DEPC-treated water RNA concentration was measured using a NanoDrop.

Lysis buffer

20 mM	Tris, pH 8
0.1 M	KCl
0.2 mM	EDTA
20 %	Glycerol
0.5 mM	DTT
100 U	RNaseOUT

Complete protease inhibitor
Diluted in PBS

2.2.6.3 Reverse Transcription (RT)-PCR

Immunoprecipitated RNA from RNA-protein immunoprecipitation experiment was subjected to RT-PCR to analyze the binding of mRNA targets to OTUD4.
For this, the following more stringent washing buffers were used during the RNA-IP. Washing: 2x in lysis buffer and 2x in high salt buffer (500 mM NaCl, 50 mM Tris, pH 7.5, 2 mM EDTA, 0.5 % NP-40, 0.5 mM DTT, 1.25 µl/ml RNaseOUT). Purified RNA was used as a template for reverse transcription and amplification, carried out with the OneStep RT-PCR Kit according to manufacturer's instructions.

Lysis buffer

50 mM	Tris, pH 7.5
150 mM	NaCl
2 mM	EDTA
0.5 %	NP-40
0.5 mM	DTT
100 U	RNaseOUT

Complete protease inhibitor
Diluted in PBS

2.2.7 Immunocytochemistry

Cells were seeded on poly-L-lysine-coated glass coverslips (1 µg/ml), one day prior to treatment or transfections. Cells were fixed with 4% paraformaldehyde (PFA) diluted in PBS for 10 min at RT. This was followed by three times washing with PBS. All incubation steps were performed in a wet chamber. The cells were incubated for 30 min in 5% (v/v) ChemiBLOCKER solution containing 0.5% TritonX-100 diluted in PBS for permeabilization and blocking. All antibodies were diluted in 2.5% ChemiBLOCKER solution containing 0.25% Triton X-100. Cells were incubated with primary antibodies with appropriate dilution for 1 h at RT. The coverslips were washed three times for 7 minutes with PBS to remove unbound primary antibodies and incubated with fluorescently-conjugated secondary antibodies diluted 1:500 for 1 h, RT. After washing two times with PBS, cells were incubated with DAPI (1 µg/ml) diluted in PBS to stain the cellular genomic DNA. After washing, coverslips were mounted on microscopic slides using ProLong Gold Antifade Reagent and were allowed to dry before proceeding with imaging.

For high throughput analysis using cell voyager, cells were seeded in poly-L-lysine coated 96-well plates one day prior to treatments. Cells were grown at least 24 h in the plates before proceeding for further treatments.

The cultured neurons seeded on the poly-L-lysine coated coverslips were fixed with pre-warmed 4% PFA/4% Sucrose in PBS for 15 min at RT. After three times washing with PBS, fixed neurons were quenched for 10 min with 50 mM NH_4Cl to reduce the autofluorescence generated due to free aldehyde groups. This was followed by three times washing and permeabilization with 0.1% TritonX-100 for 3 min. Longer permeabilization of neurons was avoided as it destroys the neuronal structure. After washing, neurons were blocked for 1 h at RT with blocking solution (see below). Subsequently, cells were incubated with primary and secondary antibodies diluted in 10% blocking solution for 1 h each at RT. Coverslips were mounted on microscopic slides using ProLong Gold Antifade Reagent and air dried before proceeding with imaging.

Blocking solution for neuronal cells

2%	FBS
2%	BSA
0.2%	Fish gelatin

Diluted in PBS

2.2.8 Oligo(dT)-fluorescence in situ hybridization (FISH)

Hela cells were exposed to arsenite stress, washed once with PBS and fixed with 4% PFA for 10 min. Cultured neurons were fixed with 4% PFA/4% Sucrose for 15 min. Cells were washed three times with PBS and then permeabilized with 0.2% TritonX-100 for 10 min, washed twice in PBS, followed by a 5 min wash with 2X saline-sodium citrate (SSC). Cells were prehybridized in prehybridization solution for 30 min. This was followed by hybridization in 4X SSC containing 50% formamide, 10% dextran sulfate, 1% BSA, 0.5 mM EDTA and 100 nM Cy3-oligo(dT)30 probe, overnight at 37°C in a dark humidified chamber. Subsequently, the following washing steps were applied: twice 5 min 2X SSC at RT, twice 15 min 2X SSC at 37°C, 10 min 2X SSC at RT, 10 min 0.2X SSC at RT. Hybridization was subsequently combined with immunocytochemistry starting with the blocking step as described in section 2.2.7.

2.2.9 Microscopy

2.2.9.1 Confocal laser scanning microscopy

Confocal imaging was performed to obtain highly magnified images with a better resolution to ascertain colocalization. Imaging was performed using Zeiss LSM 780 laser scanning confocal microscope with ZEN 2010 software (Zeiss, black edition), equipped with lasers at 405, 488, 561 and 633 nm. Images were captured using 40x and 63x oil objectives by sequential imaging to prevent 'bleed through'. For quantification purposes, random images from different view fields but from the same coverslip were acquired using identical settings. For cells and neurons, z-stacks were generated to obtain maximum projections of images.
For high throughput analysis, automated confocal imaging was performed using CellVoyager 6000 (Yokogawa, Tokyo, Japan) using 40x water objective.

2.2.9.2 Live Cell Imaging

Live cell imaging of transfected neurons was performed using GE DeltaVision Elite microscope running softWoRx 7.00 software. Images were captured using 60x oil objective with 1.42 NA, excitation bandpass at 542/27 nm for mNeonGreen-SMN1 and 597/45 nm for mOrange2-OTUD4. Time course images were captured at 500 ms interval up to 4 min. While imaging, neurons were maintained in a humidified 5% CO2 incubator at 37°C. All images were deconvolved to obtain better resolution using standard softWoRx deconvolution algorithm.

2.2.10 Image Analysis and Quantifications

2.2.10.1 Image adjustments

Maximum intensity projections from z-stacks were generated in Fiji software (Schindelin et al., 2012). Fiji was used to adjust the brightness and contrast, to crop images and create scale bars.

2.2.10.2 Live cell granule tracking

The trajectories of moving granules were generated with MTrackJ plugin in Fiji. The kymograph from the region of interest was generated using KymoResliceWide plugin in Fiji. The "Straighten" tool in Fiji was used to straighten the neurites.

2.2.10.3 Quantification of FMRP/OTUD4 co-localization

For determining FMRP/OTUD4 colocalization, maximum intensity projections were used. Images were smoothened by applying a Gaussian filter (Fiji). Granules were separated from the background by adjusting the threshold of the smoothened image, followed by the detection of local maxima. Clumped particles were separated by applying the watershed algorithm. Using the 'Analyze particle' plugin, OTUD4-positive granules were detected. The average fluorescence intensity of FMRP was measured in each OTUD4 granule with the 'measure' plugin in the ROI manager. A stringent cut-off value for FMRP fluorescence intensity was set to filter out the noise.

2.2.10.4 Quantification of granule mobility

Granule mobility over a period of 4 min was analyzed from kymographs using the "Velocity Measurement Tool" plugin. Granules with maximum displacement (dx) > 4 µm were considered as moving, with a dx < 1 µm as stationary. Granules with dx values between 1-4 µm were scored as oscillating.

2.2.10.5 Quantification of stress granules

Average number and mean area of cytoplasmic stress granules in Hela cells were quantified using a customized pipeline in CellProfiler (Carpenter et al., 2006). For this, an image analysis pipeline was developed. Individual images were exported as tiff images and imported into CellProfiler where each image was individually analyzed. For all SG quantification experiments, between 200-365 cells per condition were counted from at least 25 random fields of view at 63x magnification. For rescue experiments, between 55-100 transfected cells were counted from at least 20 random fields of view.
In brief, nuclei were segmented using the DAPI signal. Whole cells were segmented as secondary objects, by extrapolating a specified distance from the edges of the nuclei based on the Alexa488-TIAR signal. The punctate structures in the Alexa488 channel were enhanced and detected as 'Speckles' with a feature size of 30 pixels in diameter. These enhanced speckles were annotated as stress granules. Only the granules in the cytoplasm region were quantified. Finally, feature count and mean feature area for stress granules were calculated and were exported for statistical analysis. I analyzed data from three repeat experiments.

2.2.10.6 Statistical Analysis

Statistical analyses were performed using R. Graphs were plotted using GraphPad Prism 5.0 and Microsoft Office Excel. For statistically analyzed data, at least three biological replicates ($n \geq 3$) were analyzed. For stress granule quantification experiments, we analyzed the data using Generalized Linear Model (GLM) and accounted for a confounding effect of the experimental data. For the average SG count/cell quasi-Poissonian regression model and for the mean SG area/cell Gamma regression model were used. A p-value of ≤ 0.05 was considered statistically significant.

3 Results

3.1 OTUD4 interactome reveals strong association with RNA-binding proteins

At the inception of this project, only limited knowledge existed regarding the physiological functions of OTUD4. OTUD4 was found to regulate the dorsoventral patterning in zebrafish (Tse et al., 2013). Additionally, a homozygous mutation in OTUD4 was reported in a familial case of Gordon Holmes Syndrome in which patients displayed fertility defects (hypogonadotropic hypogonadism), ataxia and dementia (Margolin et al., 2013). To ascertain the importance of OTUD4 in the nervous system and investigate key cellular processes controlled by OTUD4, novel interacting partners of OTUD4 were identified from mouse brain. Towards this approach, affinity purification was performed followed by mass spectrometry. HEK293T cells were transfected with empty pN3HA vector (as negative control) or HA-tagged OTUD4, and anti-HA-affinity purification was carried out using HA-agarose beads. Following immunoprecipitation, the HA-OTUD4 bound beads and the empty HA-peptide beads were incubated with cortex or cerebellum lysates from mouse brain. After the pulldown, the beads were subjected to stringent washing to remove the unspecific binders and the eluate was resolved by SDS-PAGE. Coomassie Blue staining showed that OTUD4 interacted with numerous proteins, whereas there were far fewer proteins bound with empty HA-peptide beads (Figure 8A). This was observed for both cerebellum and cortex lysates in three independent experiments. The immunopurified protein complexes were identified by liquid chromatography tandem mass spectrometry (LC-MS/MS).

To identify highly specific interactors of OTUD4, the potential interactors were subjected to stringent filtering. All the interactors that appeared in at least 2 out of 3 replicates were selected. The proteins that were found with ≥30-fold enrichment based on peak area in comparison with control samples were qualified as high scoring interaction partners. 298 proteins were scored as specific interaction partners in the cerebellum and 290 proteins were specific to the cortex.

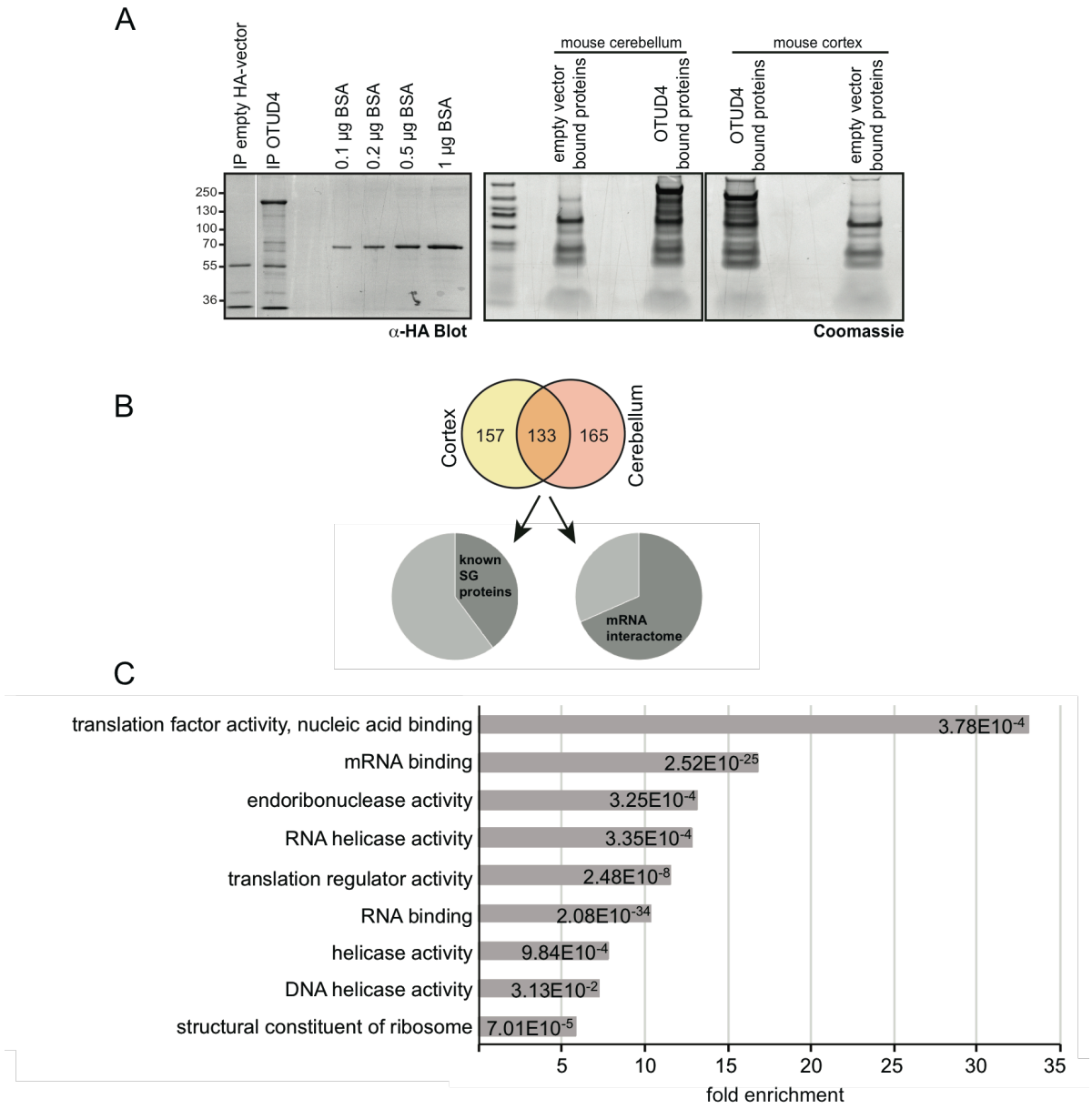

Figure 8: Identification of OTUD4-interacting proteins in mouse brain by affinity purification (A) WB showing IP of HA-OTUD4 and empty pN3HA vector expressed in HEK293T cells. Known amounts of BSA were loaded as standard to have an approximate estimation of the concentration of purified HA-OTUD4. HA-OTUD4 or empty vector bound immunoprecipitates from mouse cerebellum or cortex lysate were resolved on 4-12% Bis-Tris NuPAGE gradient gels and proteins were visualized by Coomassie staining.
(B) OTUD4 or empty vector bound proteins were identified by mass spectrometry. OTUD4-precipitates with more than 30-fold enrichment compared to controls were identified as potential interactors. Venn diagram illustrates the overlap between OTUD4-bound proteins in

cortex and cerebellum. Out of 133 shared interactors, 68% accounted for RNA-binding proteins and 40% were associated with SGs. These results are represented from 3 independent experiments. MS data are shown in Table 19.
(C) Gene Ontology analysis using the PANTHER GO-Slim tool (molecular function) showing enrichment in proteins related to RNA metabolism and translation. Shown are all terms with a fold enrichment factor >5. The fold enrichment of terms is calculated with reference to the mouse genome. The FDR for each of the terms is indicated in the respective bar. The analysis was performed for 298 potential interactors from the cerebellum. Figure is modified from (Das et al., 2019).

Among these, a subset of 133 overlapping proteins was found in both the cerebellum and cortex lysates (Figure 8B). The lists of specific interactors have been shown in Table 19 with their corresponding enrichment scores. In order to predict which biological functions were overrepresented, the list of interactors was subjected to Gene Ontology enrichment analysis using the Panther GO Slim tool (Mi et al., 2013; Thomas et al., 2003). This analysis annotates biological terms (gene ontology terms) to describe a given selection of genes and clustering them together based on functionally related GO terms. This was used to predict the likelihood of particular biological functions relevant to our study. Interestingly, the gene ontology analyses with respect to the molecular function revealed GO terms like mRNA binding, nucleic acid binding and translation were overrepresented in the cerebellum interactome (Figure 8C). Among the overlapping interactors from both the tissues, 68% of them were identified as RNA-binding proteins (Beckmann et al., 2015). Furthermore, 40% of the potential interactors have been previously shown to associate with SGs (against a manually curated list of proteins from literature). Well-known SG-associated proteins like G3BP1, TIA-1/TIAR were identified as interactors (Kedersha et al., 1999; Tourriere et al., 2003). Identification of the SG proteome in a recent study accounted for approximately 150 newly annotated SG proteins in HEK293T cells and neural precursor cells (Markmiller et al., 2018). Including these new data sets, ~50% of OTUD4 interactome accounted as SG proteins. Moreover, well-characterized proteins such as SMN1, Staufen and FMRP known to be constituents of mobile RNA transport granules in neurons were also found as significant hits in the list (Kiebler & Bassell, 2006).

3.2 Verification of OTUD4 interacting proteins by co-immunoprecipitation

In order to validate interactors from the proteomic analysis, co-immunoprecipitation was performed using HEK293T cells using a subset of RNA-binding proteins from the list of putative interactors. For this purpose, GFP-tagged SMN1 or flag-tagged HuB or myc-tagged IGF2BP3 was transiently co-expressed along with epitope-tagged OTUD4 in HEK293T cells. 48 hours post-transfection the cells were lysed and immunoprecipitation was performed using beads conjugated with antibodies against the respective tag (Figure 9). Interestingly, SMN1, HuB and IGF2BP3 were found in the IP fraction along with OTUD4. As a negative control, empty GFP vector was used as indicated, to exclude the chance of unspecific binding to the GFP tag. Similarly, in order to validate the physical interaction of the two core stress granule proteins G3BP1 and TIAR with OTUD4, immunoprecipitation was performed with overexpressed OTUD4. Interestingly, both the endogenous core SG proteins co-immunoprecipitated with OTUD4 but not with empty vector control (Figure 9D & E). As all the above interacting proteins are RNA-binding proteins, the interaction with OTUD4 could be mediated through RNA transcripts. Therefore, to conclude whether the observed co-immunoprecipitation depended on the presence of RNA, the lysates were treated with RNase A. Treatment of the lysates with RNase A, prior to immunoprecipitation showed a reduced or abolished interaction of OTUD4 with SMN1, HuB and G3BP1 pointing towards a RNA-dependent interaction (Figure 9A, B, D). In contrast, the interaction of IGF2BP3 and TIAR with OTUD4 was unaffected or even stronger after RNase treatment indicating a protein-protein interaction. This suggested, OTUD4 binding to some of the interaction partners is direct and for others, RNA binding could be a pre-requisite for the interaction.

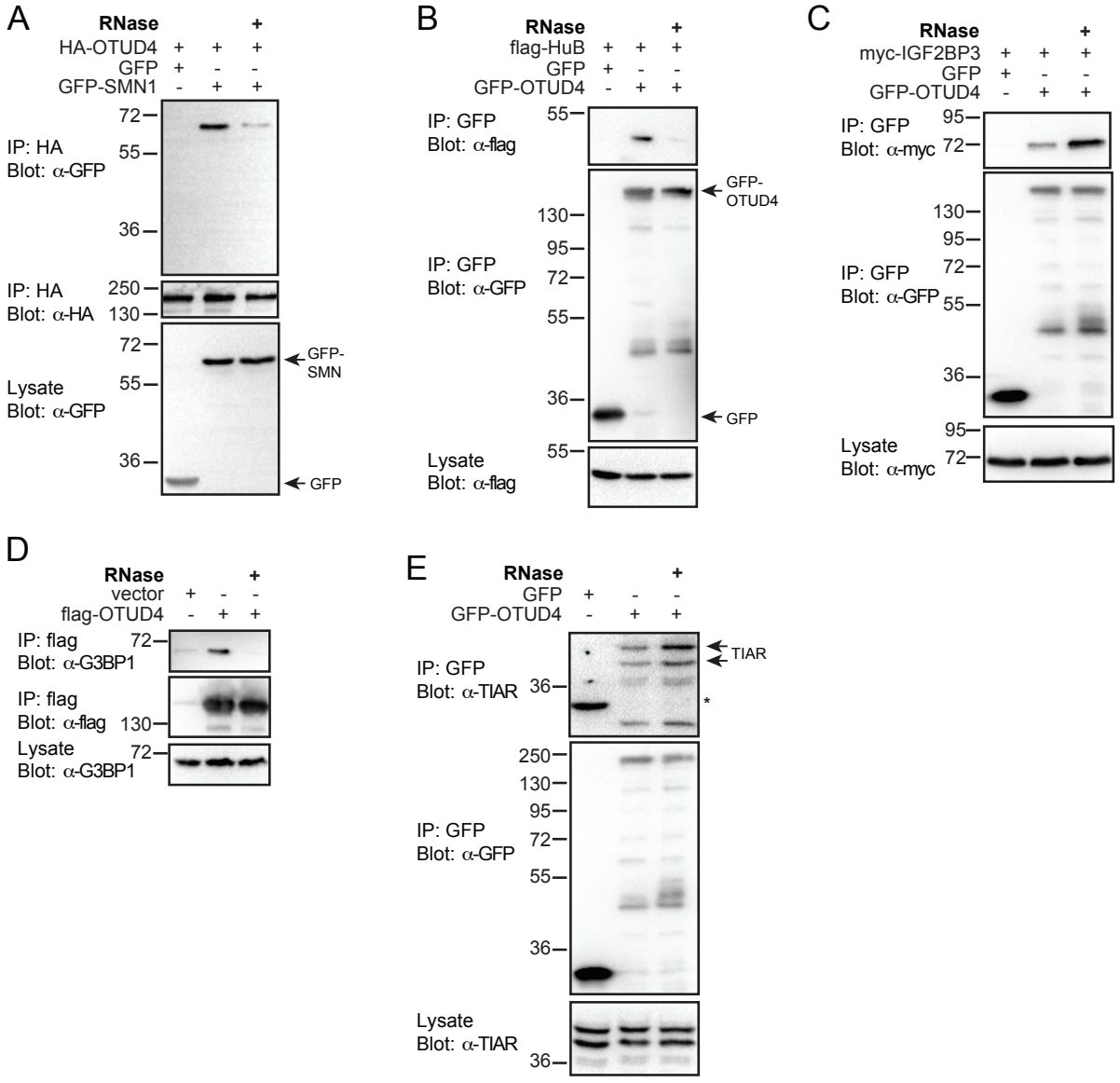

Figure 9: Verification of potential OTUD4 interactors identified in LC-MS/MS
The interaction of proteins with OTUD4 was verified by co-immunoprecipitation experiments. HEK293T cells were overexpressed with tagged-OTUD4 or corresponding empty vector as indicated. Following co-IP, the interaction was verified by immunoblotting with indicated antibodies. 10% of the lysate used for IP is shown as input. Interaction between exogenously expressed OTUD4 with SMN1 (A), ELAV-like protein 2/HuB (B) and IGF2BP3 (C) and interaction with endogenous SG-associated proteins G3BP1 and TIAR (D, E) is shown. Lysates were incubated at 37°C for 15 min in the absence or presence of RNase A (50 µg/ml) as indicated (third lane in each blot) and subjected to IP. Each co-IP is representative of at least 3 independent experiments. Figure is modified from (Das et al., 2019).
(* denotes cross-reaction with anti-TIAR-antibody)

3.3 OTUD4 associates with stress granules upon cellular stress

The newly identified interactors of OTUD4 have been extensively studied regarding their association with stress granules. In eukaryotic cells, SGs are cytoplasmic assemblies formed due to inhibition of protein translation in response to various stresses.

The biochemical interaction of OTUD4 with well-known SG core proteins like TIA-1/TIAR and G3BP1 (Gilks et al., 2004; Tourriere et al., 2003), prompted me to test whether OTUD4 is recruited to SGs. Towards this, subcellular localization of endogenous OTUD4 was examined in Hela cells in the absence and presence of stress. Following treatment with sodium arsenite (SA), cells were visualized by indirect immunofluorescence microscopy using antibodies against endogenous OTUD4 and TIA-1, as bona fide SG marker. SA has been widely used to generate oxidative stress in cells, thus inducing SG formation. In the unstressed cells, OTUD4 was diffusely distributed throughout the cytoplasm as reported in previous studies (Urbe et al., 2012) and showed partial colocalization with TIA-1 (Figure 10A). Upon exposure to SA, OTUD4 was substantially enriched in cytoplasmic foci, co-localizing with the SG marker protein TIA-1. To confirm the presence of OTUD4 in SGs, G3BP1 was used as a second SG marker. Therefore, Hela cells expressing flag-tagged OTUD4 were stained using antibodies against flag and G3BP1 following arsenite stress. Strong co-localization of overexpressed OTUD4 with G3BP1-positive puncta was observed (Figure 10B). These results identified OTUD4 as a novel component of SGs in cells. Previous studies revealed cell type and stress-specific compositional diversity of SGs (Aulas et al., 2017; Markmiller et al., 2018). To address whether the recruitment of OTUD4 is restricted to specific cell types and specific kinds of stress, Hela cells were treated with different SG inducing stimuli such as arsenite, heat shock, MG132 (proteasome inhibitor) and stained with antibodies against TIA-1 and OTUD4. TIA-1 is associated with granules under all conditions (Figure 10A). OTUD4 was also found in the SGs irrespective of the type of stress. To test whether the recruitment of OTUD4 to SG is cell-type specific, SH-SY5Y and N2a cells were also treated with different stressors like arsenite and heat shock and were stained using antibodies against endogenous OTUD4 and TIA-1. OTUD4 was efficiently recruited to SGs in SH-SY5Y and N2a cells (Figure 11). Hence, the results conclude that OTUD4 is recruited to SGs across different cell types under various stress conditions.

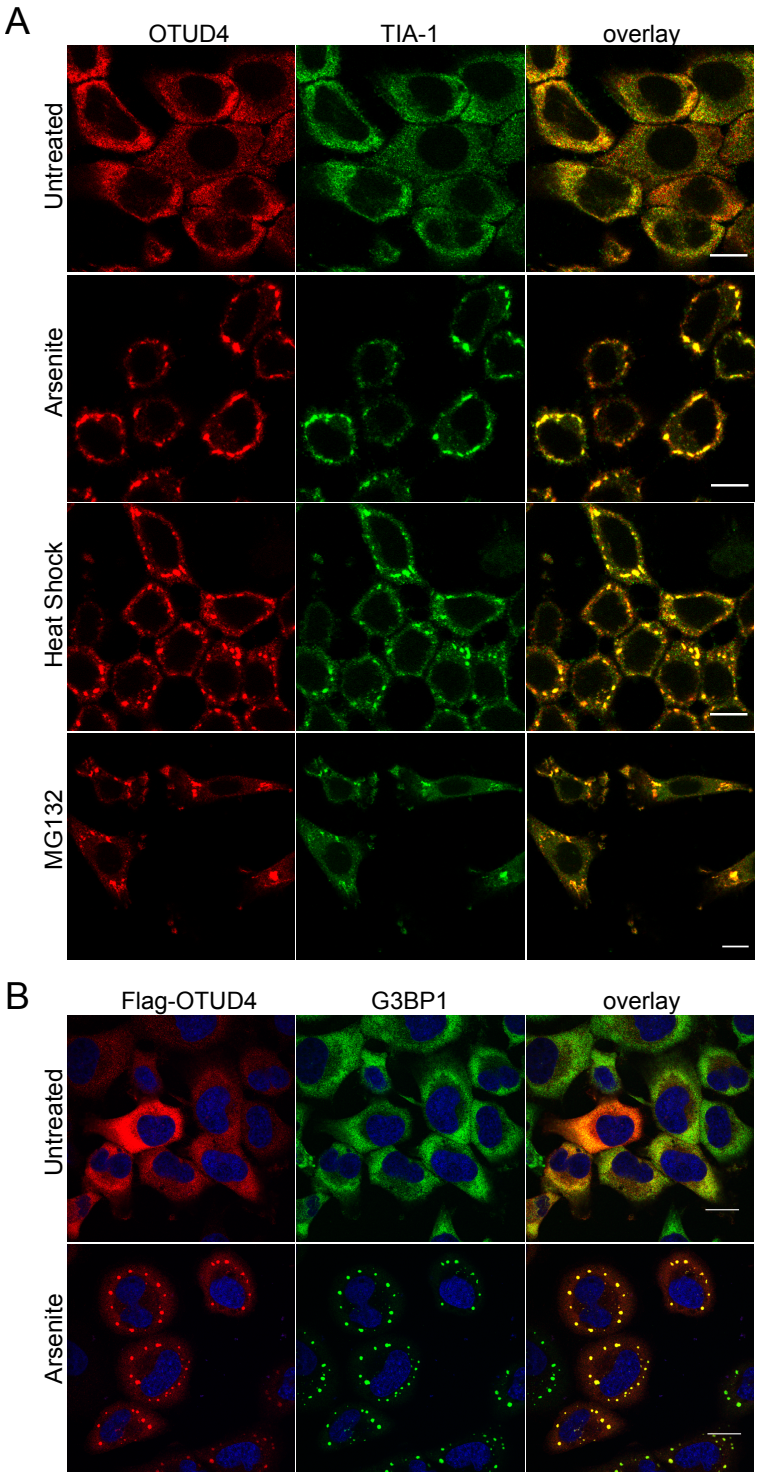

Figure 10: OTUD4 localizes to SGs in Hela cells upon various stress stimuli
(A) Hela cells were either untreated or subjected to sodium arsenite treatment (0.5 mM, 1 h), heat shock (42°C, 1 h) or MG132 (100 µM, 90 min) as indicated. The localization of endogenous

OTUD4 (shown in red) and TIA-1 (green) to SGs was monitored by confocal immunofluorescence microscopy. Representative confocal image from 3 independent experiments is shown here. Scale bar = 10 µm
(B) Hela cells were transfected with flag-OTUD4 and treated with arsenite (0.5 mM, 1 h) to induce SGs. Immunostainings with α-flag antibody and α-G3BP1 (another SG-core protein) showed co-localization of flag-OTUD4 (in red) with endogenous G3BP1 (green) (n=3 experiments). Figure is modified from (Das et al., 2019). Scale bar = 20 µm

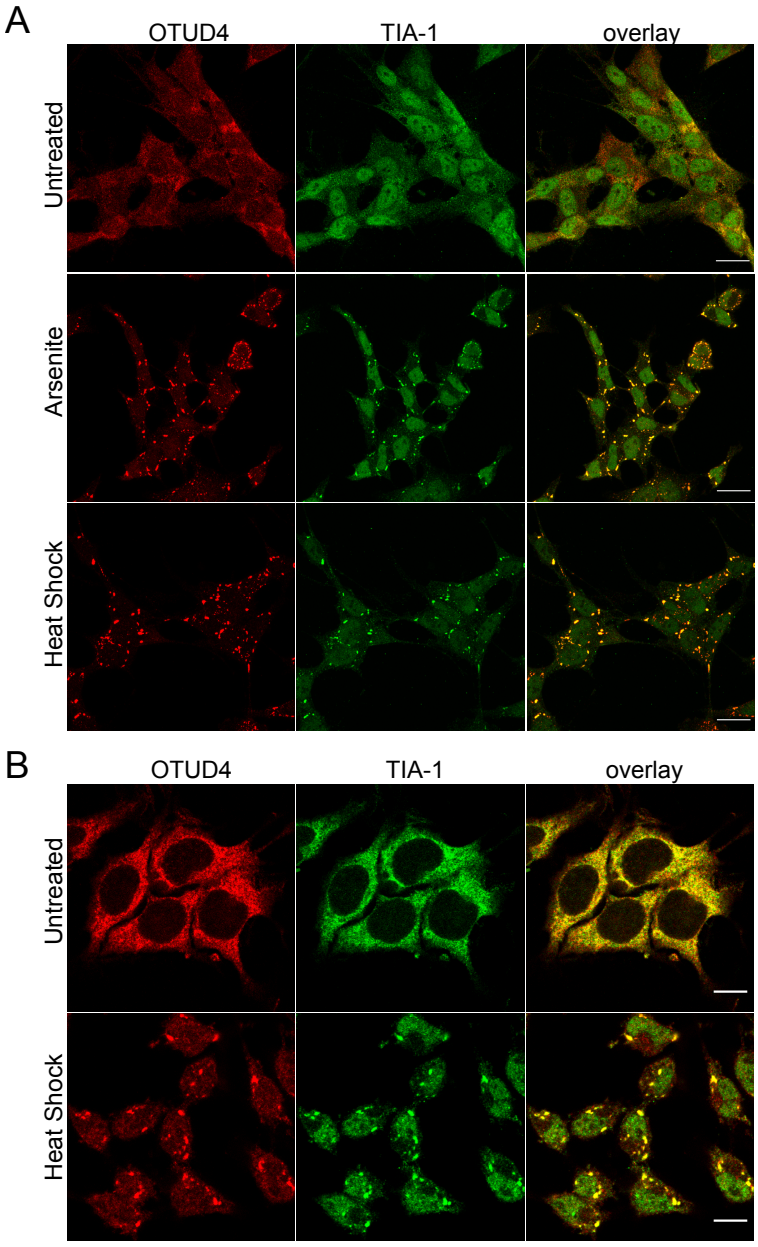

Figure 11: OTUD4 associates with SGs in neuronal cell types
(A) SH-SY5Y cells were either untreated or stressed by exposure to arsenite (0.5 mM, 30 min) or heat shock (42°C, 1 h). Subsequently, the cells were fixed and immunostained for endogenous OTUD4 (in red) and SG-marker TIA-1 (in green). The co-localization of endogenous OTUD4 and TIA-1 in SGs (in yellow) was monitored by confocal microscopy (n=2 experiments). Scale bar = 20 µm
(B) OTUD4 distributed to SGs in N2a cells upon heat shock (42°C, 1 h) as visualized by immunofluorescence images (n=2 experiments). Figure is modified from (Das et al., 2019). Scale bar = 10 µm

3.4 OTUD4-positive SGs contain poly(A)+ RNA in Hela cells

SGs are primarily sites to protect and store untranslated mRNAs and proteins during deleterious phases (Kedersha & Anderson, 2002). To identify whether OTUD4-positive SGs contained polyadenylated (poly(A)) RNA, fluorescence *in situ* hybridization (FISH) was performed using fluorescently Cy3-labeled Oligo(dT) probes to detect endogenous poly(A) RNA. This was followed by endogenous OTUD4 immunostaining in Hela cells. This indicated that after arsenite treatment, Cy3 signal strongly co-localized with OTUD4-positive stress granules (Figure 12). This confirmed OTUD4 as a *bona fide* component of SGs enriched with polyadenylated mRNA.

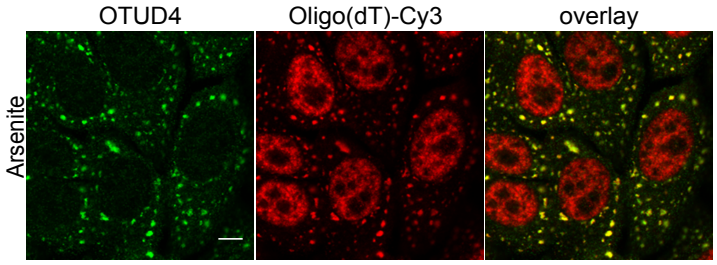

Figure 12: OTUD4-positive stress granules contain mRNA
Representative images of combined FISH/ICC performed in Hela cells treated with arsenite (0.5 mM, 30 min). FISH was first carried out with Cy3-labelled Oligo(dT) probe (red) to stain endogenous mRNA and was followed by immunostaining with α-OTUD4 antibody (shown in green). Representative image shows OTUD4 granules containing mRNA. Scale bar = 10 µm

3.5 OTUD4 is an intrinsically disordered protein

SGs are formed due to liquid-liquid phase separation (LLPS) behavior mediated by proteins possessing IDRs (Lin et al., 2015; Molliex et al., 2015). To determine if OTUD4

is intrinsically disordered, the FoldIndex© algorithm (Prilusky et al., 2005) and "Predictor of Natural Disordered Regions" (PONDR®, www.pondr.com) were used to identify intrinsically disordered domains of OTUD4 (Figure 13). FoldIndex© uses hydrophobicity values and absolute net charge of residues to depict the unstructured regions in a protein. FoldIndex predicted 59% of OTUD4 to be intrinsically unfolded. PONDR® algorithm identifies short and long disordered regions based on combining neural network predictors (Peng et al., 2006). This identified 69% of the sequence in OTUD4 were disordered. Amino acids 317-554 in the N-terminus and amino acids 886-1114 in the C-terminus were predicted to form two large stretches of intrinsically unfolded regions according to FoldIndex© algorithm.

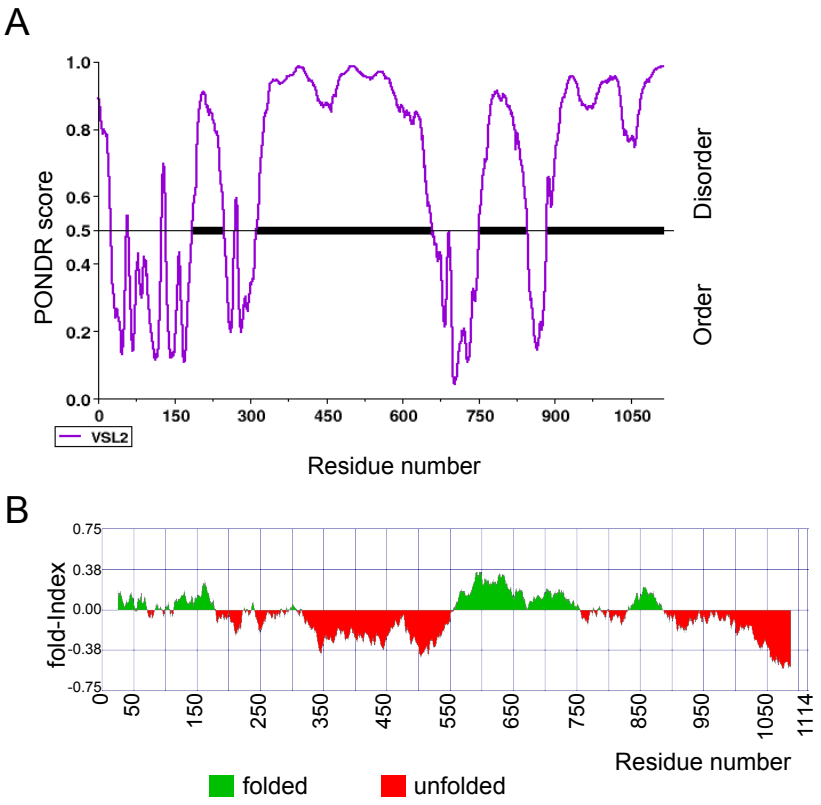

Figure 13: OTUD4 possesses intrinsically disordered regions
OTUD4 was identified to contain intrinsically disordered regions by utilizing two different algorithms
(A) PONDR-VSL2 algorithm identifies the short and the long disordered regions based on combining neural network predictors (Peng et al., 2006). If the PONDR score of an amino acid residue is ≥0.5, the residue is considered as disordered.
(B) FoldIndex implements an algorithm based on average residue hydrophobicity and net charge of the sequence. Figure is modified from (Das et al., 2019).

The predictions by PONDR® algorithm were also similar to FoldIndex© algorithm. Although OTUD4 does not possess any classical RNA-binding domains, a closer look at the C-terminal disordered region showed arginine(R)/glycine(G) and arginine(R)/serine(S)-rich motifs which have been reported to modulate RNA-binding activities (Castello et al., 2016; Jarvelin et al., 2016). Taken together, these predictions suggest that OTUD4 bears intrinsically disordered regions.

3.6 Mapping sequence determinants of OTUD4 responsible for SG recruitment

In order to map the region(s) of OTUD4 responsible for SG recruitment, several truncated EGFP-fusion constructs were generated (Figure 14A).
The N-terminal EGFP-OTUD4$_{1\text{-}551}$ contains the folded OTU-domain, putative Tudor-like domain and the predicted intrinsically disordered region (aa 317-554).
The C-terminal EGFP-OTUD4$_{550\text{-}1114}$ consists of the other predicted intrinsically disordered region (aa 886-1114) with RG/RGG/RS elements. And EGFP-OTUD4$_{1\text{-}900}$ is a version with deletion of aa 901-1114 residues containing the RG/RGG/RS- motifs. Hela cells were transfected with the EGFP-tagged full-length OTUD4 and other truncated constructs. After 24 h of expression, cells were harvested and confocal microscopy was performed.
Interestingly, the truncated version OTUD4$_{550\text{-}1114}$ containing the IDR rich in RG/RS motifs and lacking the OTU-domain showed relatively strong expression in cells with widespread formation of cytoplasmic granules positive for SG protein TIAR even in the absence of stress. The cells expressing the OTUD4$_{1\text{-}551}$ and OTUD4$_{1\text{-}900}$ lacking the C-terminal IDR showed a diffused cytoplasmic distribution with few cells showing TIAR-positive granules. In cells with expression levels similar to EGFP-OTUD4$_{550\text{-}1114}$ expression, these two constructs did not form any granules. Full-length OTUD4 was weakly expressed with diffused distribution in the cytoplasm with a negligible degree of granule formation in the absence of stress (Figure 14B).
When cells were exposed to arsenite stress, all the truncated OTUD4 constructs were recruited to SGs co-localizing with TIAR signal similar to the full-length OTUD4. The C-terminal construct EGFP-OTUD4$_{550\text{-}1114}$ formed large and intense puncta in contrast to less intense granules formed by the N-terminal EGFP-OTUD4$_{1\text{-}551}$ and OTUD4$_{1\text{-}900}$ lacking the RG/RS-rich IDR (Figure 14C).
Taken together, these data demonstrate that the C-terminal IDR fragment OTUD4$_{550\text{-}1113}$ rich in RG/RS-motifs have a higher propensity to form granules in the absence of

stress. Similarly, the constructs lacking this part showed reduced propensity to form granules.

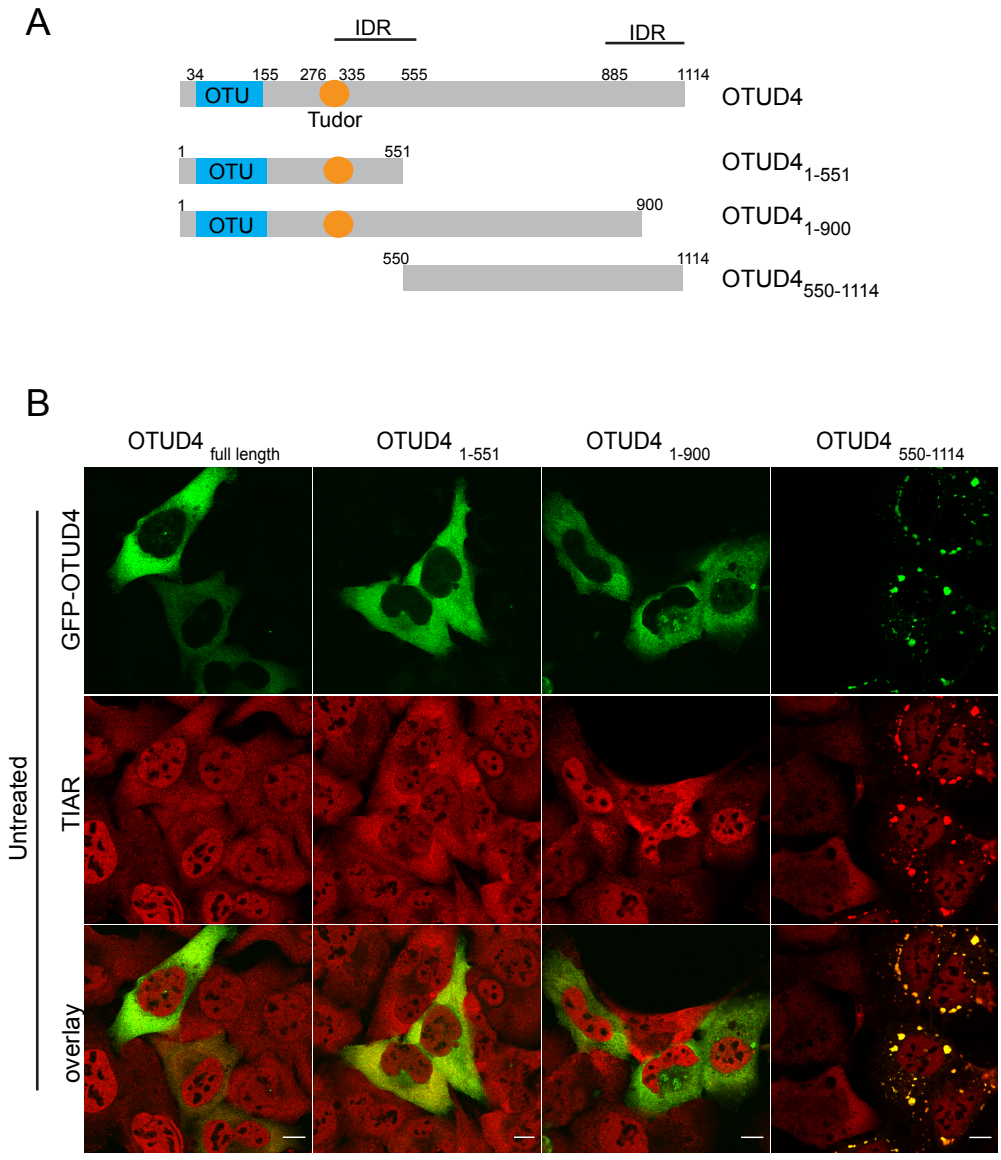

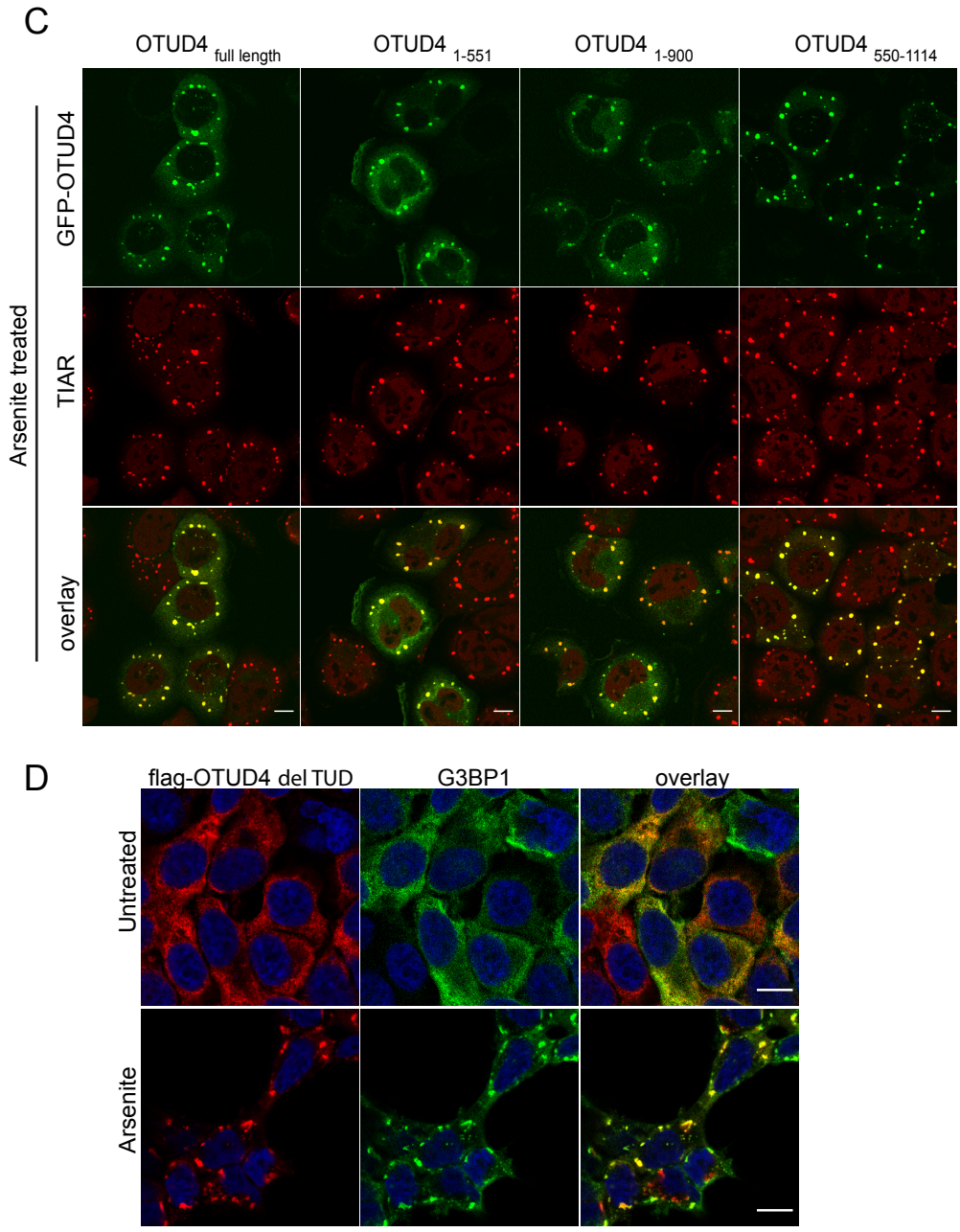

Figure 14: Subcellular localization of different deletion mutants of OTUD4
(A) Domain structure of human OTUD4. It exhibits the ovarian tumor (OTU) domain responsible for its catalytic activity to cleave linkage specific Ub chains as well as a putative Tudor domain. The scheme illustrates the OTUD4 deletion constructs used in this study. IDR represents the intrinsically disordered regions as predicted by FoldIndex (Figure 13).
(B), (C) Shown is the subcellular localization of OTUD4 deletion mutants and their SG localization. GFP-tagged OTUD4 deletion constructs were expressed in Hela cells and were either untreated or stressed with arsenite (0.5 mM, 30 min). Cells were fixed and co-stained with endogenous TIAR antibody. GFP-OTUD4 constructs (in green) and TIAR (in red)

localization was visualized by confocal microscopy. Representative images are from n=4 experiments. Scale bar = 10 μm
(D) Shown here is the subcellular localization of OTUD4 Tudor deletion mutant in stressed and unstressed conditions. Hela cells expressing flag-tagged OTUD4 Tudor domain deletion mutant were stained with α-flag (in red) and α-G3BP1 (in green) antibodies and visualized under a confocal microscope. Figure is modified from (Das et al., 2019). Scale bar = 10 μm

OTUD4 harbors a putative Tudor-like domain at residues 276-335 (Clague et al., 2013). Tudor domains might possess RNA-binding ability (Ponting, 1997). They are reported to bind the methylated arginine residues in different RNA-binding proteins and this interaction subsequently mediates the recruitment of Tudor domains into SGs (Cote & Richard, 2005; Goulet et al., 2008).
Therefore, to verify whether OTUD4's Tudor domain might play a role in localizing it to SGs, we generated a flag-tagged Tudor-domain deleted construct (Flag-ΔTUD) and transiently transfected in HEK293T cells. The ΔTUD construct was predominantly distributed in the cytoplasm in the absence of stress (Figure 14D). Upon treatment with arsenite, its localization to the SGs did not seem to be impaired. Overall, the intracellular distribution pattern of the ΔTUD deletion construct was similar to full-length OTUD4. The Tudor domain does not seem to be essential to localize OTUD4 to SGs.

3.7 OTUD4 point mutations C45A and G398V do not influence SG localization

Polyubiquitylated proteins are reported to be a component of SGs (Kwon et al., 2007; Mateju et al., 2017; Turakhiya et al., 2018).
Although OTUD4 localizes to the SGs independent of its OTU-domain, it is possible that catalytic activity could regulate its tendency to associate with SGs. For this, a Flag-tagged OTUD4^{C45A} point mutant was generated. The cysteine residue of this construct that is critical for its catalytic activity was replaced with alanine (Mevissen et al., 2013). To test this, enzymatically inactive mutant Flag-OTUD4^{C45A} was transfected in Hela cells and its subcellular localization was examined in the presence and absence of arsenite by indirect immunofluorescence. The catalytic inactive mutant displayed similar behavior as wild type OTUD4 (Figure 15A). Flag-OTUD4^{C45A} exhibited a diffused localization in the cytoplasm of unstressed cells whereas addition of arsenite recruited it to SGs, co-localizing with the G3BP1 signal in these foci. Thus, the DUB activity does not determine OTUD4's association with SGs.

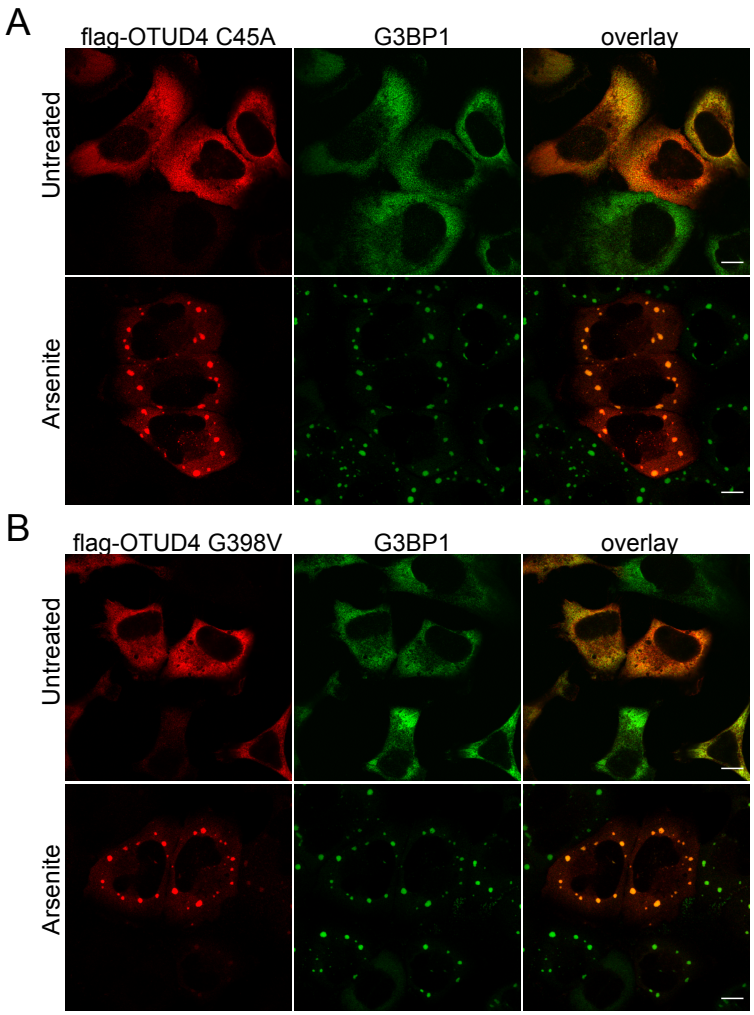

Figure 15: Subcellular localization of different point mutants of OTUD4
Shown here is the subcellular localization of OTUD4 point mutants in stressed and unstressed conditions. Hela cells expressing flag-OTUD4 C45A catalytic inactive mutant (A) and flag-OTUD4 G398V disease mutant (B) were left untreated or were treated with arsenite (0.5 mM, 30 min). To monitor OTUD4 localization, cells were stained with α-flag and α-G3BP1 antibodies and visualized by confocal microscopy. Scale bar = 10 µm

OTUD4 has been reported to a carry mutation at G398V associated with Gordon Holmes syndrome (Margolin et al., 2013). Several disease-linked mutations in the IDRs of SG-associated proteins such as TIA-1, FUS, TDP43, hnRNPA2/B1 have been reported to accelerate their propensity to form SGs in the absence of stress and subsequently

altering SG dynamics (Kim et al., 2013; Liu-Yesucevitz et al., 2014; Mackenzie et al., 2017; Murakami et al., 2015). Thus, we investigated the behavior of disease-associated mutant OTUD4^{G398V} under basal and stress conditions. To test this, we examined the subcellular localization of the Flag-OTUD4^{G398V} in Hela cells before and after SG induction with arsenite. In unstressed conditions, mutated OTUD4^{G398V} was localized to the cytoplasm similar to wildtype OTUD4. It did not form any constitutive SGs as reported for other disease-associated mutations in RNA-binding proteins. OTUD4 ^{G398V} mutant was incorporated to the SGs immunopositive for G3BP1 upon treatment with arsenite. This was similar to the wildtype OTUD4 (Figure 15B). Hence, the disease-associated mutation does not impact the recruitment of OTUD4 to SGs.

3.8 Loss of OTUD4 by CRISPR/Cas does not impact stress granule formation

Next, I addressed the requirement of OTUD4 in SG metabolism. To investigate the importance of OTUD4 in SG assembly, stable knockout (KO) cells were generated by using the CRISPR/Cas system in N2a mouse neuroblastoma cells. Four independent knockout clones were generated. Analysis of protein levels confirmed the loss of OTUD4 (Figure 16B). High throughput analysis was performed to determine the ability of KO cells to assemble SGs following stress. To this end, N2a wildtype and knockout clones were seeded in 96-well plate followed by exposure to 1 h of arsenite stress. The cells were stained with SG marker G3BP1 and were imaged with an automated confocal microscope (Cell Voyager 6000, Yokogawa, Tokyo, Japan). G3BP1-positive SGs were counted for quantification purposes. The wildtype N2a cells readily assembled G3BP1-positive SGs upon exposure to arsenite. In three out of four knockout clones, OTUD4 depletion did not affect the formation of SGs. However, in the knockout clone no.4 (KO4) the cells exhibited a defect in forming discrete SGs (Figure 16A). Quantitative analysis of the percentage of cells bearing G3BP1-positive SGs shows that more than 80% of the wild-type N2a cells possessed SGs; in contrast, in OTUD4-deficient clone KO4 not more than 25% of the cells exhibited SGs (Figure 17A). However, the other three OTUD4 KO clones behaved identical to the wildtype N2a cells with no defect in the SG formation (Figure 16A & Figure 17A). Quantifying differences in the average SG count per cell; a reduction in the SG count in the OTUD4 KO4 was observed compared to the wildtype N2a cells. The other three clones behaved similarly as the wildtype cells (Figure 17B). Summarizing these findings, the results obtained in

CRISPR-KO clones do not give strong evidence for the requirement of OTUD4 for SG formation.

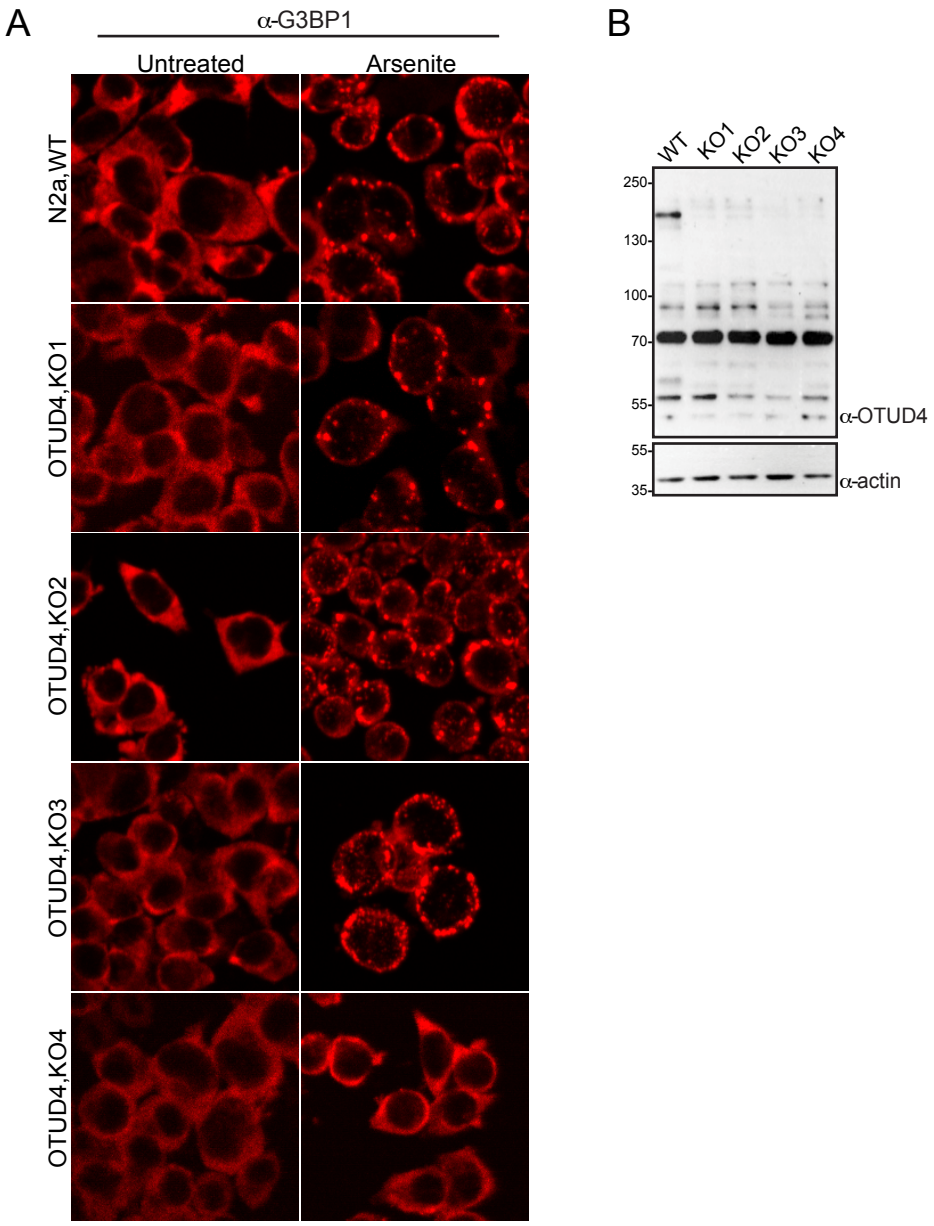

Figure 16: Formation of SGs in WT and OTUD4 knockout N2a cells
(A) Representative confocal images of N2a WT cells and OTUD4 KO cells (4 different KO clones), untreated or treated with arsenite (0.5 mM, 60 min) and stained with α-G3BP1 to monitor SG formation upon loss of OTUD4. Images were acquired by automated confocal microscopy (Cell Voyager 6000). Shown are representative images from n=3 experiments.
(B) WB showing OTUD4 protein levels in N2a, WT and CRISPR/Cas9 generated OTUD4 KO cells. Actin levels are shown as a loading control.

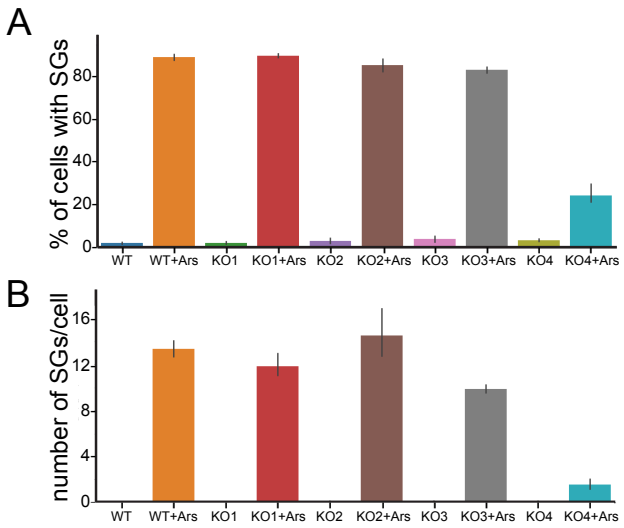

Figure 17: Quantification of SGs in N2a, WT and KO cells
The image analysis from Figure 9 was performed using CellProfiler. (A) Percentage of cells bearing at least one SG. (B) Average number of SGs per cell in both treated and untreated conditions. Data are represented as mean values ± SD from n=3 replicates. At least 10000 cells were imaged per condition.

3.9 Loss of OTUD4 by RNAi impairs stress granule formation

In KO cells, compensatory effects can make it difficult to learn about the function of a protein, therefore we employed RNAi for acute depletion of OTUD4 gene expression. Additionally, human-derived Hela cells were used, which were sturdier upon exposure to arsenite and exhibited robust SG phenotype. In contrast, delicate mouse N2a cells used before displayed smaller and roundish morphology with tiny granules in response to arsenite. This made it challenging to visualize the SGs in N2a cells under the microscope. Therefore, I performed siRNA-mediated knockdown of OTUD4 in Hela cells utilizing two different siRNA oligonucleotides (siRNA5 & siRNA7). The knockdown was carried out for 48 h. The siRNAs strongly abolished the endogenous OTUD4 gene expression compared to cells transfected with control siRNA (siNeg.Ctrl) (Figure 18A & B). After induction of SGs upon arsenite treatment for 30 min, loss of OTUD4 caused a changed SG morphology. As judged by the granules positive for SG marker protein TIAR, loss of OTUD4 resulted in smaller, dispersed and more numerous SGs as compared to the larger, compact and lesser SGs in cells treated with control siRNA (Figure 18A). Quantifications of TIAR-positive SG count per cell and mean area

of granules per cell confirmed a highly significant effect on cells deficient in OTUD4 (Figure 18C, D).

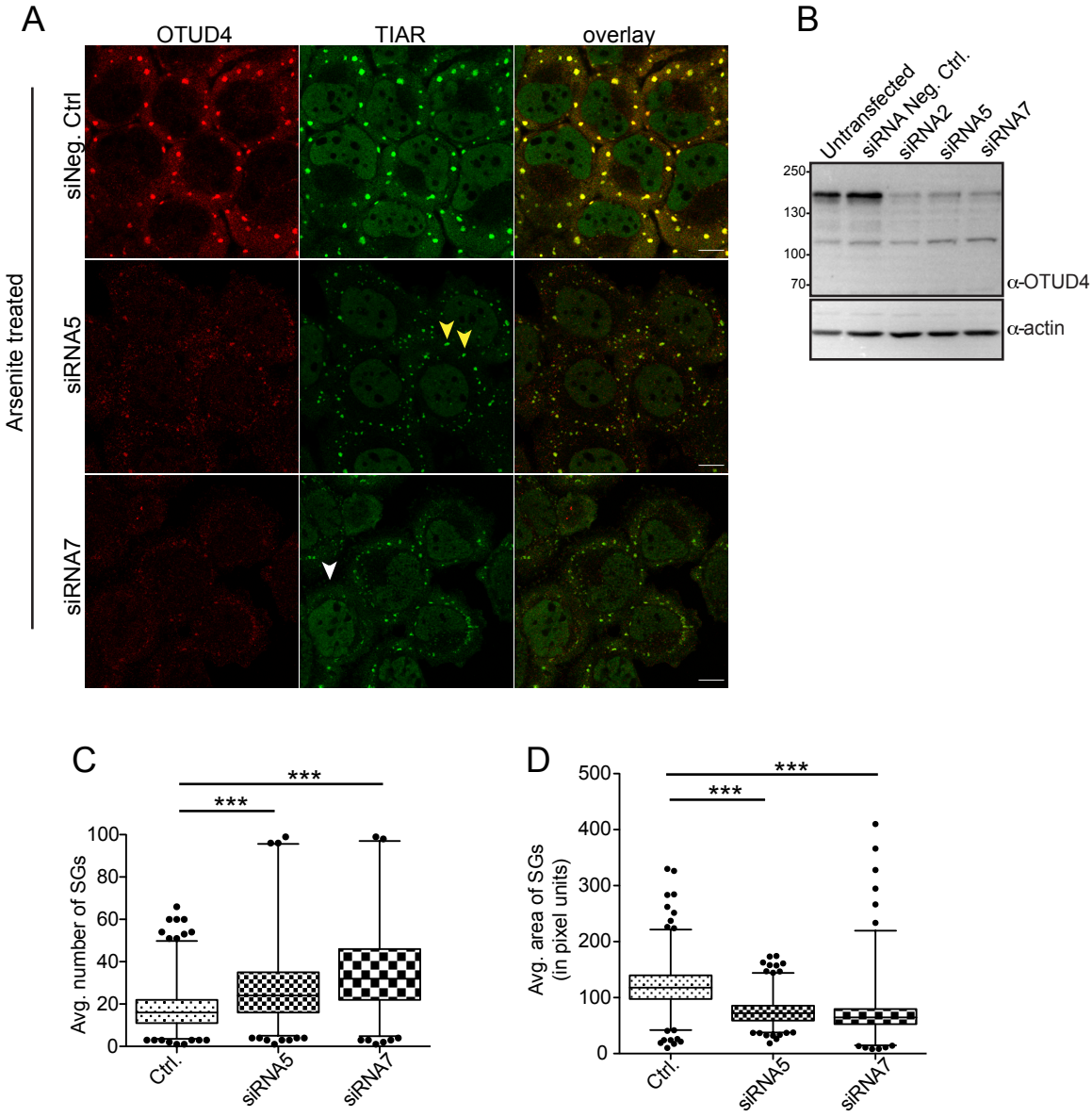

Figure 18: Knockdown of OTUD4 alters SG formation

(A) Hela cells were transfected with negative control siRNA and two different oligos targeting OTUD4. At 48 h post-transfection, cells were stressed with sodium arsenite (0.5 mM, 30 min) and immunostained with α-OTUD4 and α-TIAR antibodies. SGs were visualized by TIAR staining using confocal immunofluorescence microscopy. Loss of OTUD4 resulted in fragmented SG morphology. Yellow arrowheads indicate granules with incomplete OTUD4 knockdown. White arrowhead indicates cell with almost complete OTUD4 knockdown. Scale bar = 10 µm

(B) WB showing OTUD4 protein levels in Hela cells transfected with control siRNA or siRNA against OTUD4. Cells were lysed 48 h post-transfection and immunoblotted using α-OTUD4 antibody. Actin levels are shown as a loading control.
(C) Quantification of average number of SGs per cell determined by CellProfiler. For statistical analysis, quasi-Poissonian regression model was used in R.
(D) Quantification of average area of SGs per cell determined by CellProfiler. For statistical analysis, Gamma regression model was used in R.
In (C & D) data are represented as a box-and-whiskers plot from 3 independent experiments with at least 200 cells counted per condition. Figure is modified from (Das et al., 2019).
For statistical significance: * $p \leq 0.05$, ** $p \leq 0.01$, *** $p \leq 0.001$

Importantly, the individual cells that displayed almost complete abrogation of OTUD4 showed a complete absence of SGs (indicated by white arrow) and cells with incomplete OTUD4 knockdown showed SGs similar in morphology as to control cells (indicated by yellow arrows)(Figure 18A).
Furthermore, to investigate if this effect is exclusive only to TIAR-positive granules or stress granules in general, also G3BP1-positive SGs were analyzed. As shown in Figure 19A, all the G3BP1-positive puncta co-localized with TIA-1 signal. Upon loss of OTUD4, G3BP1-positive granules displayed a similar morphology as TIAR-positive granules.
To assess, if the observed defect in the phenotype of SGs was specific to arsenite stress only, the cells were heat-shocked at 46°C for 1 h and SGs were analyzed. Confocal microscope images revealed smaller and fragmented TIAR-positive SGs upon loss of OTUD4 in comparison with control cells upon heat shock (Figure 19B). This effect was similar to SG morphology under arsenite stress. Taken together, our results demonstrate that OTUD4 is required for proper formation of SGs in Hela cells under different types of stress.

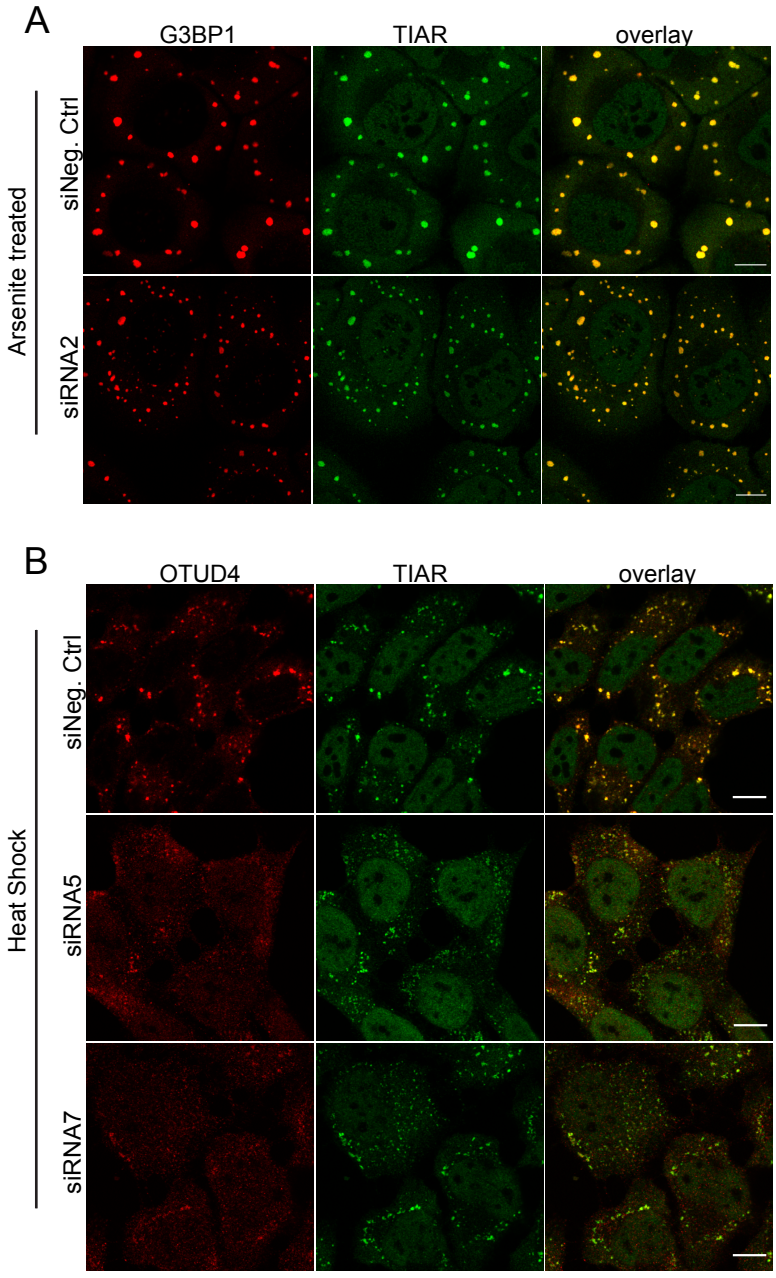

Figure 19: Knockdown of OTUD4 alters SG formation
(A) OTUD4 was depleted in Hela cells by knockdown as indicated and cells were subjected to arsenite treatment (0.5 mM, 30 min). Cells were co-stained with TIAR and G3BP1 antibodies. Confocal images showed all the G3BP1-positive SGs completely overlapped with TIAR-positive granules, displaying a similar impairment in SG morphology upon OTUD4 depletion as TIAR-positive SGs. Scale bar = 10 µm (B) Loss of OTUD4 in Hela cells exhibited fragmented SG morphology upon heat shock (46°C, 1 h) as well, as compared to control siRNA transfected cells. Representative confocal images shown here are immunostained with α-TIAR antibody to visualize SGs. Figure is modified from (Das et al., 2019). Scale bar = 10 µm

3.10 Re-introduction of OTUD4 restores stress granule morphology

To verify that the observed SG phenotype upon loss of OTUD4 was not due to off-target effects of RNAi, OTUD4-depleted Hela cells were transfected with plasmids RNAi resistant plasmids or control plasmid. To approach this, I generated flag-tagged siRNA resistant, wildtype OTUD4 construct. This was achieved by inserting silent mutations in siRNA-targeted sequence (siRNA7) of wildtype OTUD4. The siRNA-resistant Flag-OTUD4^{WT} plasmid was transfected in Hela cells 24 h after knockdown of OTUD4 and was expressed until the next day (Figure 20A). Following this, the cells were immunostained using OTUD4 and TIAR specific antibodies after arsenite treatment. There was a clear distinction in the immunofluorescence signal between cells with endogenous OTUD4 staining and cells with overexpressed Flag-OTUD4. In order to avoid artifacts from OTUD4 overexpression, half of the normal amount of OTUD4 cDNA was used for transfections. Only the cells with expression levels of exogenous OTUD4 near to the endogenous levels were considered for analysis. Cells with strong expression signal exhibited numerous cytoplasmic aggregates and were excluded from the analysis.

Re-introduction of OTUD4 led to a significant rescue of the impaired SG formation as determined by analyzing the TIAR-positive granule size and number. These results suggest that the SG formation defect was due to the lack of OTUD4 (Figure 20B-D).

3.11 OTUD4 point mutants C45A and G398V rescues impaired SG morphology

Several SG-associated proteins have been shown to be ubiquitinated. Hence, it is possible that OTUD4 can deubiquitinate these proteins during the assembly of SGs and maintain their intact morphology. To test whether catalytic inactive mutant of OTUD4 was able to restore normal SG formation, siRNA-resistant catalytic inactive mutant of OTUD4 (Flag-OTUD4^{C45A}) was transfected in OTUD4-depleted Hela cells and immunostaining was performed. Confocal images showed OTUD4^{C45A} was able to restore the normal SG formation in a manner similar to the rescue by OTUD4^{WT} (Figure 20B). This was quantified by analyzing the TIAR-positive granules for their size and number (Figure 20C, D). Hence these results demonstrate that catalytic activity of OTUD4 is dispensable for intact SG formation.

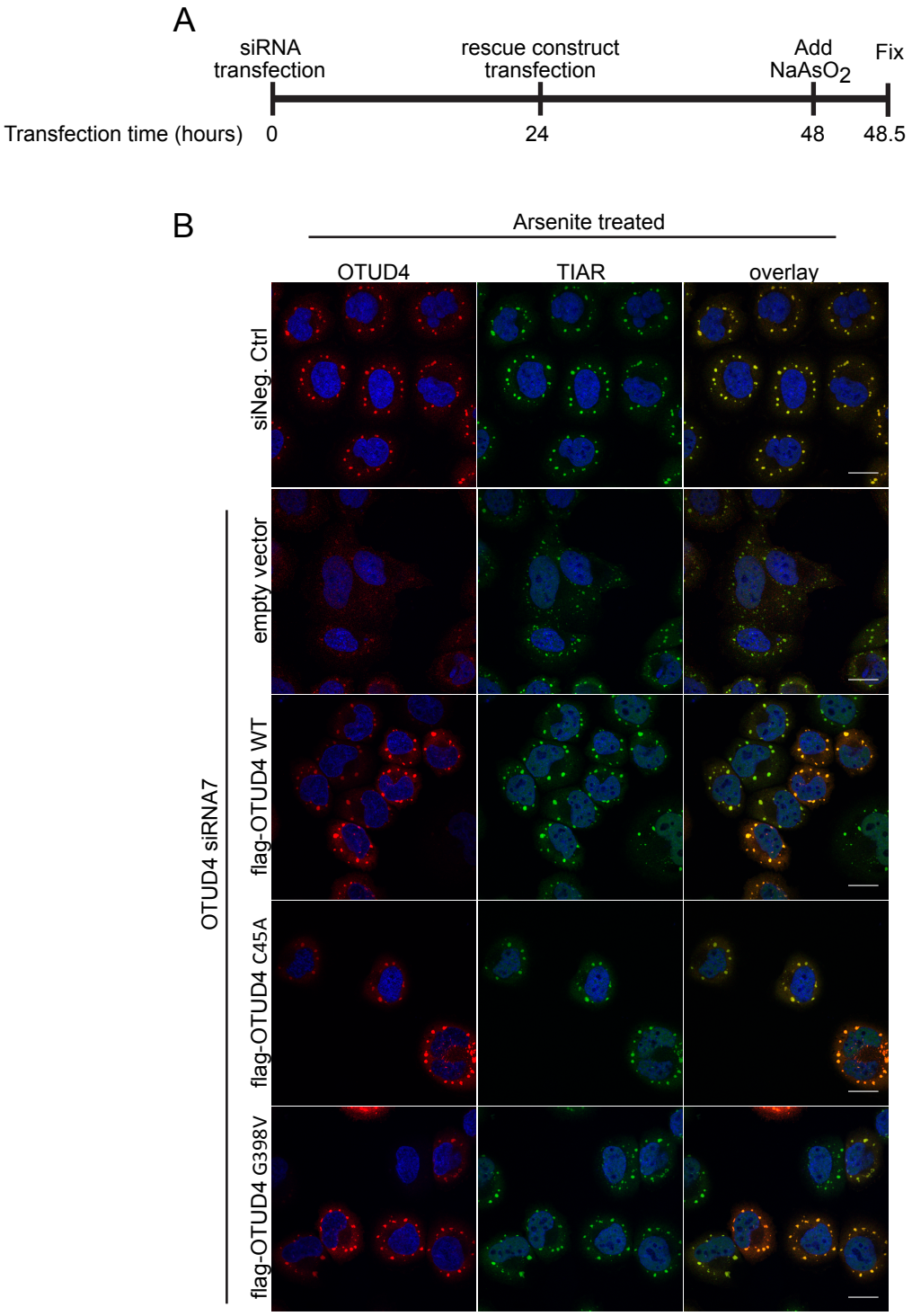
A
siRNA transfection
rescue construct transfection
Add NaAsO2
Fix
Transfection time (hours)
0
24
48
48.5
B
Arsenite treated
OTUD4
TIAR
overlay
siNeg. Ctrl
empty vector
flag-OTUD4 WT
flag-OTUD4 C45A
flag-OTUD4 G398V
OTUD4 siRNA7

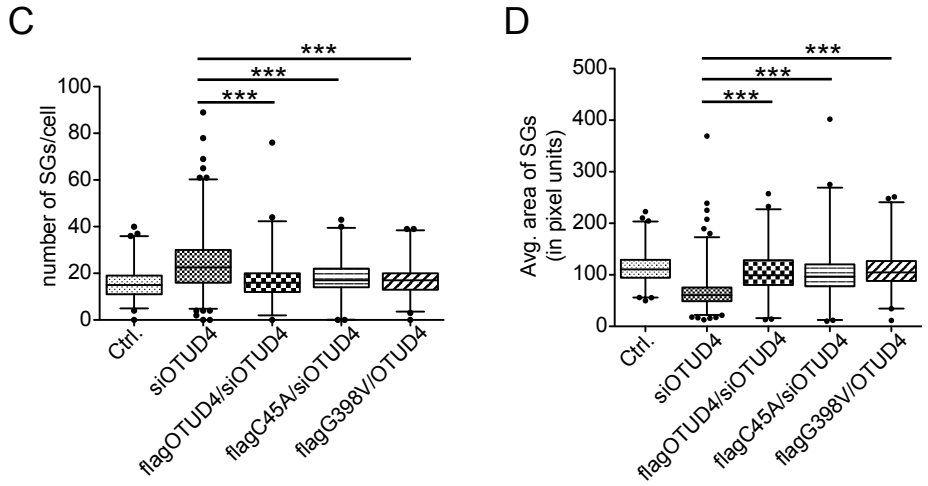

Figure 20: OTUD4 rescues impaired SG morphology in Hela cells
(A) Experimental design showing time points of siRNA-resistant construct transfections and arsenite treatment (0.5 mM, 30 min) in OTUD4-depleted cells.
(B) Hela cells were transfected with siRNA resistant flag-OTUD4, its catalytic inactive mutant (C45A) or disease mutant (G398V) 24 h after OTUD4 knockdown. Arsenite-treated cells were stained with α-OTUD4 and α-TIAR antibodies to visualize SGs.
Scale bar = 20 µm
(C) Quantification of the average number of SGs per cell determined by using CellProfiler. For statistical analysis, quasi-Poissonian regression model was used in R.
(D) Quantification of average area of SGs per cell determined by using CellProfiler. For statistical analysis, Gamma regression model was used in R.
In (C & D) data are represented as a box-and-whiskers plot from 3 independent experiments with 55-100 transfected cells counted per condition. Figure is modified from (Das et al., 2019).
For statistical significance: * $p \leq 0.05$, ** $p \leq 0.01$, *** $p \leq 0.001$

Next, the effect of disease-associated OTUD4^{G398V} in the process of SG formation was evaluated. Similarly, a siRNA-resistant OTUD4 construct carrying the disease-associated mutation (Flag-OTUD4^{G398V}) was generated and transiently expressed in OTUD4-depleted Hela cells. Immunofluorescence and quantitation results showed that the disease-associated mutant was able to significantly rescue the impaired SG formation compared to the control OTUD4-depleted cells (Figure 20B-D). This result indicates that the disease-associated point mutation in the IDR of OTUD4 does not compromise the function of OTUD4 in SG formation.

3.12 Loss of OTUD4 impairs maturation during SG assembly

Stress granules are membraneless organelles formed by a stable core structure surrounded by a dynamic shell of numerous protein-RNA complexes. First, the formation of the stable core takes place followed by assembly of a diffused shell around the cores (Jain et al., 2016; Wheeler et al., 2016). Our results show that OTUD4 is required for SG assembly after 30 min arsenite treatment. It could be possible that the observed phenotype in OTUD4 knockdown cells is a delay in the initiation of SG formation or the maturation phase of granule formation could also be affected. To investigate the dynamics of stress granules at different stages of their assembly upon loss of OTUD4, knockdown was performed for 48 h and the cells were stained for TIAR post-fixation. The morphology of TIAR-positive granules at indicated time points of arsenite treatment was analyzed (Figure 21). SG assembly in Hela cells was first detected at 15 min of arsenite stress. The same was seen for siRNA-treated cells. However, the knockdown of OTUD4 led to an accumulation of smaller and more numerous SGs at this stage as compared to control Hela cells. This phenotype of (numerous, small, dispersed in size) was also evident at 30 min of SG induction when they were still in the growth phase. This persisted throughout up to 90 min of stress induction. The negative control Hela cells showed a clear initiation event with smaller stress granules at 15 min that eventually matured over time to form larger granules at 90 min of stress exposure. Taken together, we concluded that in the absence of OTUD4, SGs formed less efficiently with a persistent decline over time in their size but remained numerous in number. This indicates impairment in the maturation phase of granule formation, possibly affecting fusion events during SG assembly.

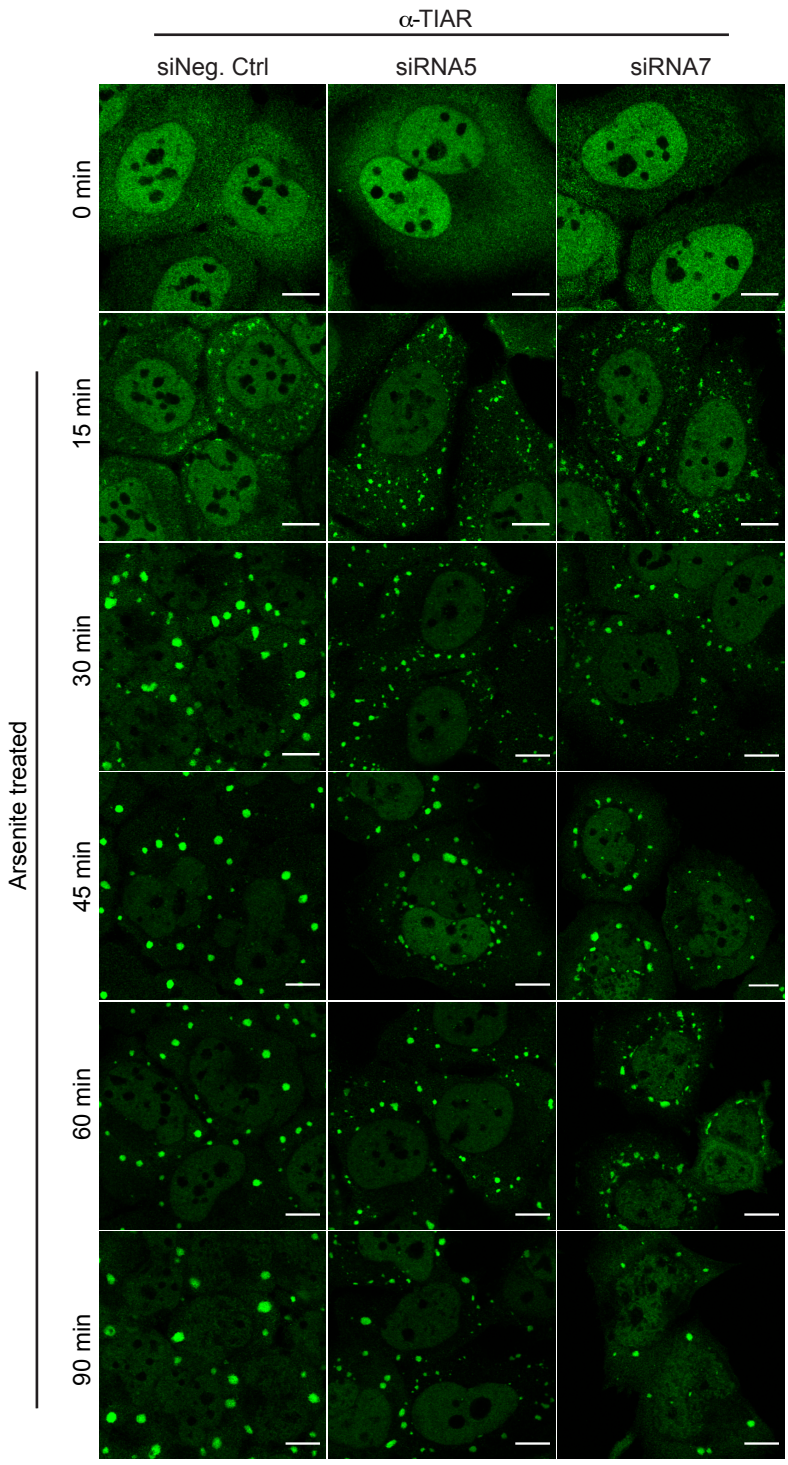

Figure 21: Loss of OTUD4 causes defect in the maturation phase of SG assembly
Time course analysis of SG assembly in control cells and OTUD4 knockdown cells. Hela cells were treated with sodium arsenite (0.5 mM) for various time points as indicated and

immunostained for endogenous TIAR to visualize the SGs by confocal microscopy. Figure is modified from (Das et al., 2019). Scale bar = 10 μm

3.13 OTUD4 is present in neuronal RNA transport granules

To accomplish on-site translation of proteins, RNA transcripts are carried to distal neurites in form of ribonucleoprotein complexes (RNPs) as neuronal transport granules (Eliscovich & Singer, 2017). The essential components of transport granules apart from mRNAs are RNA binding proteins such as Staufen, FMRP, hnRNPA1/A2, SMN and Dead-box proteins, which are also known to be sequestered into SGs (Elvira et al., 2006; Kanai et al., 2004; Markmiller et al., 2018; Thomas et al., 2009; Zalfa et al., 2006). Since OTUD4 co-purified with several of these RBPs, we hypothesized that OTUD4 is a constituent of neuronal transport granules under physiological conditions. To verify this, the subcellular distribution of OTUD4 in primary rat hippocampal neurons was assessed. Due to the lack of an antibody to specifically visualize endogenous OTUD4 in rodents, neurons were transfected with GFP-OTUD4 and were cultured for 4 days *in vitro* (DIV4). Confocal images revealed that GFP-OTUD4 primarily resided in the cell soma and also displayed a prominent granular pattern of distribution in the proximal axons and dendrites extending to the distal parts of immature neurons (Figure 22A). This pattern of distribution was similar to what was characterized as transport granules formed by other RNA-binding proteins (Fallini et al., 2012; Tang et al., 2001). To investigate whether overexpression of the bulky EGFP-tag caused the formation of these punctate structures, we used cultured DIV4 neurons transfected with the same amount of empty EGFP vector as a negative control. As seen in Figure 22B, we observed the EGFP-tag alone showed a diffused signal in the cell body and proximal axon but was reduced or absent in the distal processes. In another approach to exclude overexpression artifacts by the EGFP-tag (27 kDa), neurons were transfected using OTUD4 fused with the short 3x flag-tag (3 kDa). Overexpression of flag-OTUD4 in DIV4 cultured neurons showed granular distribution similar to those formed by GFP-OTUD4 along the length of the axons and dendrites. This proved that overexpressed OTUD4 spatially distributes along the neurites of rat hippocampal neurons (Figure 22C).

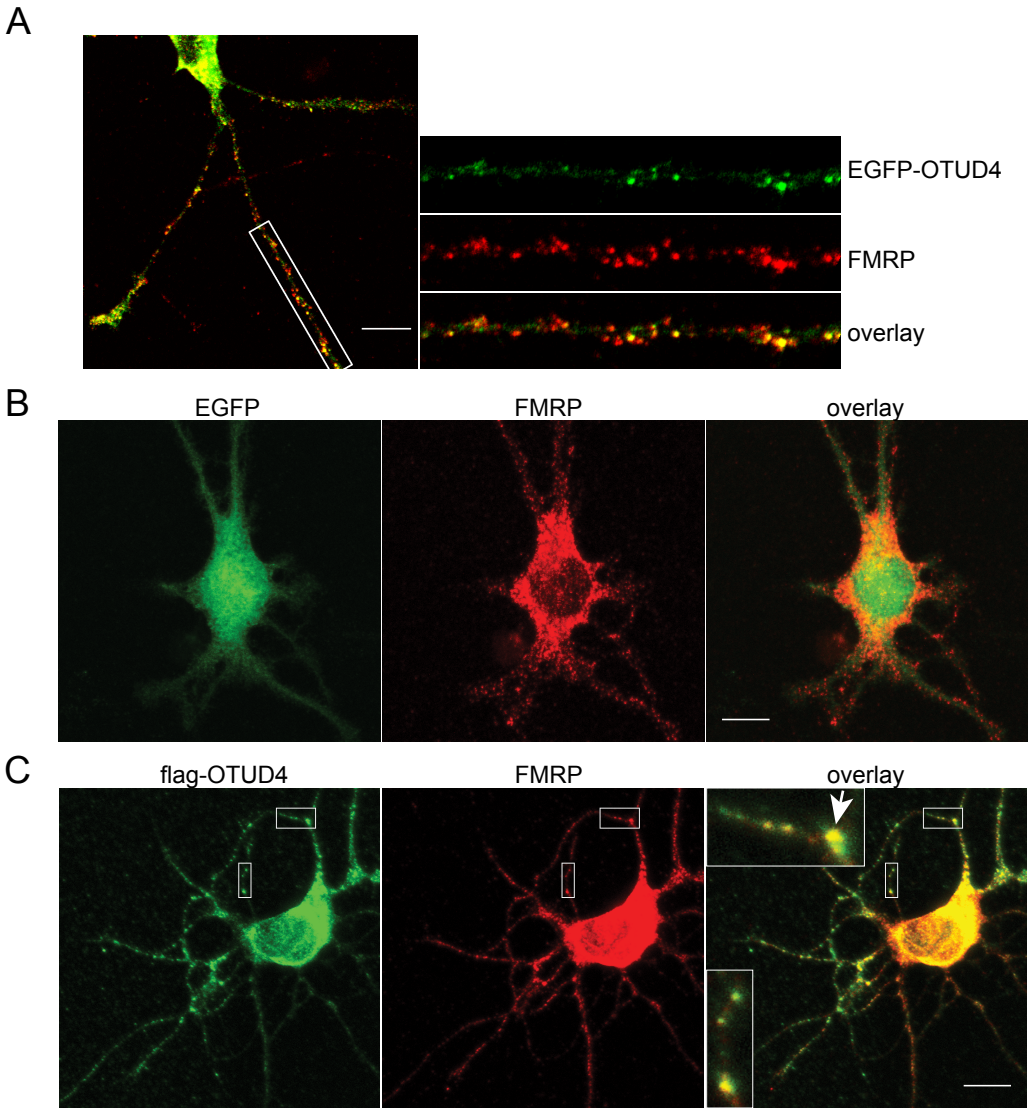

Figure 22: OTUD4 co-localizes with FMRP in RNA transport granules in neurons
(A) Primary rat hippocampal neurons were transfected with GFP-OTUD4 (green) and stained with α-FMRP antibody (red) at DIV4. Representative confocal images demonstrate co-localization of OTUD4 and FMRP in the neuronal granules in dendrites. The adjacent insets show higher magnification of the cropped dendritic region marked by a white box on the overlay image. Scale bar = 10 µm
(B) DIV4 hippocampal neurons transfected with EGFP and stained with α-FMRP were taken as control. EGFP does not display neuronal granules. Scale bar = 10 µm
(C) Hippocampal neurons were transfected with flag-OTUD4 (green) and stained with α-FMRP antibody (red) at DIV4. Insets show higher magnification of the cropped regions marked by white boxes on the overlay image. The white arrow in the inset demonstrates co-localization of OTUD4 with FMRP at dendritic branch points. Figure is modified from (Das et al., 2019).
Scale bar = 10 µm

RNA transport granules are heterogeneous in their composition. The RNA binding proteins and the mRNAs transported in these units are present in different binding combinations with one another. FMRP has been well characterized as a stable component of the neuronal granules, which is involved in activity-dependent translation (El Fatimy et al., 2016; Zalfa et al., 2006). Moreover, OTUD4 co-purified with the FXR proteins namely, Fxr1, Fxr2, Fmr1 (protein name: FMRP) in our proteomic analysis (see Table 19). Hence, the distribution and localization of OTUD4 and FMRP in the immature hippocampal neurons (DIV4) was investigated. To test this, neurons were transfected with EGFP-OTUD4 and subsequently stained for endogenous FMRP. FMRP expression in the cell soma was observed and it exhibited a granular staining pattern along the dendrites as seen in other findings (El Fatimy et al., 2016). Furthermore, our results indicated co-localization of GFP-OTUD4 with endogenous FMRP in the cell body as well as a major fraction of OTUD4 granules partially co-localized with FMRP in the proximal and distal parts of the dendrites. The co-localization of OTUD4 granules with FMRP was quantified. After stringent filtering of noise, 76% ± 11.8% of OTUD4 granules were quantified positive for FMRP. However, a small subset of FMRP granules was found to be negative for OTUD4 signal, most likely due to the heterogeneous composition of RNA granules (Figure 22A).

To rule out the overexpression artifact of EGFP-tag, neurons were transfected with flag-tagged OTUD4 and co-stained with FMRP-specific antibody. Flag-tagged OTUD4 granules co-localized with FMRP granules in the proximal axons and in the distal dendrites, thus confirming the previous results (Figure 22C). Interestingly, immunofluorescence images also identified an overlap of OTUD4 and FMRP at dendritic branch points where previous findings had reported a pronounced accumulation of FMRP along with ribosomes and proteins responsible for mRNA trafficking and translation (Wang et al., 2014) (white arrow, Figure 22C).

3.14 OTUD4-positive granules contain poly(A)+ RNA in hippocampal neurons

To further characterize OTUD4-positive granules as RNA transport granules, the presence of mRNA in these granules was examined. To test this, fluorescence *in situ* hybridization (FISH) was employed using a Cy3-labelled Oligo(dT) probe in neurons transfected with flag-OTUD4. Immunofluorescence microscopy showed Oligo(dT) probe labeled the endogenous poly(A) RNA in the cell somata as well in the axons as

represented by the red Cy3-signal. The Cy3 signal displayed a granular pattern in the proximal dendrites but comparatively weaker distribution towards the distal neurites. A strong co-localization of flag-OTUD4 with the intense mRNA signal was visualized within the granules in the proximal parts. Owing to the lower intensity of the mRNA signal in the distal dendrites, weak co-localization was detected there (Figure 23A). Overall the mRNA signal was quite faint. Therefore the brightness of the images was adjusted to observe the granules in the distal neurites. This explains the saturated signal observed in the cell body. As a control, hippocampal neurons transfected with empty-flag vector were used for FISH with Cy3-Oligo(dT) followed by immunostaining with flag antibody. The endogenous mRNA signal was observed as granules in dendrites and a faint, diffused flag signal was observed with the control transfected neurons without any colocalization with mRNA signal (Figure 23B). Taken together, OTUD4-positive granules contain mRNAs in rat hippocampal neurons, suggesting that OTUD4 is a component of RNA transport granules in neurons.

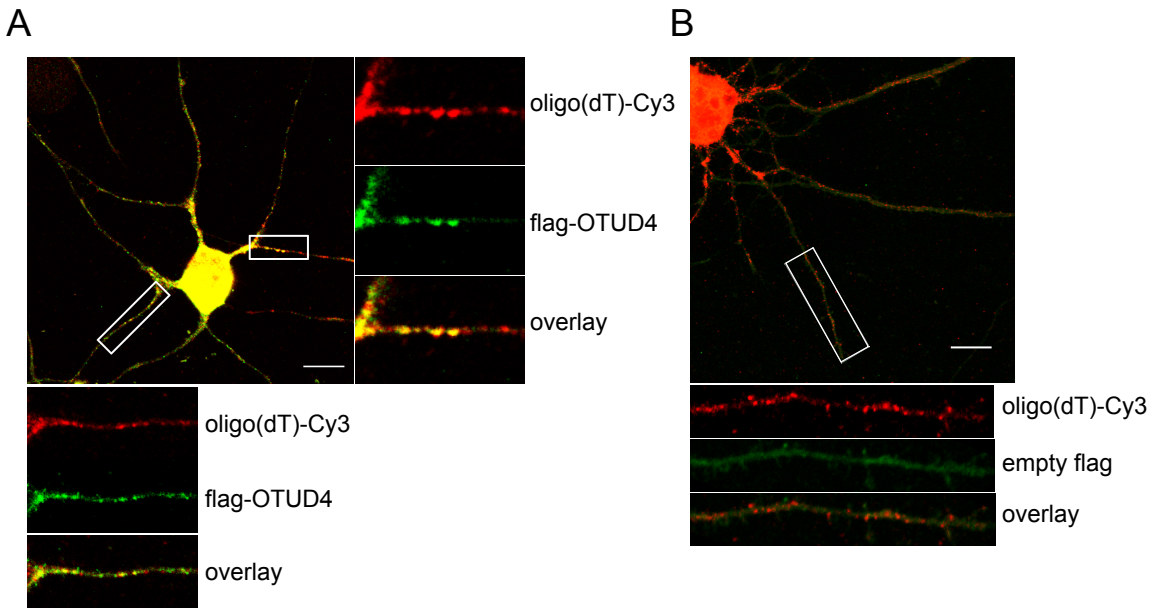

Figure 23: OTUD4-positive granules contain mRNA in neurons

(A) DIV4 hippocampal neurons were transfected with flag-OTUD4 and FISH was performed using Cy3-labelled Oligo(dT) (shown in red) to visualize endogenous mRNA. This was combined with immunostaining with α-flag antibody. Confocal images showed flag-OTUD4 granules stained positive for mRNA. The adjacent insets represent magnified and straightened dendritic regions shown as white boxes in the overlay image. Scale bar = 20 µm

(B) Confocal representative image of DIV4 hippocampal neuron transfected with empty flag vector. Combined FISH/ICC was performed as described in (A). Control vector showed weak and diffused staining pattern. Figure is modified from (Das et al., 2019). Scale bar = 10 µm

3.15 OTUD4-containing granules are trafficked along the neurites

As previously identified, OTUD4 interacted with a network of RNA-binding proteins which includes numerous proteins that have been reported to play a role in RNA-trafficking. Therefore, it can be hypothesized that as a constituent of transport granules, OTUD4 granules might exhibit a similar kind of mobile behavior while transporting mRNAs along axons and dendrites.

To track the dynamics of OTUD4-positive granules, time-lapse live-cell imaging was carried out. Rat hippocampal neurons were transfected with mOrange2-tagged OTUD4. The neurons were maintained in culture for 4 days *in vitro* at 37°C. For live cell imaging, OTUD4 was cloned into p-βactin-mOrange2-C1, under the chicken β-actin promoter to obtain a robust neuron-specific expression of OTUD4. Images were captured in intervals of 500 ms for up to 4 min (120 images/min). Time-lapse imaging of mOrange2-tagged OTUD4 in rat hippocampal neurons revealed OTUD4 granules of various sizes moving along the length of the axons. As a control, hippocampal neurons were transfected with the same amount of empty-mOrange2 vector. Contrary to the mOrange2-OTUD4 expressing neurons, which displayed granular, punctate structures in the neurites, empty-mOrange2 expressing neurons showed strong, homogenous fluorescent signal without any granular patterns (Figure 24A, D). Thus, the granular, punctate structures were specific to mOrange2-OTUD4 expression in neurons.

Furthermore, OTUD4 granules displayed different kinds of trafficking behavior along the processes: (a) large granules were stationary, or displayed slow, oscillatory movements (to and fro movements over short distances) without any net displacement, (b) smaller OTUD4 granules exhibited continuous, rapid movements in either retrograde or anterograde directions or bi-directionally. Some smaller granules were transported across long distances along the neurons (Figure 24A) as seen for other proteins such as SMN1 (Zhang et al., 2003). Analyzing n=30 neurons from three independent experiments, a majority of mOrange2-OTUD4 granules exhibited stationary behavior while a smaller fraction of granules displayed rapid, continuous movements. The behavior of OTUD4 granules was quantified based on their distance travelled (dx) over the duration of 4 min. I found that 35% of OTUD4-containing granules were stationary (dx < 1 µm) and 34% were oscillating (dx = 1-4 µm), while 30% of the granules travelled distances more than 4 µm in either direction (Figure 24C).

This is also illustrated by a kymograph (Figure 24B). Each vertical line represents one granule. The thick vertical lines in the kymograph represent the large, stationary or oscillating granules, whereas the thinner and fainter lines towards the left or right

represent the of the smaller OTUD4 granules with retrograde or anterograde movements, respectively. Hence, these experiments confirm that granules containing overexpressed OTUD4 are mobile in hippocampal neurons and are that OTUD4 is constituent of mRNP complexes actively transported in primary neurons.

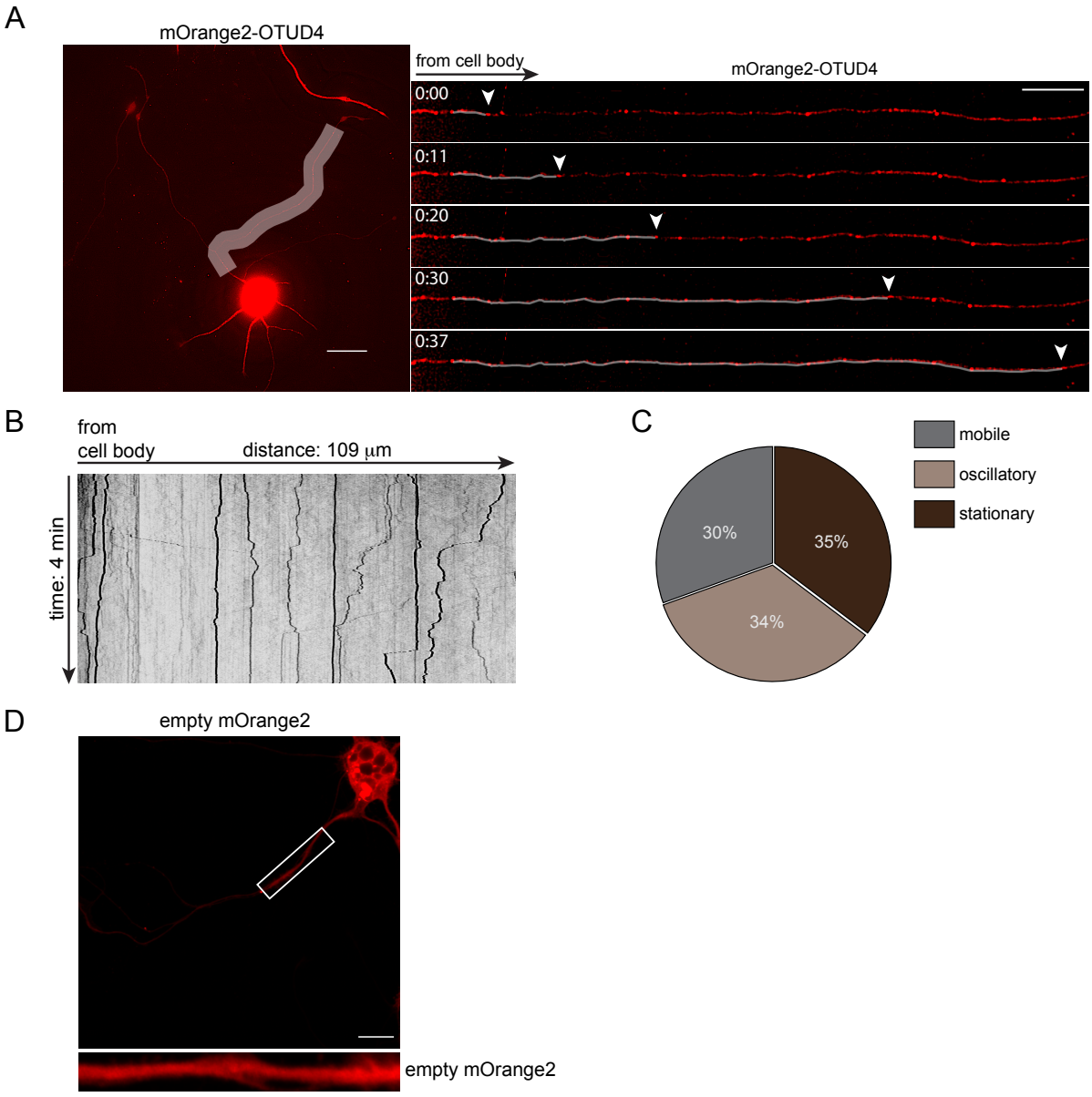

Figure 24: OTUD4 displays trafficking behavior along the neurites

(A) Representative image of primary rat hippocampal neuron (DIV4) expressing mOrange2-OTUD4 (in red) used for live cell imaging. The tracing shown as a diffused white segment represents 109 µm dendritic region corresponding to adjacent insets displaying time-lapse series. The region of interest was straightened for illustration. The white tracings shown in the

adjacent insets correspond to an anterograde movement of an OTUD4-granule in a time span of 37 s. The individual granule is indicated with white arrowheads. Scale bar = 20 µm
(B) Kymograph tracing mOrange2-OTUD4 granules in the selected dendritic region from (A). OTUD4 granules display dynamic movements during the entire length of the movie (4 min).
(C) Quantification of OTUD4-granules displaying stationary, oscillating or mobile movement behavior. The percentage of OTUD4-granules classified into three groups is visualized as a pie chart. The behavior of 367 granules was analyzed from a total of 13 neurons from three independent experiments. (D) Representative image of primary rat hippocampal neuron (DIV4) expressing empty mOrange2 vector was used as a negative control. Figure is modified from (Das et al., 2019). Scale bar = 10 µm

3.16 OTUD4 associates with SMN1 in transport granules in neurons

Survival motor neuron protein 1 (SMN1) has been demonstrated to associate with several RNA-binding proteins within mRNP complexes in neurons and plays a critical role in their assembly (Donlin-Asp et al., 2017; Fallini et al., 2014). OTUD4 has been shown to interact with SMN1 in an RNA-dependent manner using pull-down and co-immunoprecipitation experiments (Figure 9A). Therefore, to assess the behavior of OTUD4 and SMN1 in cultured neurons, primary hippocampal neurons were co-transfected with mOrange2-OTUD4 and neonGreen-SMN1 and live cell imaging was performed at DIV4. n=30 neurons from three independent experiments were imaged. Interestingly, we found that a large subset of mOrange2-OTUD4 granules showed strong co-localization with neonGreen-SMN1 within granular structures along the length of axons and dendrites in neurons (Figure 25A). All the images were deconvolved to reduce the blurred signal due to background noise, hence avoiding false co-localization signal.
Further, we investigated if OTUD4 and SMN1 are transported as parts of the same granule. Tracking the movements of the granules, it was observed that the majority of the granules that contained both the proteins displayed a stationary behaviour, consistent with the movements displayed by association of SMN-HuD and SMN-Gemin2 in the neurons (Fallini et al., 2011; Zhang et al., 2006; Zhang et al., 2003). There was also a small fraction of granules, which displayed fast movements in both anterograde and retrograde directions. During the rapid movements, mOrange2-OTUD4 and neonGreen-SMN1 granules seemed to be separate granules, still travelling in very close proximity to one another with the same speed. And while pausing they merged again seemingly to be one granular structure. It is likely that sequential imaging of the individual channels might cause the apparent separation of granules while being transported (marked by white arrows in Figure 25A).

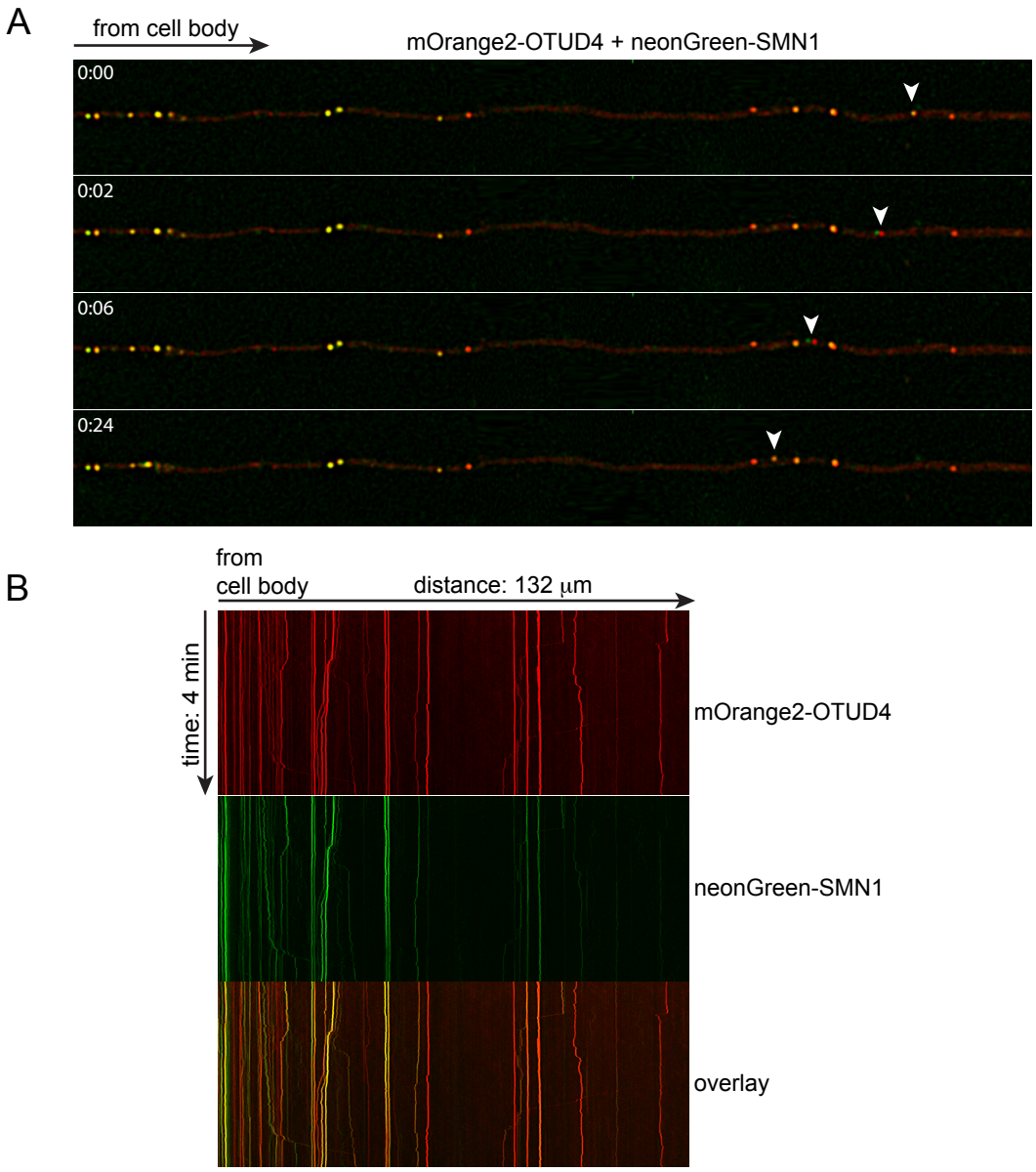

Figure 25: OTUD4 and SMN mostly reside in the same transport granules in neurons
(A) Rat hippocampal neurons (DIV4) were transfected with mOrange2-OTUD4 and neonGreen-SMN1 for live cell imaging. Shown are representative time-lapse series of a 132 µm dendritic region of a neuron expressing tagged OTUD4 and SMN1. The yellow granules represent co-localization of OTUD4 and SMN1 in the same granules. The white arrowhead indicates the association of OTUD4 and SMN1 granule while trafficking together in a retrograde direction over a time span of 24 s. (B) Kymograph representation of the OTUD4 and SMN granules in the selected dendritic region from (A). The overlay kymograph displays yellow lines indicating most of the granules contain both OTUD4 and SMN1. The graphs are displayed for the entire duration of the movie (4 min). Figure is modified from (Das et al., 2019).

As illustrated in the kymograph, major fraction of SMN1 granules associated with OTUD4-containing granules in the neurons. These are depicted as yellow lines in the overlay kymograph (Figure 25B).
Hence, these observations indicate that OTUD4 associates with SMN1 in the mobile neuronal RNA granules. It might play a role in the transport and translation of mRNAs contributing together with RNA-binding proteins such as FMRP and SMN1, which has to be investigated in detail.

3.17 OTUD4 is not a constituent of Processing bodies (P-bodies)

P-bodies are another set of cytoplasmic, non-membranous mRNP complexes, which have been studied as sites of mRNA degradation. Although SGs and P-bodies are distinctly regulated, both are dynamically linked to each other. Spatially, P-bodies are found closely juxtaposed to SGs in cells. There have been several reports describing the exchange of constituents between SGs and P-bodies influencing translation control and RNA metabolism in cells (Kedersha et al., 2005). Although there are proteins, which are exclusively associated with SGs or P-bodies, certain proteins such as eIF4E, HuR, YB1 or AGO2 are residents of both kinds of granular structures (Ivanov et al., 2019). Therefore, to investigate if OTUD4 is exclusively restricted to SGs or might also be present in P-bodies, Hela cells were stained with antibody against decapping enzyme 1a (Dcp1a), a marker protein of P-bodies. Confocal images revealed Dcp1a-positive P-bodies were present constitutively as discrete spots in unstressed Hela cells, in agreement with previous studies (Kedersha et al., 2005) (Figure 26). Upon arsenite stress, SGs and P-bodies were both induced in treated cells with an increased number of P-bodies as compared to unstressed cells. Clearly, OTUD4 was recruited to SGs; with DCP1a-positive P-bodies found juxtaposed next to OTUD4-positive SGs. As indicated in Figure 26, arsenite-treated Hela cells exhibited numerous P-bodies many of which could be found lying adjacent to OTUD4-positive SGs. No co-localization of OTUD4 was observed with P-bodies. Hence, OTUD4 is an exclusive constituent of SGs.

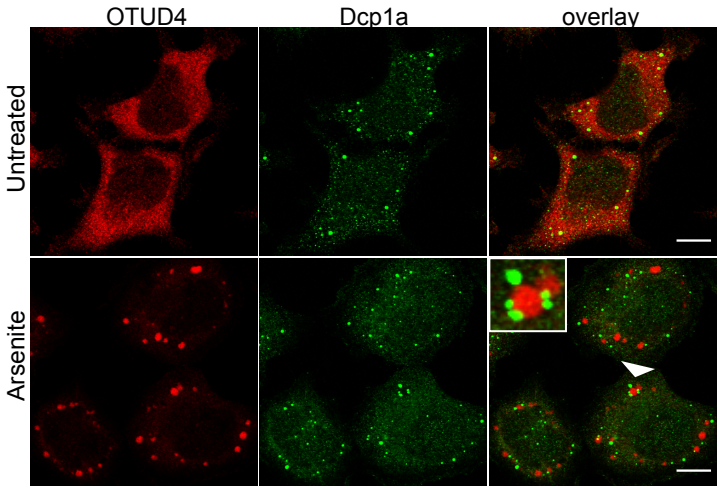

Figure 26: OTUD4 does not localize to P-bodies
Hela cells were untreated or treated with arsenite (0.5 mM, 30 min). Cells were fixed and immunostained with α-OTUD4 and α-Dcp1a (P-body marker) and analyzed by confocal microscopy. Immunofluorescence images shown here indicate OTUD4-positive granules do not associate with P-bodies. The inset shows the granule indicated by the white arrowhead in higher magnification. Scale bar = 10 µm

3.18 OTUD4 interacts with RNA and binds to its own mRNA

The RNA transport granules present physiologically in neurons and stress granules accumulated under stressful stimulus are formed as a result of the interplay between diverse RNA-binding proteins and multiple mRNA transcripts. There are several examples of RBPs, which have been largely known to bind specific RNA transcripts that are constituents of these mRNPs. For example, Imp1 is known to bind the 3' UTR region of ß-actin mRNA forming IMP1-ß-actin mRNP complexes (Donlin-Asp et al., 2017; Farina et al., 2003).
Recently published articles have identified OTUD4 in mRNA-interactome studies (Baltz et al., 2012; Beckmann et al., 2015). From the aforementioned results, it has been shown that OTUD4 interacts with RBPs in an RNA-dependent manner (Figure 9). These observations along with the categorization of OTUD4 as intrinsically disordered, prompted us to validate the RNA-binding ability of OTUD4. To test this, RNA-immunoprecipitation assay (RNA-IP) was performed. For this purpose, HEK293T cells were transfected with flag-OTUD4. The transfected cells were subsequently UV cross-linked to freeze the proteins in extremely close proximity to the mRNAs for efficient capture of protein-mRNA complexes. Then OTUD4-flag IP was performed using specific

monoclonal anti-flag antibody. The immunoprecipitated OTUD4-RNA complex was subjected to phenol/chloroform RNA extraction to isolate the bound RNA transcripts. The integrity and the concentration of the precipitated RNA was assessed by using the RNA Integrity Number (RIN) on TapeStation instrument. As a negative control, HEK293T cells transfected with pCMV flag vector was used. Analyzing the immunopurified RNA concentration showed approximately 5-fold enrichment of RNA transcripts with flag-OTUD4 as compared to RNA bound to control (Figure 27A). Therefore, the above result indicates an overall RNA enrichment with OTUD4 immunoprecipitate suggesting OTUD4 might putatively bind to RNA transcripts.

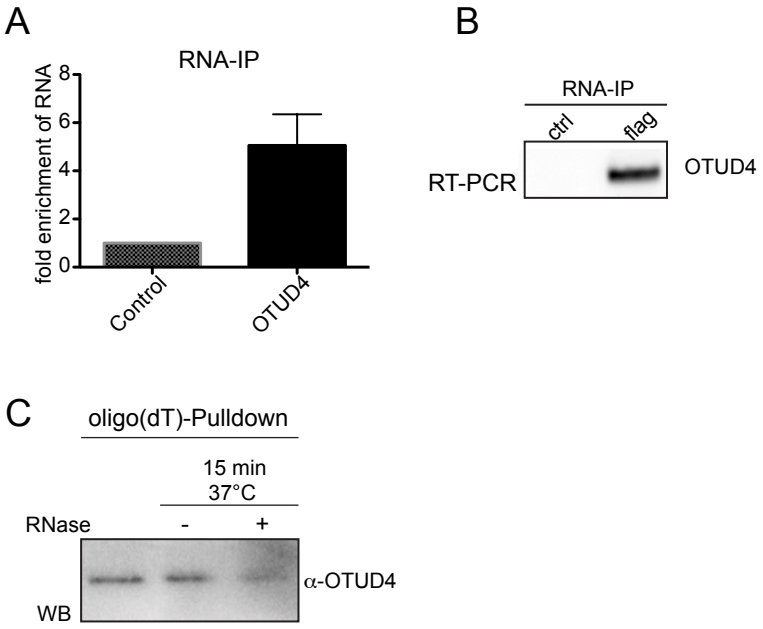

Figure 27: OTUD4 binds to RNA
(A) RNA-protein immunoprecipitation assay shows 5-fold enrichment of RNA immunoprecipitated with OTUD4-flag from HEK293T cells as compared to control vector. Shown is the SEM from n=6 experiments.
(B) RT-PCR experiments shown here indicate OTUD4 binds to OTUD4 mRNA. RNA-protein immunoprecipitation assay was performed from flag-OTUD4 or empty vector (control) transfected HEK293T cells using stringent buffer conditions. RNA was isolated using anti flag-beads and an equal volume of RNA was used for RT-PCR reactions.
(C) Oligo(dT) pulldown experiment performed with HEK293T lysates showed OTUD4 protein co-purified with poly(A)-RNA as visualized by α-OTUD4 western blot. RNase treatment (50 µg/ml) at 37°C reduced the amount of OTUD4 bound to the oligo(dT)-beads. This result is representative of n=4 independent experiments. Figure is modified from (Das et al., 2019).

RNA-binding proteins such as FMRP are known to bind their own mRNA, thus we speculated that OTUD4 binds to its own mRNA too (Schaeffer et al., 2001). In order to investigate this, Reverse-Transcription (RT)-PCR was performed. The extracted RNA from the RNA-IP experiments was subjected to cDNA synthesis using gene-specific primers for the 3'UTR of OTUD4 mRNA. Clearly, OTUD4 interacted with its own mRNA, as enrichment of OTUD4 product was observed in flag-OTUD4 immunoprecipitate as compared to negative control. As a negative control, immunoprecipitation was performed from cells transfected with pCMV flag vector only (Figure 27B).

In a parallel attempt to identify OTUD4 as an RNA-binding protein, oligo(dT)-pulldown experiment was performed by Dr. Lukas Schwintzer. For this purpose, HEK293T cells were subjected to covalent UV crosslinking. The endogenous mRNA-protein complexes were captured from the cell lysates by incubation with oligo(dT)-coated beads, which binds to the poly(A)-RNA in the extracts. This was followed by extensive washing to eliminate the non-specific binding to poly(A) RNA. The captured isolates were subjected to western blot analysis for the assessment of OTUD4 association with mRNA. Detection of the western blot with OTUD4 specific antibody revealed that OTUD4 protein was pulled down with mRNA in HEK293T cells. As a control, RNA-protein complexes immobilized to oligo(dT) beads were treated with RNase, which led to a reduction in the OTUD4 signal (Figure 27C). Hence, this result confirms the association of endogenous OTUD4 with mRNA extracted from cells.

3.19 Loss of OTUD4 causes increased apoptosis but does not affect the stability of SG-resident proteins

Next, I wanted to determine the mechanism by which OTUD4 regulates SG formation. It was speculated that OTUD4 might regulate the abundance of SG-core proteins such as G3BP1 and TIAR. To test this hypothesis, OTUD4 was depleted in Hela cells by siRNA knockdown and protein expression levels were analyzed by western blot. Notably, the basal expression levels of the two SG core proteins were not reduced upon loss of OTUD4, even though the SG formation was impaired (Figure 28A). Rather, there was a slight increase in the G3BP1 protein levels in OTUD4 deficient cells. A Similar effect was observed under arsenite-treated conditions.

Interestingly, depletion of OTUD4 in Hela cells after 48 h of knockdown showed reduced cell viability. Hence, cell lysates were checked for markers of apoptosis.

Western blot analysis showed an increase in the activation of caspase-3 and increased levels of cleaved PARP (a cellular substrate of caspase) in OTUD4-deficient cells as compared to control cells (Figure 28A). However, under oxidative stress conditions, OTUD4-deficient Hela cells did not show any additional sensitivity to apoptosis. Hence, loss of OTUD4 causes apoptotic cell death under basal conditions.

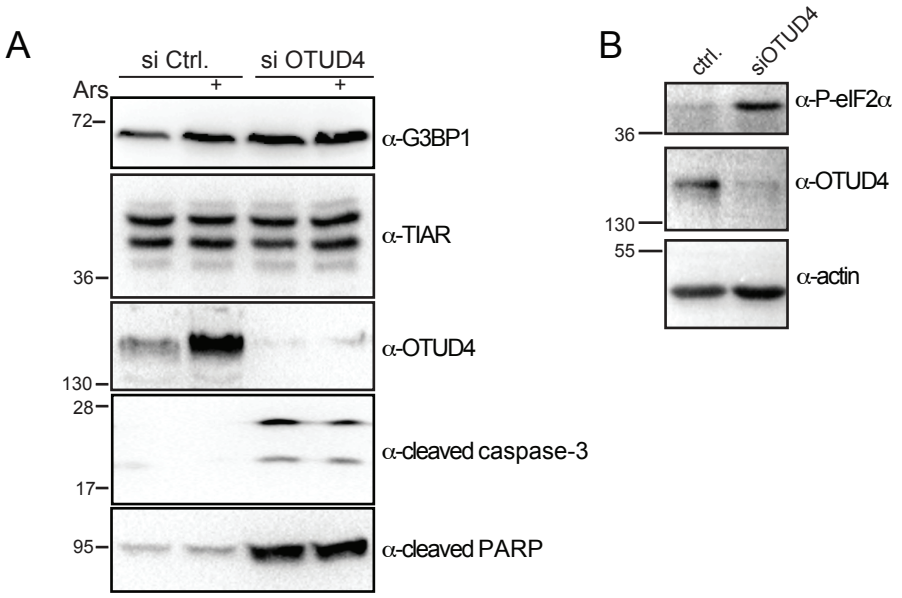

Figure 28: Analysis of protein levels of SG-marker proteins and apoptotic markers upon loss of OTUD4
Hela cells transfected with siControl or siRNA against OTUD4 were left untreated or treated with arsenite (0.5 mM, 30 min). Lysates were analyzed by immunoblotting using antibodies against SG-proteins G3BP1 and TIAR and apoptotic markers as indicated (A). Increased phosphorylated eIF2α level upon loss of OTUD4 is indicated in (B). Actin is shown as a loading control. Figure is modified from (Das et al., 2019).

In stressed cells, protein synthesis is shut down by the induction of phosphorylation of eIF2α by a family of stress activated-kinases that constitute the integrated stress response (ISR) (Holcik & Sonenberg, 2005). Phosphorylation of eIF2α at serine 51 blocks translation initiation by inhibiting the formation of ternary preinitiation complexes, which subsequently initiates SG formation (Jackson et al., 2010; Wek, 2018). To test whether OTUD4 depletion influences eIF2α phosphorylation, cell extracts from control and OTUD4-depleted cells were immunoblotted using phospho-

specific eIF2α antibody. As shown in Figure 28B, OTUD4-deficient cells exhibited an increase in phopho-eIF2α levels. Even a small amount of eIF2α phosphorylation inhibits the activity of guanine nucleotide exchange factor eIF2B, consequently depleting ternary complex that inhibits translation and initiates SG formation (Jackson et al., 2010; Wek, 2018). Increase in phosphorylation of eIF2α in the absence of OTUD4 indicates a role of OTUD4 in protein synthesis. Thus, absence of OTUD4 might cause stress-mediated translational repression by triggering phosphorylation of eIF2α.

4 Discussion

In the recent years, OTUD4 has been implicated in a variety of functions such as DNA damage response serving as a scaffold for two other DUBs namely USP7 and USP9X (Zhao et al., 2015), regulating innate immune signaling by controlling K63-linked deubiquitination of Myd88 (Zhao et al., 2018) and also in antiviral innate immune response (Liuyu et al., 2019). In our study, we have undertaken an approach to identify the function of OTUD4 in a neuronal context. Our study reveals OTUD4 as an RNA-binding protein. We show its association with higher order ribonucleoprotein assemblies. Importantly, we discovered previously unknown roles of OTUD4 in the regulation of stress granule formation and in cellular stress response. Identification of OTUD4 in neuronal RNA granules suggests the potential involvement of OTUD4 in mRNA transport and local translation regulation.

4.1 Interactome analysis reveals OTUD4 exists in a network with RNA-binding proteins

Here, we have employed an unbiased approach to identify the interactome of OTUD4 in the cortex and cerebellum of an adult mouse brain. The affected siblings bearing homozygous mutations in OTUD4 deubiquitinase and RNF216 E3 ligase showed a neuronal loss in the hippocampus and cerebellar Purkinje cells (Margolin et al., 2013). Also, OTUD4 has been shown to play a critical role in the structural integrity and organization of the cerebellum in zebrafish embryos (Margolin et al., 2013; Tse et al., 2013). These findings suggest crucial roles of OTUD4 in the nervous system, which so far have remained unaddressed.

To answer this, we performed a two-step strategy: affinity purification of HA-tagged OTUD4 from HEK293T cells followed by pull down from mouse brain lysates. The associated proteins were identified using mass spectrometry as described before. Due to the lack of a specific antibody against rodents, endogenous OTUD4 affinity purification was not possible to perform. Hence, we used HA-tagged OTUD4 as bait against the brain extracts. This approach gave us a certain advantage that purification of tagged OTUD4 from HEK293T cells would still preserve the folding and post-

translational modifications of OTUD4 similar to native environment. A recent study identified that the phosphorylation state of OTUD4, critically required for its K63-linked DUB activity, is intact only when it is purified from HEK293 cells and not from *E.coli* (Zhao et al., 2018).

It was surprising to find a large number of RNA-binding proteins in the interactome analysis of OTUD4 deubiquitinase as there has been no previous connection reported between OTUD4 and RNA. In the screen, many of the OTUD4-interacting proteins formed higher order membraneless granules namely RNA transport granules and stress granules. RNA binding proteins possessing low complexity domains (LCDs) have been quite thoroughly investigated to undergo phase separation behavior *in vitro*, a phenomenon responsible for driving the formation of stress granules (Kato et al., 2012; Lin et al., 2015). Therefore, it is not surprising that a larger fraction of proteins in the list of OTUD4 identified interactors possess LCDs.

My data provides a systematic identification of binding partners of OTUD4 in the nervous system. Recently, two separate studies have identified the OTUD4 interactome from HEK293 cells (Sowa et al., 2009; Zhao et al., 2018).
Cross-comparison of my data set with the previously identified interactomes in HEK293 cells reveals about 20% overlap between the data sets. Most of the overlapping proteins between both cell types are well-known RBPs. Notably, RBPs which have been verified in our biochemical interactions in HEK293T cells (TIAR, G3BP1, HuB, IGF2BP3) also appeared in these previous interactomes, which confirms our result. Together, this suggests that OTUD4 exists within the interconnected network of RNA-binding proteins in steady state conditions.

4.2 OTUD4 is a component of stress granules

Upon diverse stresses, SGs are readily assembled due to protein translation inhibition, accumulating RNA-protein condensates. As soon as the stress subsides, SGs are disassembled and the translation is resumed again (Anderson & Kedersha, 2008; Protter & Parker, 2016). Purification of SGs has revealed that more than 80% of SGs is composed of mRNAs. In this study, I have thoroughly characterized OTUD4 as a novel component of stress granules. SA-induced OTUD4-positive cytoplasmic foci are canonical SGs in their composition and behavior. First, OTUD4 interacts with core SG assembly components such as TIAR and G3BP1 *in vitro* and localizes to SGs in cells upon stressful stimulus. Second, OTUD4-positive granules contain endogenous poly(A)

mRNA, indicating mRNAs as constituents of these assemblies. Third, 60 min after stress removal, complete disassembly of OTUD4-positive granules was observed demonstrating SG-like dynamic behavior (data not shown here).

SGs display certain levels of heterogeneity in their composition upon different stresses and cell-types. For instance, in a recent screen conducted by Markmiller and colleagues, SG component EIF3A was exclusively identified in Hela cells but absent in neural progenitor cells (Markmiller et al., 2018). Upon exposure to different stress stimuli, HSP27 is exclusively present in heat-induced SGs (Kedersha et al., 1999). Similarly, ZFAND1 is present only in arsenite-induced SGs and excluded in granules induced by heat stress (Turakhiya et al., 2018). Therefore, I investigated the presence of OTUD4 in SGs in response to diverse stresses such as oxidative stress, heat shock and proteasome inhibition (MG132) in both neuronal and non-neuronal cells of human and mouse origin. Altogether, my data conclude OTUD4 as a *bona fide* component of SGs across different cell types and stress conditions.

During the course of our investigation, two groups in separate studies, employed quantitative proteomics to reveal the SG proteome. They identified OTUD4 present in the interaction network of SG proteins (Markmiller et al., 2018; Youn et al., 2018). Interestingly, both the studies recovered OTUD4 as SG-associated protein in the absence of exogenous stress. Same holds true for our interactome analysis from the wild-type mouse brain. Many SG-associated proteins were recovered as interactors of OTUD4 under non-stress conditions. This supports our finding that OTUD4 exists in a tightly connected network of SG proteins in steady state, which condenses as granules upon stressful insults.

4.3 OTUD4 is required for correct stress granule formation

My results demonstrate that loss of OTUD4 interferes with SG formation during oxidative and heat stress. This phenotype was observed for both TIAR and G3BP1-positive SGs. In fact, I observed all the G3BP1-positive foci co-localized with TIAR signal in contrast to the observation made by Tourriere et al that SGs containing G3BP lack TIA-1 (Tourriere et al., 2003). During SG formation, first, the dense 'core' is formed followed by the assembly of secondary 'shell' composed of loosely connected proteins (Jain et al., 2016; Wheeler et al., 2016). Time course analysis of SG formation showed that in the absence of OTUD4, SGs remained small and fragmented. This suggests the secondary aggregation of SGs is impaired in the absence of OTUD4 expression. These

observed changes in SG formation could be rescued by expression of siRNA-resistant OTUD4.

We employed two different approaches to characterize SGs in the absence of OTUD4: (1) the CRISPR-Cas9 generated OTUD4 knockout clones which showed inconsistent phenotypes (2) RNAi mediated knockdown of OTUD4 expression which led to smaller and fragmented SG appearance. Clearly, both approaches resulted in distinct responses to SG formation in the absence of OTUD4. This discrepancy could be explained as follows:

Although the knockout clones are OTUD4-deficient as confirmed by sequencing and western blot, this does not rule out potential off-target genomic modifications by the CRISPR/Cas9 technology, one of the primary concerns regarding this kind of genome editing technique. Additionally, since the OTUD4 knockout cells are a stable population selected by puromycin over a period of time and puromycin itself being an SG inducer due to its interference with translation (Kedersha et al., 2000), there is a possibility that these isogenic cell lines have developed compensation mechanisms by gene products that serve similar function as OTUD4. This might prevent us to see an immediate phenotype during the assembly of SGs in the KO clones no. 1-3. Hence, due to the above-mentioned factors, the different OTUD4-deficient clonal lines might exhibit conflicting and inconclusive results.

On the other hand, RNAi leads to acute depletion of OTUD4. Knockdown of OTUD4 during oxidative or heat stress led to characteristic changes in stress granule appearance, e.g. granules are smaller in size but more numerous. Incomplete knockdown of OTUD4 might hide the true extent of effect observed in SG formation. The observed SG phenotype was observed with several siRNA oligonucleotides to exclude that these could be an off-target effect.

Interestingly, cells depleted for other identified core SG proteins such as G3BP1, SMN, TDP-43 and Ataxin2 also displayed similar phenotypes (Aulas et al., 2015; Aulas et al., 2012; Nonhoff et al., 2007; Zou et al., 2011). Even lack of valosin-containing protein (VCP) mediating the autophagic clearance of SGs similarly impairs the formation and morphology of SGs (Seguin et al., 2014). Reducing levels of key SG-associated proteins critically impacts the granule formation. Many of these proteins provide a scaffold to hold the architecture of SGs together. For instance, RNA-binding proteins TDP-43 and YB-1 bind and stimulate translation of G3BP1 mRNA, thus critically influencing SG formation and dynamics (McDonald et al., 2011; Somasekharan et al., 2015). However, our results showed that knockdown of OTUD4 did not alter the protein levels of key SG-proteins, G3BP1 and TIAR1. Additionally, the levels of other RNA-binding proteins

FMRP and SMN1 also remained unaffected (data not shown). Future investigations will have to address the reason behind impaired SG assembly upon loss of OTUD4.

4.4 Loss of OTUD4 hyper-sensitizes cells in response to oxidative stress

Formation of SGs can be seen as a cellular defense mechanism to adapt to stressful conditions. Prior studies have established that impaired SG formation has detrimental effects on cell survival by inducing apoptosis (Arimoto et al., 2008; Eisinger-Mathason et al., 2008; Kwon et al., 2007).
Our findings show that under basal conditions, loss of OTUD4 in HEK293T and Hela cells triggers apoptotic cell death. There was no additional increase in sensitivity of OTUD4-depleted Hela cells upon stress induction. However, additional experiments performed in the lab revealed that lack of OTUD4 in SH-SY5Y cells led to stronger activation of apoptotic markers PARP and caspase-3 post-oxidative stress compared to unstressed conditions (data not shown). Thus, loss of OTUD4 rendered these cells more sensitive to stress, suggesting that the sensitivity of OTUD4-deficient cells might be regulated in a cell-type specific manner. Taken together, OTUD4 might exert its protective effects against oxidative stress by facilitating proper SG assembly. Additionally, OTUD4 affects cell viability under basal conditions.

Liuyu and colleagues demonstrated that loss of OTUD4 compromised a virus-triggered signaling pathway, thus underscoring the importance of OTUD4 in cellular stress response (Liuyu et al., 2019). OTUD4 levels were upregulated upon viral infection to promote virus-triggered signaling in human cell lines (Liuyu et al., 2019). Although we occasionally observed increased protein levels of OTUD4 upon arsenite exposure, it is still unclear whether OTUD4 levels are regulated upon oxidative stress.

4.5 Does OTUD4 have an ubiquitin-dependent role in SGs?

Several post-translational modifications of SG-associated proteins have been reported that regulate the assembly of SGs. For instance, phosphorylation of G3BP1 reduced its ability to nucleate SG (Kedersha et al., 2016; Tourriere et al., 2003). Also, O-Glc-Nac glycosylation of ribosomal proteins contributes to SG assembly (Ohn et al., 2008). Other post-translational modifications such as acetylation and neddylation are also involved in regulating SG formation (Jayabalan et al., 2016; Kwon et al., 2007). Although Tudor domains and methylation of arginine residues have been shown to be

necessary and sufficient for SG recruitment under certain conditions (De Leeuw et al., 2007; Goulet et al., 2008), I could not identify a role of OTUD4's Tudor domain in this context.
Presence of ubiquitin and polyubiquitinated proteins in SGs has been clearly demonstrated by several studies so far (Kwon et al., 2007; Mateju et al., 2017; Seguin et al., 2014; Turakhiya et al., 2018). Despite these findings, there is no evidence addressing the role of ubiquitination in regulating SG dynamics. Until recently, a study concluded that acute inhibition of ubiquitination has no impact on arsenite-induced SG dynamics (Markmiller et al., 2019).

An obvious question arising from these findings is, whether OTUD4 influences granule formation through its catalytic activity. When DUBs remove ubiquitin chains from other proteins, they can alter protein stability, protein localization or the function of their substrates (Clague et al., 2013; Reyes-Turcu et al., 2009). I found that catalytically inactive mutant OTUD4 did not alter its localization to SGs. It also restored normal granule formation upon knockdown of OTUD4. However, this does not exclude the possibility that OTUD4 might deubiquitinate one or several components of SGs, with implications on the function of these individual proteins or for the whole process of stress granule formation. Several other DUBs are part of stress granules, including USP10 (Kedersha et al., 2016; Takahashi et al., 2013), its yeast homolog Ubp3 (Nostramo et al., 2016), USP5 and USP13 (Xie et al., 2018). So far, no stress granule-specific substrate proteins of these DUBs have been identified and diverging results exist for the requirement of catalytic activity for the assembly or disassembly of granules (Nostramo & Herman, 2016; Xie et al., 2018). Preliminary experiments show an increase in the polyubiquitin levels in SGs upon OTUD4 knockdown (data not shown).
It will be interesting to identify ubiquitinated proteins in SGs and to further assess whether OTUD4 possess specific substrates in SGs or whether it exerts only ubiquitin-independent roles in this context.
Of note, a role for the 26S proteasome in the clearance of SGs following acute stress (Turakhiya et al., 2018) and evidence of the presence of several DUBs, including OTUD4 in SGs hint towards ubiquitin-dependent events occurring in SGs.

4.6 OTUD4 is a component of neuronal RNA transport granules

My data establish OTUD4 as a component of RNA transport granules in neurons. Its punctate pattern along the dendrites is similar to that of other RBPs such as Staufen

and Pumilio2, which are known to be a part of RNA transport and local translation (Kohrmann et al., 1999; Vessey et al., 2006). Usually, these granules in neurons are highly dynamic and this provides them the ability to deliver mature mRNA transcripts to distal dendrites for local translation (Krichevsky & Kosik, 2001). For instance, RNA-binding protein TDP-43 associates with Nefl mRNA promoting its anterograde transport along the dendrites (Alami et al., 2014). OTUD4 granules displayed both stationary and directed movements along the neurites and contained mRNA. This hints towards OTUD4's association with mRNA transcripts for their transport.

These results were obtained with several overexpression constructs due to the lack of specific antibody for staining in rodent cells. The finding that OTUD4 granules actively move along the neurites underlines that these are functionally active entities and not mere aggregates due to OTUD4 overexpression. In a previous report, overexpression of RNA-binding protein Pumilio2 in neurons induced the formation of TIA-1 positive SGs (Vessey et al., 2006). In my experiments, OTUD4-containing granules in neurons did not stain positive for TIAR, thus concluding that these are not SGs induced upon overexpression of OTUD4 in neurons. Of note, SGs (for example induced by SA treatment) in primary neurons usually locate to the cell body.
Motor proteins usually drive the directed movements of these granules along microtubules in neurons (Bramham & Wells, 2007; Kiebler & Bassell, 2006). In fact, microtubule-dependent localization of FMRP-containing granules has been demonstrated by several studies (Antar et al., 2005; Ling et al., 2004). OTUD4-positive granules displayed anterograde and retrograde movements along dendritic arbors. It will be interesting to test the requirement of these components for OTUD4-granule mobility.

OTUD4 shows an RNA-dependent interaction with SMN1 and co-localizes with this protein in transport granules. Previous studies have shown that proteins such as HuD and Gemin2 co-transport with SMN1 as part of the same granule in motor neurons. Reduced protein levels of SMN1 impaired the recruitment of mRNAs and mRNA-binding proteins to the transport granules in axons (Akten et al., 2011; Fallini et al., 2011; Zhang et al., 2006). Also, SMN1 has been established as a chaperone promoting the mRNP assembly of IMP1 (ZBP1) protein and ß-actin mRNA (Donlin-Asp et al., 2017; Li et al., 2014). Given these facts, OTUD4 might be recruited to transport granules in an SMN1-dependent manner, which would require further investigation. Altogether, my work identifies for the first time the cellular localization of OTUD4 in

neurons and gives a completely new direction to the function of OTUD4 regarding protein synthesis and synaptic plasticity.

4.7 OTUD4 as an RNA-binding protein

The presence of OTUD4 in ribonucleoprotein complexes and its interaction with other RNA-binding proteins in an RNA-dependent manner suggests RNA-binding ability of OTUD4. This is further emphasized by the identification of OTUD4 in various mRNA-interactome studies (Baltz et al., 2012; Beckmann et al., 2015). By employing RNA-immunoprecipitation and Oligo(dT) pulldown, I and colleagues from our lab could successfully demonstrate that OTUD4 binds to mRNA transcripts. Typically, RNA-binding proteins consist of classical RNA-binding domains such as RRM, KH or zinc finger domain among others (Anantharaman et al., 2002). Over the last years, an increasing number of proteins has been reported to interact with RNA through their IDRs (Castello et al., 2016). Proteins such as FMRP are reported to selectively bind RNA targets through disordered sequences such as arginine-rich motifs (e.g. RGG/RS) (Jarvelin et al., 2016; Phan et al., 2011). Although, OTUD4 lacks a classical RNA-binding domain, we speculate that it might engage in RNA interactions through RGG/RS motifs present in its C-terminal intrinsically disordered region (aa 886-1114). In fact, many of these unconventional RBPs are classified as metabolic enzymes such as kinases and ubiquitin proteases among others (Castello et al., 2012; Mitchell et al., 2013).
During our investigation, we also undertook a pilot study to identify specific mRNA targets of OTUD4 by next-generation sequencing of enriched transcripts from our RNA-immunoprecipitation experiments. Although we obtained strong enrichment of transcripts with OTUD4 over the control sample, and some of the RNA targets were confirmed by RT-PCR, we could not find enrichment of specific binding motifs within the RNA sequences. Therefore, it can be speculated that OTUD4 non-selectively binds RNA sequences due to a lack of a classical RNA-binding domain. Binding of enzymes to RNA has also been reported to aid protein folding and contribute to its catalytic activity upon interaction with RNA (Basu & Bahadur, 2016; Casu et al., 2013; Choudhury et al., 2017). This would be an interesting possibility also for OTUD4.

4.8 Potential role of OTUD4 in translation regulation

RNA transport granules in neurons are transported to precise subcellular locations to facilitate synaptic growth and dendritic arborization by local protein synthesis (Wong et al., 2017; Yoon et al., 2016). Presence of ribosomes and translation initiation factors

in the RNA granules indicates their roles in local protein production at the synapse (Elvira et al., 2006; Krichevsky & Kosik, 2001). Dendritic transport of RNA-binding protein FMRP regulates the local translation of CamKII, MAP1b and PSD-95 transcripts in response to neuronal stimulation (Kao et al., 2010; Lu et al., 2004; Todd et al., 2003). Also, deficiency of SMN1 has been reported to disrupt local protein synthesis in motor neurons (Fallini et al., 2016). Therefore, it is tempting to speculate the contribution of OTUD4-containing granules to local protein synthesis, which is unclear at this point. This might depend on OTUD4's DUB activity, e.g. by tuning the levels of proteins that directly regulate translation in the granules. Intriguingly, the dendritic levels of FMRP, an interactor of OTUD4 and suppressor of translation during transport, can be regulated by ubiquitylation and proteasomal degradation upon metabotropic glutamate receptor stimulation (Hou et al., 2006; Nalavadi et al., 2012). Given these facts, the catalytic activity of OTUD4 could indeed play a role here.

Phosphorylation of eIF2α leads to a decrease in the global protein synthesis as a part of the integrated stress response to maintain cellular homeostasis (Pakos-Zebrucka et al., 2016). It blocks the translation initiation by inhibiting the formation of the preinitiation complex (Holcik & Sonenberg, 2005). Our study demonstrates that loss of OTUD4 is associated with reduced cell viability and enhanced levels of phosphorylated eIF2α. This might result in a stress-mediated inhibition of protein synthesis. A well-established 'SUnSET' assay monitors translation rate by using puromycin, which incorporates into nascent polypeptides by mimicking aminoacyl-tRNA. Thus, the rate of puromycin incorporation reflects the rate of protein synthesis (Schmidt et al., 2009). In fact, 'SUnSET' assay performed in the lab showed a reduced rate of mRNA translation in OTUD4-deficient Hela cells by monitoring the levels of puromycylated proteins (data not shown). This suggests an important connection of OTUD4 with translation regulation.
In line with a potential role of OTUD4 in translation regulation, we also found several eukaryotic translation initiation factors (eIF3, eIF4A, eIF4E, eIF4G) and ribosomal proteins in our interactome study (Table 19). Also, previous proteomic studies detected these proteins as potential OTUD4 interactors (Sowa et al., 2009; Zhao et al., 2018). Potential future work should further investigate the connection between OTUD4 and translation regulation.

4.9 RNA-binding proteins and their role in neurodegenerative disorders

Interestingly, my findings have established OTUD4 as a highly disordered protein. The IDR within 550-1114 residues of OTUD4, which is rich in RG/RGG/RS-motifs showed higher propensity to form spontaneous granules upon overexpression in cells. Proteins possessing intrinsically disordered regions are not only implicated in the formation of membraneless organelles such as SGs but also possess RNA binding ability (Castello et al., 2016; Jarvelin et al., 2016; Kato et al., 2012; Nott et al., 2015). These RBPs containing IDRs and prion-like domains can promote spontaneous self-aggregation by concentration-dependent oligomerization (Kato et al., 2012; Lin et al., 2015; Molliex et al., 2015).

Mutations in RBPs such as TDP-43 or FUS lead to ALS/FTD (Lagier-Tourenne et al., 2010; Vance et al., 2009), while mutations in Ataxin-2 can cause Spinocerebellar Ataxia type 2 or ALS (Elden et al., 2010; Gispert et al., 1993). To date, many disease-causing mutations reported are concentrated within the IDRs of these RBPs (Uversky et al., 2008; Vacic et al., 2012). Recent evidence has linked mutated RBPs such as TIA1, FUS, hnRNPA2/B1 and TDP-43 to impairment of SG dynamics and protein translation and eventually to the formation of aberrant aggregates (Kim et al., 2013; Mackenzie et al., 2017; Murakami et al., 2015; Vacic et al., 2012; Vance et al., 2009). Interestingly, a homozygous mutation in *OTUD4* gene in a familial form of Gordon Holmes syndrome, leading to hypogonadotropism, ataxia and dementia, also lies within IDR coding region of the gene (Margolin et al., 2013). Although our data showed that the disease mutant could rescue the SG phenotype in OTUD4 knockdown cells, it would be quite insightful to study the phase-transition behavior of disease mutant OTUD4 *in vitro*, as disruptions in liquid-liquid phase separation have been suggested to contribute to pathogenesis in the neurodegenerative diseases (Gitler & Shorter, 2011; Li et al., 2013). Also, it cannot be ruled out that OTUD4's disease-associated mutation could alter the kinetics of SGs, which needs to be thoroughly examined.

To further emphasize the importance of RBPs in neurodegenerative diseases, recent work has shown reduction of RBPs such as Ataxin-2 or TIA-1 inhibits SG assembly by size and number and considerably suppresses neuronal toxicity in disease models of ALS and tauopathies (Apicco et al., 2018; Kim et al., 2014). In fact, inhibition of SG assembly by therapeutic reduction of Ataxin-2 has been shown to suppress TDP-43 pathological aggregates in a disease mouse model (Becker et al., 2017). As an SG assembly regulator, it would be very exciting to address the effects of OTUD4 in diseased models in future studies.

In summary, this study gives important new insights into the function of OTUD4 and elucidates its requirement in cellular stress response. These results place OTUD4 within the large network of RNA-binding proteins and establish it as a non-canonical RNA-binding protein. This work provides a new platform of research regarding the role of OTUD4 in RNA granules and potential implications in translation regulation.

5 Bibliography

Aalto, A. L., Mohan, A. K., Schwintzer, L., Kupka, S., Kietz, C., Walczak, H., . . . Meinander, A. (2019). M1-linked ubiquitination by LUBEL is required for inflammatory responses to oral infection in Drosophila. *Cell Death Differ, 26*(5), 860-876. doi:10.1038/s41418-018-0164-x

Abdul Rehman, S. A., Kristariyanto, Y. A., Choi, S. Y., Nkosi, P. J., Weidlich, S., Labib, K., . . . Kulathu, Y. (2016). MINDY-1 Is a Member of an Evolutionarily Conserved and Structurally Distinct New Family of Deubiquitinating Enzymes. *Mol Cell, 63*(1), 146-155. doi:10.1016/j.molcel.2016.05.009

Adjibade, P., St-Sauveur, V. G., Quevillon Huberdeau, M., Fournier, M. J., Savard, A., Coudert, L., . . . Mazroui, R. (2015). Sorafenib, a multikinase inhibitor, induces formation of stress granules in hepatocarcinoma cells. *Oncotarget, 6*(41), 43927-43943. doi:10.18632/oncotarget.5980

Akten, B., Kye, M. J., Hao le, T., Wertz, M. H., Singh, S., Nie, D., . . . Sahin, M. (2011). Interaction of survival of motor neuron (SMN) and HuD proteins with mRNA cpg15 rescues motor neuron axonal deficits. *Proc Natl Acad Sci U S A, 108*(25), 10337-10342. doi:10.1073/pnas.1104928108

Alami, N. H., Smith, R. B., Carrasco, M. A., Williams, L. A., Winborn, C. S., Han, S. S. W., . . . Taylor, J. P. (2014). Axonal transport of TDP-43 mRNA granules is impaired by ALS-causing mutations. *Neuron, 81*(3), 536-543. doi:10.1016/j.neuron.2013.12.018

Alexander, E. J., Ghanbari Niaki, A., Zhang, T., Sarkar, J., Liu, Y., Nirujogi, R. S., . . . Wang, J. (2018). Ubiquilin 2 modulates ALS/FTD-linked FUS-RNA complex dynamics and stress granule formation. *Proc Natl Acad Sci U S A, 115*(49), E11485-e11494. doi:10.1073/pnas.1811997115

Anantharaman, V., Koonin, E. V., & Aravind, L. (2002). Comparative genomics and evolution of proteins involved in RNA metabolism. *Nucleic Acids Res, 30*(7), 1427-1464. doi:10.1093/nar/30.7.1427

Anderson, P., & Kedersha, N. (2006). RNA granules. *J Cell Biol, 172*(6), 803-808. doi:10.1083/jcb.200512082

Anderson, P., & Kedersha, N. (2008). Stress granules: the Tao of RNA triage. *Trends Biochem Sci, 33*(3), 141-150. doi:10.1016/j.tibs.2007.12.003

Anderson, P., Kedersha, N., & Ivanov, P. (2015). Stress granules, P-bodies and cancer. *Biochim Biophys Acta, 1849*(7), 861-870. doi:10.1016/j.bbagrm.2014.11.009

Antar, L. N., Dictenberg, J. B., Plociniak, M., Afroz, R., & Bassell, G. J. (2005). Localization of FMRP-associated mRNA granules and requirement of microtubules for activity-dependent trafficking in hippocampal neurons. *Genes Brain Behav, 4*(6), 350-359. doi:10.1111/j.1601-183X.2005.00128.x

Apicco, D. J., Ash, P. E. A., Maziuk, B., LeBlang, C., Medalla, M., Al Abdullatif, A., . . . Wolozin, B. (2018). Reducing the RNA binding protein TIA1 protects against tau-mediated

neurodegeneration in vivo. *Nat Neurosci, 21*(1), 72-80. doi:10.1038/s41593-017-0022-z

Arimoto, K., Fukuda, H., Imajoh-Ohmi, S., Saito, H., & Takekawa, M. (2008). Formation of stress granules inhibits apoptosis by suppressing stress-responsive MAPK pathways. *Nat Cell Biol, 10*(11), 1324-1332. doi:10.1038/ncb1791

Ascano, M., Hafner, M., Cekan, P., Gerstberger, S., & Tuschl, T. (2012). Identification of RNA-protein interaction networks using PAR-CLIP. *Wiley Interdiscip Rev RNA, 3*(2), 159-177. doi:10.1002/wrna.1103

Aulas, A., Caron, G., Gkogkas, C. G., Mohamed, N. V., Destroismaisons, L., Sonenberg, N., . . . Vande Velde, C. (2015). G3BP1 promotes stress-induced RNA granule interactions to preserve polyadenylated mRNA. *J Cell Biol, 209*(1), 73-84. doi:10.1083/jcb.201408092

Aulas, A., Fay, M. M., Lyons, S. M., Achorn, C. A., Kedersha, N., Anderson, P., & Ivanov, P. (2017). Stress-specific differences in assembly and composition of stress granules and related foci. *J Cell Sci, 130*(5), 927-937. doi:10.1242/jcs.199240

Aulas, A., Stabile, S., & Vande Velde, C. (2012). Endogenous TDP-43, but not FUS, contributes to stress granule assembly via G3BP. *Mol Neurodegener, 7*, 54. doi:10.1186/1750-1326-7-54

Bakthavachalu, B., Huelsmeier, J., Sudhakaran, I. P., Hillebrand, J., Singh, A., Petrauskas, A., . . . Ramaswami, M. (2018). RNP-Granule Assembly via Ataxin-2 Disordered Domains Is Required for Long-Term Memory and Neurodegeneration. *Neuron, 98*(4), 754-766 e754. doi:10.1016/j.neuron.2018.04.032

Baltz, A. G., Munschauer, M., Schwanhausser, B., Vasile, A., Murakawa, Y., Schueler, M., . . . Landthaler, M. (2012). The mRNA-bound proteome and its global occupancy profile on protein-coding transcripts. *Mol Cell, 46*(5), 674-690. doi:10.1016/j.molcel.2012.05.021

Banerjee, A., Ifrim, M. F., Valdez, A. N., Raj, N., & Bassell, G. J. (2018). Aberrant RNA translation in fragile X syndrome: From FMRP mechanisms to emerging therapeutic strategies. *Brain Res, 1693*(Pt A), 24-36. doi:10.1016/j.brainres.2018.04.008

Basu, S., & Bahadur, R. P. (2016). A structural perspective of RNA recognition by intrinsically disordered proteins. *Cell Mol Life Sci, 73*(21), 4075-4084. doi:10.1007/s00018-016-2283-1

Becker, L. A., Huang, B., Bieri, G., Ma, R., Knowles, D. A., Jafar-Nejad, P., . . . Gitler, A. D. (2017). Therapeutic reduction of ataxin-2 extends lifespan and reduces pathology in TDP-43 mice. *Nature, 544*(7650), 367-371. doi:10.1038/nature22038

Beckmann, B. M., Horos, R., Fischer, B., Castello, A., Eichelbaum, K., Alleaume, A. M., . . . Hentze, M. W. (2015). The RNA-binding proteomes from yeast to man harbour conserved enigmRBPs. *Nat Commun, 6*, 10127. doi:10.1038/ncomms10127

Bradford, M. M. (1976). A rapid and sensitive method for the quantitation of microgram quantities of protein utilizing the principle of protein-dye binding. *Anal Biochem, 72*, 248-254. doi:10.1006/abio.1976.9999

Bramham, C. R., & Wells, D. G. (2007). Dendritic mRNA: transport, translation and function. *Nat Rev Neurosci, 8*(10), 776-789. doi:10.1038/nrn2150

Brangwynne, C. P. (2013). Phase transitions and size scaling of membrane-less organelles. *The Journal of Cell Biology, 203*(6), 875-881. doi:10.1083/jcb.201308087

Brown, V., Jin, P., Ceman, S., Darnell, J. C., O'Donnell, W. T., Tenenbaum, S. A., . . . Warren, S. T. (2001). Microarray identification of FMRP-associated brain mRNAs and altered mRNA translational profiles in fragile X syndrome. *Cell, 107*(4), 477-487.

Buchan, J. R. (2014). mRNP granules. Assembly, function, and connections with disease. *RNA Biol, 11*(8), 1019-1030. doi:10.4161/15476286.2014.972208

Buchan, J. R., Kolaitis, R. M., Taylor, J. P., & Parker, R. (2013). Eukaryotic stress granules are cleared by autophagy and Cdc48/VCP function. *Cell, 153*(7), 1461-1474. doi:10.1016/j.cell.2013.05.037

Buchan, J. R., & Parker, R. (2009). Eukaryotic stress granules: the ins and outs of translation. *Mol Cell, 36*(6), 932-941. doi:10.1016/j.molcel.2009.11.020

Buchan, J. R., Yoon, J. H., & Parker, R. (2011). Stress-specific composition, assembly and kinetics of stress granules in Saccharomyces cerevisiae. *J Cell Sci, 124*(Pt 2), 228-239. doi:10.1242/jcs.078444

Cajigas, I. J., Tushev, G., Will, T. J., tom Dieck, S., Fuerst, N., & Schuman, E. M. (2012). The local transcriptome in the synaptic neuropil revealed by deep sequencing and high-resolution imaging. *Neuron, 74*(3), 453-466. doi:10.1016/j.neuron.2012.02.036

Carpenter, A. E., Jones, T. R., Lamprecht, M. R., Clarke, C., Kang, I. H., Friman, O., . . . Sabatini, D. M. (2006). CellProfiler: image analysis software for identifying and quantifying cell phenotypes. *Genome Biol, 7*(10), R100. doi:10.1186/gb-2006-7-10-r100

Castello, A., Fischer, B., Eichelbaum, K., Horos, R., Beckmann, B. M., Strein, C., . . . Hentze, M. W. (2012). Insights into RNA biology from an atlas of mammalian mRNA-binding proteins. *Cell, 149*(6), 1393-1406. doi:10.1016/j.cell.2012.04.031

Castello, A., Fischer, B., Frese, C. K., Horos, R., Alleaume, A. M., Foehr, S., . . . Hentze, M. W. (2016). Comprehensive Identification of RNA-Binding Domains in Human Cells. *Mol Cell, 63*(4), 696-710. doi:10.1016/j.molcel.2016.06.029

Casu, F., Duggan, B. M., & Hennig, M. (2013). The arginine-rich RNA-binding motif of HIV-1 Rev is intrinsically disordered and folds upon RRE binding. *Biophys J, 105*(4), 1004-1017. doi:10.1016/j.bpj.2013.07.022

Chau, V., Tobias, J. W., Bachmair, A., Marriott, D., Ecker, D. J., Gonda, D. K., & Varshavsky, A. (1989). A multiubiquitin chain is confined to specific lysine in a targeted short-lived protein. *Science, 243*(4898), 1576-1583. doi:10.1126/science.2538923

Chen, C., & Okayama, H. (1987). High-efficiency transformation of mammalian cells by plasmid DNA. *Mol Cell Biol, 7*(8), 2745-2752. doi:10.1128/mcb.7.8.2745

Chen, Z. J., & Sun, L. J. (2009). Nonproteolytic functions of ubiquitin in cell signaling. *Mol Cell, 33*(3), 275-286. doi:10.1016/j.molcel.2009.01.014

Chen-Plotkin, A. S., Lee, V. M., & Trojanowski, J. Q. (2010). TAR DNA-binding protein 43 in neurodegenerative disease. *Nat Rev Neurol, 6*(4), 211-220. doi:10.1038/nrneurol.2010.18

Cherkasov, V., Hofmann, S., Druffel-Augustin, S., Mogk, A., Tyedmers, J., Stoecklin, G., & Bukau, B. (2013). Coordination of translational control and protein homeostasis during severe heat stress. *Curr Biol, 23*(24), 2452-2462. doi:10.1016/j.cub.2013.09.058

Choudhury, N. R., Heikel, G., Trubitsyna, M., Kubik, P., Nowak, J. S., Webb, S., . . . Michlewski, G. (2017). RNA-binding activity of TRIM25 is mediated by its PRY/SPRY domain and is required for ubiquitination. *BMC Biol, 15*(1), 105. doi:10.1186/s12915-017-0444-9

Clague, M. J., Barsukov, I., Coulson, J. M., Liu, H., Rigden, D. J., & Urbe, S. (2013). Deubiquitylases from genes to organism. *Physiol Rev, 93*(3), 1289-1315. doi:10.1152/physrev.00002.2013

Clague, M. J., Heride, C., & Urbe, S. (2015). The demographics of the ubiquitin system. *Trends Cell Biol, 25*(7), 417-426. doi:10.1016/j.tcb.2015.03.002

Clague, M. J., Urbe, S., & Komander, D. (2019). Breaking the chains: deubiquitylating enzyme specificity begets function. *Nat Rev Mol Cell Biol, 20*(6), 338-352. doi:10.1038/s41580-019-0099-1

Clemens, K., Wolf, V., McBryant, S., Zhang, P., Liao, X., Wright, P., & Gottesfeld, J. (1993). Molecular basis for specific recognition of both RNA and DNA by a zinc finger protein. *Science, 260*(5107), 530-533. doi:10.1126/science.8475383

Costa-Mattioli, M., Sossin, W. S., Klann, E., & Sonenberg, N. (2009). Translational control of long-lasting synaptic plasticity and memory. *Neuron, 61*(1), 10-26. doi:10.1016/j.neuron.2008.10.055

Cote, J., & Richard, S. (2005). Tudor domains bind symmetrical dimethylated arginines. *J Biol Chem, 280*(31), 28476-28483. doi:10.1074/jbc.M414328200

D'Arcy, P., Wang, X., & Linder, S. (2015). Deubiquitinase inhibition as a cancer therapeutic strategy. *Pharmacol Ther, 147*, 32-54. doi:10.1016/j.pharmthera.2014.11.002

Damgaard, C. K., & Lykke-Andersen, J. (2011). Translational coregulation of 5'TOP mRNAs by TIA-1 and TIAR. *Genes Dev, 25*(19), 2057-2068. doi:10.1101/gad.17355911

Darnell, J. C., Jensen, K. B., Jin, P., Brown, V., Warren, S. T., & Darnell, R. B. (2001). Fragile X mental retardation protein targets G quartet mRNAs important for neuronal function. *Cell, 107*(4), 489-499.

Das, R., Schwintzer, L., Vinopal, S., Aguado Roca, E., Sylvester, M., Oprisoreanu, A. M., . . . Broemer, M. (2019). New roles for the de-ubiquitylating enzyme OTUD4 in an RNA-protein network and RNA granules. *J Cell Sci, 132*(12). doi:10.1242/jcs.229252

Daubner, G. M., Clery, A., & Allain, F. H. (2013). RRM-RNA recognition: NMR or crystallography...and new findings. *Curr Opin Struct Biol, 23*(1), 100-108. doi:10.1016/j.sbi.2012.11.006

De Hoop, M., Meyn, L., & Dotti, C. (1998). Culturing hippocampal neurons and astrocytes from fetal rodent brain. *Cell biology: a laboratory handbook, 1*, 154-163.

De Leeuw, F., Zhang, T., Wauquier, C., Huez, G., Kruys, V., & Gueydan, C. (2007). The cold-inducible RNA-binding protein migrates from the nucleus to cytoplasmic stress granules by a methylation-dependent mechanism and acts as a translational repressor. *Exp Cell Res, 313*(20), 4130-4144. doi:10.1016/j.yexcr.2007.09.017

Del Campo, M., & Lambowitz, A. M. (2009). Structure of the Yeast DEAD box protein Mss116p reveals two wedges that crimp RNA. *Mol Cell, 35*(5), 598-609. doi:10.1016/j.molcel.2009.07.032

Deng, L., Wang, C., Spencer, E., Yang, L., Braun, A., You, J., . . . Chen, Z. J. (2000). Activation of the IkappaB kinase complex by TRAF6 requires a dimeric ubiquitin-conjugating enzyme complex and a unique polyubiquitin chain. *Cell, 103*(2), 351-361.

Deshaies, R. J., & Joazeiro, C. A. (2009). RING domain E3 ubiquitin ligases. *Annu Rev Biochem, 78*, 399-434. doi:10.1146/annurev.biochem.78.101807.093809

Dever, T. E., Feng, L., Wek, R. C., Cigan, A. M., Donahue, T. F., & Hinnebusch, A. G. (1992). Phosphorylation of initiation factor 2 alpha by protein kinase GCN2 mediates gene-specific translational control of GCN4 in yeast. *Cell, 68*(3), 585-596.

Didiot, M. C., Subramanian, M., Flatter, E., Mandel, J. L., & Moine, H. (2009). Cells lacking the fragile X mental retardation protein (FMRP) have normal RISC activity but exhibit altered stress granule assembly. *Mol Biol Cell, 20*(1), 428-437. doi:10.1091/mbc.E08-07-0737

Doil, C., Mailand, N., Bekker-Jensen, S., Menard, P., Larsen, D. H., Pepperkok, R., . . . Lukas, C. (2009). RNF168 binds and amplifies ubiquitin conjugates on damaged chromosomes to

allow accumulation of repair proteins. *Cell, 136*(3), 435-446. doi:10.1016/j.cell.2008.12.041

Donlin-Asp, P. G., Fallini, C., Campos, J., Chou, C. C., Merritt, M. E., Phan, H. C., . . . Rossoll, W. (2017). The Survival of Motor Neuron Protein Acts as a Molecular Chaperone for mRNP Assembly. *Cell Rep, 18*(7), 1660-1673. doi:10.1016/j.celrep.2017.01.059

Donnelly, C. J., Park, M., Spillane, M., Yoo, S., Pacheco, A., Gomes, C., . . . Twiss, J. L. (2013). Axonally synthesized beta-actin and GAP-43 proteins support distinct modes of axonal growth. *J Neurosci, 33*(8), 3311-3322. doi:10.1523/jneurosci.1722-12.2013

Eisinger-Mathason, T. S., Andrade, J., Groehler, A. L., Clark, D. E., Muratore-Schroeder, T. L., Pasic, L., . . . Lannigan, D. A. (2008). Codependent functions of RSK2 and the apoptosis-promoting factor TIA-1 in stress granule assembly and cell survival. *Mol Cell, 31*(5), 722-736. doi:10.1016/j.molcel.2008.06.025

El Fatimy, R., Davidovic, L., Tremblay, S., Jaglin, X., Dury, A., Robert, C., . . . Khandjian, E. W. (2016). Tracking the Fragile X Mental Retardation Protein in a Highly Ordered Neuronal RiboNucleoParticles Population: A Link between Stalled Polyribosomes and RNA Granules. *PLoS Genet, 12*(7), e1006192. doi:10.1371/journal.pgen.1006192

Elden, A. C., Kim, H. J., Hart, M. P., Chen-Plotkin, A. S., Johnson, B. S., Fang, X., . . . Gitler, A. D. (2010). Ataxin-2 intermediate-length polyglutamine expansions are associated with increased risk for ALS. *Nature, 466*(7310), 1069-1075. doi:10.1038/nature09320

Eliscovich, C., & Singer, R. H. (2017). RNP transport in cell biology: the long and winding road. *Curr Opin Cell Biol, 45*, 38-46. doi:10.1016/j.ceb.2017.02.008

Elvira, G., Wasiak, S., Blandford, V., Tong, X. K., Serrano, A., Fan, X., . . . Sossin, W. S. (2006). Characterization of an RNA granule from developing brain. *Mol Cell Proteomics, 5*(4), 635-651. doi:10.1074/mcp.M500255-MCP200

Eom, T., Antar, L. N., Singer, R. H., & Bassell, G. J. (2003). Localization of a β-Actin Messenger Ribonucleoprotein Complex with Zipcode-Binding Protein Modulates the Density of Dendritic Filopodia and Filopodial Synapses. *The Journal of Neuroscience, 23*(32), 10433-10444. doi:10.1523/jneurosci.23-32-10433.2003

Fallini, C., Bassell, G. J., & Rossoll, W. (2012). The ALS disease protein TDP-43 is actively transported in motor neuron axons and regulates axon outgrowth. *Hum Mol Genet, 21*(16), 3703-3718. doi:10.1093/hmg/dds205

Fallini, C., Donlin-Asp, P. G., Rouanet, J. P., Bassell, G. J., & Rossoll, W. (2016). Deficiency of the Survival of Motor Neuron Protein Impairs mRNA Localization and Local Translation in the Growth Cone of Motor Neurons. *J Neurosci, 36*(13), 3811-3820. doi:10.1523/JNEUROSCI.2396-15.2016

Fallini, C., Rouanet, J. P., Donlin-Asp, P. G., Guo, P., Zhang, H., Singer, R. H., . . . Bassell, G. J. (2014). Dynamics of survival of motor neuron (SMN) protein interaction with the mRNA-binding protein IMP1 facilitates its trafficking into motor neuron axons. *Dev Neurobiol, 74*(3), 319-332. doi:10.1002/dneu.22111

Fallini, C., Zhang, H., Su, Y., Silani, V., Singer, R. H., Rossoll, W., & Bassell, G. J. (2011). The survival of motor neuron (SMN) protein interacts with the mRNA-binding protein HuD and regulates localization of poly(A) mRNA in primary motor neuron axons. *J Neurosci, 31*(10), 3914-3925. doi:10.1523/JNEUROSCI.3631-10.2011

Farina, K. L., Huttelmaier, S., Musunuru, K., Darnell, R., & Singer, R. H. (2003). Two ZBP1 KH domains facilitate beta-actin mRNA localization, granule formation, and cytoskeletal attachment. *J Cell Biol, 160*(1), 77-87. doi:10.1083/jcb.200206003

Fox, A. H., Lam, Y. W., Leung, A. K., Lyon, C. E., Andersen, J., Mann, M., & Lamond, A. I. (2002). Paraspeckles: a novel nuclear domain. *Curr Biol, 12*(1), 13-25.

Gall, J. G., Bellini, M., Wu, Z., & Murphy, C. (1999). Assembly of the nuclear transcription and processing machinery: Cajal bodies (coiled bodies) and transcriptosomes. *Mol Biol Cell, 10*(12), 4385-4402. doi:10.1091/mbc.10.12.4385

Gallastegui, N., & Groll, M. (2010). The 26S proteasome: assembly and function of a destructive machine. *Trends Biochem Sci, 35*(11), 634-642. doi:10.1016/j.tibs.2010.05.005

Garcia, M. A., Meurs, E. F., & Esteban, M. (2007). The dsRNA protein kinase PKR: virus and cell control. *Biochimie, 89*(6-7), 799-811. doi:10.1016/j.biochi.2007.03.001

Gerstberger, S., Hafner, M., & Tuschl, T. (2014). A census of human RNA-binding proteins. *Nat Rev Genet, 15*(12), 829-845. doi:10.1038/nrg3813

Gilks, N., Kedersha, N., Ayodele, M., Shen, L., Stoecklin, G., Dember, L. M., & Anderson, P. (2004). Stress granule assembly is mediated by prion-like aggregation of TIA-1. *Mol Biol Cell, 15*(12), 5383-5398. doi:10.1091/mbc.e04-08-0715

Gispert, S., Twells, R., Orozco, G., Brice, A., Weber, J., Heredero, L., . . . et al. (1993). Chromosomal assignment of the second locus for autosomal dominant cerebellar ataxia (SCA2) to chromosome 12q23-24.1. *Nat Genet, 4*(3), 295-299. doi:10.1038/ng0793-295

Gitler, A. D., & Shorter, J. (2011). RNA-binding proteins with prion-like domains in ALS and FTLD-U. *Prion, 5*(3), 179-187. doi:10.4161/pri.5.3.17230

Goulet, I., Boisvenue, S., Mokas, S., Mazroui, R., & Cote, J. (2008). TDRD3, a novel Tudor domain-containing protein, localizes to cytoplasmic stress granules. *Hum Mol Genet, 17*(19), 3055-3074. doi:10.1093/hmg/ddn203

Graber, T. E., Hébert-Seropian, S., Khoutorsky, A., David, A., Yewdell, J. W., Lacaille, J.-C., & Sossin, W. S. (2013). Reactivation of stalled polyribosomes in synaptic plasticity. *Proceedings of the National Academy of Sciences, 110*(40), 16205-16210. doi:10.1073/pnas.1307747110

Guo, W., Chen, Y., Zhou, X., Kar, A., Ray, P., Chen, X., . . . Wu, J. Y. (2011). An ALS-associated mutation affecting TDP-43 enhances protein aggregation, fibril formation and neurotoxicity. *Nat Struct Mol Biol, 18*(7), 822-830. doi:10.1038/nsmb.2053

Han, A. P., Yu, C., Lu, L., Fujiwara, Y., Browne, C., Chin, G., . . . Chen, J. J. (2001). Heme-regulated eIF2alpha kinase (HRI) is required for translational regulation and survival of erythroid precursors in iron deficiency. *EMBO J, 20*(23), 6909-6918. doi:10.1093/emboj/20.23.6909

Harding, H. P., Zhang, Y., & Ron, D. (1999). Protein translation and folding are coupled by an endoplasmic-reticulum-resident kinase. *Nature, 397*(6716), 271-274. doi:10.1038/16729

Harrigan, J. A., Jacq, X., Martin, N. M., & Jackson, S. P. (2018). Deubiquitylating enzymes and drug discovery: emerging opportunities. *Nat Rev Drug Discov, 17*(1), 57-78. doi:10.1038/nrd.2017.152

Hentze, M. W., Castello, A., Schwarzl, T., & Preiss, T. (2018). A brave new world of RNA-binding proteins. *Nat Rev Mol Cell Biol, 19*(5), 327-341. doi:10.1038/nrm.2017.130

Hershko, A., & Ciechanover, A. (1998). The ubiquitin system. *Annu Rev Biochem, 67*, 425-479. doi:10.1146/annurev.biochem.67.1.425

Hicke, L. (2001). Protein regulation by monoubiquitin. *Nat Rev Mol Cell Biol, 2*(3), 195-201. doi:10.1038/35056583

Hirano, M., Muto, M., Sakai, M., Kondo, H., Kobayashi, S., Kariwa, H., & Yoshii, K. (2017). Dendritic transport of tick-borne flavivirus RNA by neuronal granules affects

development of neurological disease. *Proceedings of the National Academy of Sciences, 114*(37), 9960-9965. doi:10.1073/pnas.1704454114

Hirokawa, N. (2006). mRNA transport in dendrites: RNA granules, motors, and tracks. *J Neurosci, 26*(27), 7139-7142. doi:10.1523/JNEUROSCI.1821-06.2006

Holcik, M., & Sonenberg, N. (2005). Translational control in stress and apoptosis. *Nat Rev Mol Cell Biol, 6*(4), 318-327. doi:10.1038/nrm1618

Homan, C. C., Kumar, R., Nguyen, L. S., Haan, E., Raymond, F. L., Abidi, F., . . . Jolly, L. A. (2014). Mutations in USP9X are associated with X-linked intellectual disability and disrupt neuronal cell migration and growth. *Am J Hum Genet, 94*(3), 470-478. doi:10.1016/j.ajhg.2014.02.004

Hou, L., Antion, M. D., Hu, D., Spencer, C. M., Paylor, R., & Klann, E. (2006). Dynamic translational and proteasomal regulation of fragile X mental retardation protein controls mGluR-dependent long-term depression. *Neuron, 51*(4), 441-454. doi:10.1016/j.neuron.2006.07.005

Husnjak, K., & Dikic, I. (2012). Ubiquitin-binding proteins: decoders of ubiquitin-mediated cellular functions. *Annu Rev Biochem, 81*, 291-322. doi:10.1146/annurev-biochem-051810-094654

Hyman, A. A., Weber, C. A., & Julicher, F. (2014). Liquid-liquid phase separation in biology. *Annu Rev Cell Dev Biol, 30*, 39-58. doi:10.1146/annurev-cellbio-100913-013325

Ivanov, P., Kedersha, N., & Anderson, P. (2019). Stress Granules and Processing Bodies in Translational Control. *Cold Spring Harb Perspect Biol, 11*(5). doi:10.1101/cshperspect.a032813

Jackson, R. J., Hellen, C. U., & Pestova, T. V. (2010). The mechanism of eukaryotic translation initiation and principles of its regulation. *Nat Rev Mol Cell Biol, 11*(2), 113-127. doi:10.1038/nrm2838

Jackson, S. P., & Durocher, D. (2013). Regulation of DNA damage responses by ubiquitin and SUMO. *Mol Cell, 49*(5), 795-807. doi:10.1016/j.molcel.2013.01.017

Jain, S., Wheeler, J. R., Walters, R. W., Agrawal, A., Barsic, A., & Parker, R. (2016). ATPase-Modulated Stress Granules Contain a Diverse Proteome and Substructure. *Cell, 164*(3), 487-498. doi:10.1016/j.cell.2015.12.038

Jarvelin, A. I., Noerenberg, M., Davis, I., & Castello, A. (2016). The new (dis)order in RNA regulation. *Cell Commun Signal, 14*, 9. doi:10.1186/s12964-016-0132-3

Jayabalan, A. K., Sanchez, A., Park, R. Y., Yoon, S. P., Kang, G. Y., Baek, J. H., . . . Ohn, T. (2016). NEDDylation promotes stress granule assembly. *Nat Commun, 7*, 12125. doi:10.1038/ncomms12125

Jeno, P., Mini, T., Moes, S., Hintermann, E., & Horst, M. (1995). Internal sequences from proteins digested in polyacrylamide gels. *Anal Biochem, 224*(1), 75-82. doi:10.1006/abio.1995.1010

Kall, L., Storey, J. D., MacCoss, M. J., & Noble, W. S. (2008). Assigning significance to peptides identified by tandem mass spectrometry using decoy databases. *J Proteome Res, 7*(1), 29-34. doi:10.1021/pr700600n

Kanai, Y., Dohmae, N., & Hirokawa, N. (2004). Kinesin transports RNA: isolation and characterization of an RNA-transporting granule. *Neuron, 43*(4), 513-525. doi:10.1016/j.neuron.2004.07.022

Kao, D. I., Aldridge, G. M., Weiler, I. J., & Greenough, W. T. (2010). Altered mRNA transport, docking, and protein translation in neurons lacking fragile X mental retardation

protein. *Proc Natl Acad Sci U S A, 107*(35), 15601-15606. doi:10.1073/pnas.1010564107

Kapitein, L. C., Yau, K. W., & Hoogenraad, C. C. (2010). Microtubule dynamics in dendritic spines. *Methods Cell Biol, 97*, 111-132. doi:10.1016/S0091-679X(10)97007-6

Kato, M., Han, T. W., Xie, S., Shi, K., Du, X., Wu, L. C., . . . McKnight, S. L. (2012). Cell-free formation of RNA granules: low complexity sequence domains form dynamic fibers within hydrogels. *Cell, 149*(4), 753-767. doi:10.1016/j.cell.2012.04.017

Kedersha, N., & Anderson, P. (2002). Stress granules: sites of mRNA triage that regulate mRNA stability and translatability. *Biochem Soc Trans, 30*(Pt 6), 963-969. doi:10.1042/

Kedersha, N., & Anderson, P. (2007). Mammalian stress granules and processing bodies. *Methods Enzymol, 431*, 61-81. doi:10.1016/s0076-6879(07)31005-7

Kedersha, N., Cho, M. R., Li, W., Yacono, P. W., Chen, S., Gilks, N., . . . Anderson, P. (2000). Dynamic Shuttling of Tia-1 Accompanies the Recruitment of mRNA to Mammalian Stress Granules. *The Journal of Cell Biology, 151*(6), 1257-1268. doi:10.1083/jcb.151.6.1257

Kedersha, N., Ivanov, P., & Anderson, P. (2013). Stress granules and cell signaling: more than just a passing phase? *Trends Biochem Sci, 38*(10), 494-506. doi:10.1016/j.tibs.2013.07.004

Kedersha, N., Panas, M. D., Achorn, C. A., Lyons, S., Tisdale, S., Hickman, T., . . . Anderson, P. (2016). G3BP-Caprin1-USP10 complexes mediate stress granule condensation and associate with 40S subunits. *J Cell Biol, 212*(7), 845-860. doi:10.1083/jcb.201508028

Kedersha, N., Stoecklin, G., Ayodele, M., Yacono, P., Lykke-Andersen, J., Fritzler, M. J., . . . Anderson, P. (2005). Stress granules and processing bodies are dynamically linked sites of mRNP remodeling. *J Cell Biol, 169*(6), 871-884. doi:10.1083/jcb.200502088

Kedersha, N. L., Gupta, M., Li, W., Miller, I., & Anderson, P. (1999). RNA-binding proteins TIA-1 and TIAR link the phosphorylation of eIF-2 alpha to the assembly of mammalian stress granules. *J Cell Biol, 147*(7), 1431-1442. doi:10.1083/jcb.147.7.1431

Keene, J. D. (2007). RNA regulons: coordination of post-transcriptional events. *Nat Rev Genet, 8*(7), 533-543. doi:10.1038/nrg2111

Keusekotten, K., Elliott, P. R., Glockner, L., Fiil, B. K., Damgaard, R. B., Kulathu, Y., . . . Komander, D. (2013). OTULIN antagonizes LUBAC signaling by specifically hydrolyzing Met1-linked polyubiquitin. *Cell, 153*(6), 1312-1326. doi:10.1016/j.cell.2013.05.014

Khong, A., Matheny, T., Jain, S., Mitchell, S. F., Wheeler, J. R., & Parker, R. (2017). The Stress Granule Transcriptome Reveals Principles of mRNA Accumulation in Stress Granules. *Mol Cell, 68*(4), 808-820.e805. doi:10.1016/j.molcel.2017.10.015

Kiebler, M. A., & Bassell, G. J. (2006). Neuronal RNA granules: movers and makers. *Neuron, 51*(6), 685-690. doi:10.1016/j.neuron.2006.08.021

Kim, H. J., Kim, N. C., Wang, Y. D., Scarborough, E. A., Moore, J., Diaz, Z., . . . Taylor, J. P. (2013). Mutations in prion-like domains in hnRNPA2B1 and hnRNPA1 cause multisystem proteinopathy and ALS. *Nature, 495*(7442), 467-473. doi:10.1038/nature11922

Kim, H. J., Raphael, A. R., LaDow, E. S., McGurk, L., Weber, R. A., Trojanowski, J. Q., . . . Bonini, N. M. (2014). Therapeutic modulation of eIF2alpha phosphorylation rescues TDP-43 toxicity in amyotrophic lateral sclerosis disease models. *Nat Genet, 46*(2), 152-160. doi:10.1038/ng.2853

Kim, W. J., Back, S. H., Kim, V., Ryu, I., & Jang, S. K. (2005). Sequestration of TRAF2 into stress granules interrupts tumor necrosis factor signaling under stress conditions. *Mol Cell Biol, 25*(6), 2450-2462. doi:10.1128/mcb.25.6.2450-2462.2005

Kimball, S. R., Horetsky, R. L., Ron, D., Jefferson, L. S., & Harding, H. P. (2003). Mammalian stress granules represent sites of accumulation of stalled translation initiation complexes. *Am J Physiol Cell Physiol, 284*(2), C273-284. doi:10.1152/ajpcell.00314.2002

Kirisako, T., Kamei, K., Murata, S., Kato, M., Fukumoto, H., Kanie, M., . . . Iwai, K. (2006). A ubiquitin ligase complex assembles linear polyubiquitin chains. *EMBO J, 25*(20), 4877-4887. doi:10.1038/sj.emboj.7601360

Knowles, R. B., Sabry, J. H., Martone, M. E., Deerinck, T. J., Ellisman, M. H., Bassell, G. J., & Kosik, K. S. (1996). Translocation of RNA granules in living neurons. *J Neurosci, 16*(24), 7812-7820.

Kohrmann, M., Luo, M., Kaether, C., DesGroseillers, L., Dotti, C. G., & Kiebler, M. A. (1999). Microtubule-dependent recruitment of Staufen-green fluorescent protein into large RNA-containing granules and subsequent dendritic transport in living hippocampal neurons. *Mol Biol Cell, 10*(9), 2945-2953. doi:10.1091/mbc.10.9.2945

Komander, D. (2009). The emerging complexity of protein ubiquitination. *Biochem Soc Trans, 37*(Pt 5), 937-953. doi:10.1042/BST0370937

Krichevsky, A. M., & Kosik, K. S. (2001). Neuronal RNA granules: a link between RNA localization and stimulation-dependent translation. *Neuron, 32*(4), 683-696.

Kulathu, Y., & Komander, D. (2012). Atypical ubiquitylation - the unexplored world of polyubiquitin beyond Lys48 and Lys63 linkages. *Nat Rev Mol Cell Biol, 13*(8), 508-523. doi:10.1038/nrm3394

Kwasna, D., Abdul Rehman, S. A., Natarajan, J., Matthews, S., Madden, R., De Cesare, V., . . . Kulathu, Y. (2018). Discovery and Characterization of ZUFSP/ZUP1, a Distinct Deubiquitinase Class Important for Genome Stability. *Mol Cell, 70*(1), 150-164 e156. doi:10.1016/j.molcel.2018.02.023

Kwon, S., Zhang, Y., & Matthias, P. (2007). The deacetylase HDAC6 is a novel critical component of stress granules involved in the stress response. *Genes Dev, 21*(24), 3381-3394. doi:10.1101/gad.461107

Kwon, S. C., Yi, H., Eichelbaum, K., Föhr, S., Fischer, B., You, K. T., . . . Kim, V. N. (2013). The RNA-binding protein repertoire of embryonic stem cells. *Nature Structural &Amp; Molecular Biology, 20*, 1122. doi:10.1038/nsmb.2638

https://www.nature.com/articles/nsmb.2638 - supplementary-information

Lagier-Tourenne, C., Polymenidou, M., & Cleveland, D. W. (2010). TDP-43 and FUS/TLS: emerging roles in RNA processing and neurodegeneration. *Hum Mol Genet, 19*(R1), R46-64. doi:10.1093/hmg/ddq137

Landthaler, M., Gaidatzis, D., Rothballer, A., Chen, P. Y., Soll, S. J., Dinic, L., . . . Tuschl, T. (2008). Molecular characterization of human Argonaute-containing ribonucleoprotein complexes and their bound target mRNAs. *RNA, 14*(12), 2580-2596. doi:10.1261/rna.1351608

Lewis, H. A., Musunuru, K., Jensen, K. B., Edo, C., Chen, H., Darnell, R. B., & Burley, S. K. (2000). Sequence-specific RNA binding by a Nova KH domain: implications for paraneoplastic disease and the fragile X syndrome. *Cell, 100*(3), 323-332.

Li, D. K., Tisdale, S., Lotti, F., & Pellizzoni, L. (2014). SMN control of RNP assembly: from post-transcriptional gene regulation to motor neuron disease. *Semin Cell Dev Biol, 32*, 22-29. doi:10.1016/j.semcdb.2014.04.026

Li, Y. R., King, O. D., Shorter, J., & Gitler, A. D. (2013). Stress granules as crucibles of ALS pathogenesis. *J Cell Biol, 201*(3), 361-372. doi:10.1083/jcb.201302044

Lin, Y., Protter, D. S., Rosen, M. K., & Parker, R. (2015). Formation and Maturation of Phase-Separated Liquid Droplets by RNA-Binding Proteins. *Mol Cell, 60*(2), 208-219. doi:10.1016/j.molcel.2015.08.018

Ling, S. C., Fahrner, P. S., Greenough, W. T., & Gelfand, V. I. (2004). Transport of Drosophila fragile X mental retardation protein-containing ribonucleoprotein granules by kinesin-1 and cytoplasmic dynein. *Proc Natl Acad Sci U S A, 101*(50), 17428-17433. doi:10.1073/pnas.0408114101

Ling, S. C., Polymenidou, M., & Cleveland, D. W. (2013). Converging mechanisms in ALS and FTD: disrupted RNA and protein homeostasis. *Neuron, 79*(3), 416-438. doi:10.1016/j.neuron.2013.07.033

Liu-Yesucevitz, L., Lin, A. Y., Ebata, A., Boon, J. Y., Reid, W., Xu, Y. F., . . . Wolozin, B. (2014). ALS-linked mutations enlarge TDP-43-enriched neuronal RNA granules in the dendritic arbor. *J Neurosci, 34*(12), 4167-4174. doi:10.1523/jneurosci.2350-13.2014

Liuyu, T., Yu, K., Ye, L., Zhang, Z., Zhang, M., Ren, Y., . . . Zhong, B. (2019). Induction of OTUD4 by viral infection promotes antiviral responses through deubiquitinating and stabilizing MAVS. *Cell Res, 29*(1), 67-79. doi:10.1038/s41422-018-0107-6

Lloyd, R. E. (2013). Regulation of stress granules and P-bodies during RNA virus infection. *Wiley Interdiscip Rev RNA, 4*(3), 317-331. doi:10.1002/wrna.1162

Lorson, C. L., Hahnen, E., Androphy, E. J., & Wirth, B. (1999). A single nucleotide in the SMN gene regulates splicing and is responsible for spinal muscular atrophy. *Proc Natl Acad Sci U S A, 96*(11), 6307-6311. doi:10.1073/pnas.96.11.6307

Louis, M., Hofmann, K., & Broemer, M. (2015). Evolutionary Loss of Activity in De-Ubiquitylating Enzymes of the OTU Family. *PLoS One, 10*(11), e0143227. doi:10.1371/journal.pone.0143227

Lu, R., Wang, H., Liang, Z., Ku, L., O'Donnell W, T., Li, W., . . . Feng, Y. (2004). The fragile X protein controls microtubule-associated protein 1B translation and microtubule stability in brain neuron development. *Proc Natl Acad Sci U S A, 101*(42), 15201-15206. doi:10.1073/pnas.0404995101

Lunde, B. M., Moore, C., & Varani, G. (2007). RNA-binding proteins: modular design for efficient function. *Nat Rev Mol Cell Biol, 8*(6), 479-490. doi:10.1038/nrm2178

Mackenzie, I. R., Nicholson, A. M., Sarkar, M., Messing, J., Purice, M. D., Pottier, C., . . . Rademakers, R. (2017). TIA1 Mutations in Amyotrophic Lateral Sclerosis and Frontotemporal Dementia Promote Phase Separation and Alter Stress Granule Dynamics. *Neuron, 95*(4), 808-816 e809. doi:10.1016/j.neuron.2017.07.025

Margolin, D. H., Kousi, M., Chan, Y. M., Lim, E. T., Schmahmann, J. D., Hadjivassiliou, M., . . . Seminara, S. B. (2013). Ataxia, dementia, and hypogonadotropism caused by disordered ubiquitination. *N Engl J Med, 368*(21), 1992-2003. doi:10.1056/NEJMoa1215993

Markmiller, S., Fulzele, A., Higgins, R., Leonard, M., Yeo, G. W., & Bennett, E. J. (2019). Active Protein Neddylation or Ubiquitylation Is Dispensable for Stress Granule Dynamics. *Cell Rep, 27*(5), 1356-1363 e1353. doi:10.1016/j.celrep.2019.04.015

Markmiller, S., Soltanieh, S., Server, K. L., Mak, R., Jin, W., Fang, M. Y., . . . Yeo, G. W. (2018). Context-Dependent and Disease-Specific Diversity in Protein Interactions within Stress Granules. *Cell, 172*(3), 590-604 e513. doi:10.1016/j.cell.2017.12.032

Mateju, D., Franzmann, T. M., Patel, A., Kopach, A., Boczek, E. E., Maharana, S., . . . Alberti, S. (2017). An aberrant phase transition of stress granules triggered by misfolded protein and prevented by chaperone function. *EMBO J, 36*(12), 1669-1687. doi:10.15252/embj.201695957

McDonald, K. K., Aulas, A., Destroismaisons, L., Pickles, S., Beleac, E., Camu, W., . . . Vande Velde, C. (2011). TAR DNA-binding protein 43 (TDP-43) regulates stress granule dynamics via differential regulation of G3BP and TIA-1. *Hum Mol Genet, 20*(7), 1400-1410. doi:10.1093/hmg/ddr021

Mevissen, T. E., Hospenthal, M. K., Geurink, P. P., Elliott, P. R., Akutsu, M., Arnaudo, N., . . . Komander, D. (2013). OTU deubiquitinases reveal mechanisms of linkage specificity and enable ubiquitin chain restriction analysis. *Cell, 154*(1), 169-184. doi:10.1016/j.cell.2013.05.046

Mi, H., Muruganujan, A., Casagrande, J. T., & Thomas, P. D. (2013). Large-scale gene function analysis with the PANTHER classification system. *Nat Protoc, 8*(8), 1551-1566. doi:10.1038/nprot.2013.092

Mitchell, S. F., Jain, S., She, M., & Parker, R. (2013). Global analysis of yeast mRNPs. *Nat Struct Mol Biol, 20*(1), 127-133. doi:10.1038/nsmb.2468

Mollet, S., Cougot, N., Wilczynska, A., Dautry, F., Kress, M., Bertrand, E., & Weil, D. (2008). Translationally repressed mRNA transiently cycles through stress granules during stress. *Mol Biol Cell, 19*(10), 4469-4479. doi:10.1091/mbc.E08-05-0499

Molliex, A., Temirov, J., Lee, J., Coughlin, M., Kanagaraj, A. P., Kim, H. J., . . . Taylor, J. P. (2015). Phase separation by low complexity domains promotes stress granule assembly and drives pathological fibrillization. *Cell, 163*(1), 123-133. doi:10.1016/j.cell.2015.09.015

Murakami, T., Qamar, S., Lin, J. Q., Schierle, G. S., Rees, E., Miyashita, A., . . . St George-Hyslop, P. (2015). ALS/FTD Mutation-Induced Phase Transition of FUS Liquid Droplets and Reversible Hydrogels into Irreversible Hydrogels Impairs RNP Granule Function. *Neuron, 88*(4), 678-690. doi:10.1016/j.neuron.2015.10.030

Muratani, M., & Tansey, W. P. (2003). How the ubiquitin-proteasome system controls transcription. *Nat Rev Mol Cell Biol, 4*(3), 192-201. doi:10.1038/nrm1049

Murtaza, M., Jolly, L. A., Gecz, J., & Wood, S. A. (2015). La FAM fatale: USP9X in development and disease. *Cell Mol Life Sci, 72*(11), 2075-2089. doi:10.1007/s00018-015-1851-0

Nalavadi, V. C., Muddashetty, R. S., Gross, C., & Bassell, G. J. (2012). Dephosphorylation-induced ubiquitination and degradation of FMRP in dendrites: a role in immediate early mGluR-stimulated translation. *J Neurosci, 32*(8), 2582-2587. doi:10.1523/JNEUROSCI.5057-11.2012

Nelson, M., & McClelland, M. (1992). Use of DNA methyltransferase/endonuclease enzyme combinations for megabase mapping of chromosomes. *Methods Enzymol, 216*, 279-303.

Neumann, M., Sampathu, D. M., Kwong, L. K., Truax, A. C., Micsenyi, M. C., Chou, T. T., . . . Lee, V. M. (2006). Ubiquitinated TDP-43 in frontotemporal lobar degeneration and amyotrophic lateral sclerosis. *Science, 314*(5796), 130-133. doi:10.1126/science.1134108

Nonhoff, U., Ralser, M., Welzel, F., Piccini, I., Balzereit, D., Yaspo, M. L., . . . Krobitsch, S. (2007). Ataxin-2 interacts with the DEAD/H-box RNA helicase DDX6 and interferes with P-bodies and stress granules. *Mol Biol Cell, 18*(4), 1385-1396. doi:10.1091/mbc.e06-12-1120

Nostramo, R., & Herman, P. K. (2016). Deubiquitination and the regulation of stress granule assembly. *Curr Genet, 62*(3), 503-506. doi:10.1007/s00294-016-0571-9

Nostramo, R., Varia, S. N., Zhang, B., Emerson, M. M., & Herman, P. K. (2016). The Catalytic Activity of the Ubp3 Deubiquitinating Protease Is Required for Efficient Stress Granule Assembly in Saccharomyces cerevisiae. *Mol Cell Biol, 36*(1), 173-183. doi:10.1128/MCB.00609-15

Nott, T. J., Petsalaki, E., Farber, P., Jervis, D., Fussner, E., Plochowietz, A., . . . Baldwin, A. J. (2015). Phase transition of a disordered nuage protein generates environmentally responsive membraneless organelles. *Mol Cell, 57*(5), 936-947. doi:10.1016/j.molcel.2015.01.013

Oberstrass, F. C., Auweter, S. D., Erat, M., Hargous, Y., Henning, A., Wenter, P., . . . Allain, F. H. (2005). Structure of PTB bound to RNA: specific binding and implications for splicing regulation. *Science, 309*(5743), 2054-2057. doi:10.1126/science.1114066

Ohn, T., Kedersha, N., Hickman, T., Tisdale, S., & Anderson, P. (2008). A functional RNAi screen links O-GlcNAc modification of ribosomal proteins to stress granule and processing body assembly. *Nat Cell Biol, 10*(10), 1224-1231. doi:10.1038/ncb1783

Ohshima, D., Arimoto-Matsuzaki, K., Tomida, T., Takekawa, M., & Ichikawa, K. (2015). Spatio-temporal Dynamics and Mechanisms of Stress Granule Assembly. *PLoS Comput Biol, 11*(6), e1004326. doi:10.1371/journal.pcbi.1004326

Olsen, S. K., & Lima, C. D. (2013). Structure of a ubiquitin E1-E2 complex: insights to E1-E2 thioester transfer. *Mol Cell, 49*(5), 884-896. doi:10.1016/j.molcel.2013.01.013

Onomoto, K., Jogi, M., Yoo, J. S., Narita, R., Morimoto, S., Takemura, A., . . . Fujita, T. (2012). Critical role of an antiviral stress granule containing RIG-I and PKR in viral detection and innate immunity. *PLoS One, 7*(8), e43031. doi:10.1371/journal.pone.0043031

Onomoto, K., Yoneyama, M., Fung, G., Kato, H., & Fujita, T. (2014). Antiviral innate immunity and stress granule responses. *Trends Immunol, 35*(9), 420-428. doi:10.1016/j.it.2014.07.006

Pakos-Zebrucka, K., Koryga, I., Mnich, K., Ljujic, M., Samali, A., & Gorman, A. M. (2016). The integrated stress response. *EMBO Rep, 17*(10), 1374-1395. doi:10.15252/embr.201642195

Patel, A., Lee, H. O., Jawerth, L., Maharana, S., Jahnel, M., Hein, M. Y., . . . Alberti, S. (2015). A Liquid-to-Solid Phase Transition of the ALS Protein FUS Accelerated by Disease Mutation. *Cell, 162*(5), 1066-1077. doi:10.1016/j.cell.2015.07.047

Peng, J., Schwartz, D., Elias, J. E., Thoreen, C. C., Cheng, D., Marsischky, G., . . . Gygi, S. P. (2003). A proteomics approach to understanding protein ubiquitination. *Nat Biotechnol, 21*(8), 921-926. doi:10.1038/nbt849

Peng, K., Radivojac, P., Vucetic, S., Dunker, A. K., & Obradovic, Z. (2006). Length-dependent prediction of protein intrinsic disorder. *BMC Bioinformatics, 7*(1), 208. doi:10.1186/1471-2105-7-208

Perry, R. B., Doron-Mandel, E., Iavnilovitch, E., Rishal, I., Dagan, S. Y., Tsoory, M., . . . Fainzilber, M. (2012). Subcellular knockout of importin beta1 perturbs axonal retrograde signaling. *Neuron, 75*(2), 294-305. doi:10.1016/j.neuron.2012.05.033

Phan, A. T., Kuryavyi, V., Darnell, J. C., Serganov, A., Majumdar, A., Ilin, S., . . . Patel, D. J. (2011). Structure-function studies of FMRP RGG peptide recognition of an RNA duplex-quadruplex junction. *Nat Struct Mol Biol, 18*(7), 796-804. doi:10.1038/nsmb.2064

Pickart, C. M. (2001). Mechanisms underlying ubiquitination. *Annu Rev Biochem, 70*, 503-533. doi:10.1146/annurev.biochem.70.1.503

Ponting, C. P. (1997). Tudor domains in proteins that interact with RNA. *Trends Biochem Sci, 22*(2), 51-52.

Prilusky, J., Felder, C. E., Zeev-Ben-Mordehai, T., Rydberg, E. H., Man, O., Beckmann, J. S., . . . Sussman, J. L. (2005). FoldIndex: a simple tool to predict whether a given protein sequence is intrinsically unfolded. *Bioinformatics, 21*(16), 3435-3438. doi:10.1093/bioinformatics/bti537

Protter, D. S. W., & Parker, R. (2016). Principles and Properties of Stress Granules. *Trends Cell Biol, 26*(9), 668-679. doi:10.1016/j.tcb.2016.05.004

Ramaswami, M., Taylor, J. P., & Parker, R. (2013). Altered ribostasis: RNA-protein granules in degenerative disorders. *Cell, 154*(4), 727-736. doi:10.1016/j.cell.2013.07.038

Ran, F. A., Hsu, P. D., Wright, J., Agarwala, V., Scott, D. A., & Zhang, F. (2013). Genome engineering using the CRISPR-Cas9 system. *Nat Protoc, 8*(11), 2281-2308. doi:10.1038/nprot.2013.143

Reineke, L. C., & Lloyd, R. E. (2013). Diversion of stress granules and P-bodies during viral infection. *Virology, 436*(2), 255-267. doi:10.1016/j.virol.2012.11.017

Reyes-Turcu, F. E., Ventii, K. H., & Wilkinson, K. D. (2009). Regulation and cellular roles of ubiquitin-specific deubiquitinating enzymes. *Annu Rev Biochem, 78*, 363-397. doi:10.1146/annurev.biochem.78.082307.091526

Ritorto, M. S., Ewan, R., Perez-Oliva, A. B., Knebel, A., Buhrlage, S. J., Wightman, M., . . . Trost, M. (2014). Screening of DUB activity and specificity by MALDI-TOF mass spectrometry. *Nat Commun, 5*, 4763. doi:10.1038/ncomms5763

Rosenfeld, J., Capdevielle, J., Guillemot, J. C., & Ferrara, P. (1992). In-gel digestion of proteins for internal sequence analysis after one- or two-dimensional gel electrophoresis. *Anal Biochem, 203*(1), 173-179. doi:10.1016/0003-2697(92)90061-b

Rotin, D., & Kumar, S. (2009). Physiological functions of the HECT family of ubiquitin ligases. *Nat Rev Mol Cell Biol, 10*(6), 398-409. doi:10.1038/nrm2690

Schaeffer, C., Bardoni, B., Mandel, J. L., Ehresmann, B., Ehresmann, C., & Moine, H. (2001). The fragile X mental retardation protein binds specifically to its mRNA via a purine quartet motif. *EMBO J, 20*(17), 4803-4813. doi:10.1093/emboj/20.17.4803

Schindelin, J., Arganda-Carreras, I., Frise, E., Kaynig, V., Longair, M., Pietzsch, T., . . . Cardona, A. (2012). Fiji: an open-source platform for biological-image analysis. *Nat Methods, 9*(7), 676-682. doi:10.1038/nmeth.2019

Schmid-Burgk, J. L., Schmidt, T., Gaidt, M. M., Pelka, K., Latz, E., Ebert, T. S., & Hornung, V. (2014). OutKnocker: a web tool for rapid and simple genotyping of designer nuclease edited cell lines. *Genome Res, 24*(10), 1719-1723. doi:10.1101/gr.176701.114

Schmidt, E. K., Clavarino, G., Ceppi, M., & Pierre, P. (2009). SUnSET, a nonradioactive method to monitor protein synthesis. *Nat Methods, 6*(4), 275-277. doi:10.1038/nmeth.1314

Schulman, B. A., & Harper, J. W. (2009). Ubiquitin-like protein activation by E1 enzymes: the apex for downstream signalling pathways. *Nat Rev Mol Cell Biol, 10*(5), 319-331. doi:10.1038/nrm2673

Schwanhausser, B., Busse, D., Li, N., Dittmar, G., Schuchhardt, J., Wolf, J., . . . Selbach, M. (2011). Global quantification of mammalian gene expression control. *Nature, 473*(7347), 337-342. doi:10.1038/nature10098

Scoles, D. R., Meera, P., Schneider, M. D., Paul, S., Dansithong, W., Figueroa, K. P., . . . Pulst, S. M. (2017). Antisense oligonucleotide therapy for spinocerebellar ataxia type 2. *Nature, 544*(7650), 362-366. doi:10.1038/nature22044

Seguin, S. J., Morelli, F. F., Vinet, J., Amore, D., De Biasi, S., Poletti, A., . . . Carra, S. (2014). Inhibition of autophagy, lysosome and VCP function impairs stress granule assembly. *Cell Death Differ, 21*(12), 1838-1851. doi:10.1038/cdd.2014.103

Sheth, U., & Parker, R. (2003). Decapping and Decay of Messenger RNA Occur in Cytoplasmic Processing Bodies. *Science, 300*(5620), 805-808. doi:10.1126/science.1082320

Shpargel, K. B., & Matera, A. G. (2005). Gemin proteins are required for efficient assembly of Sm-class ribonucleoproteins. *Proc Natl Acad Sci U S A, 102*(48), 17372-17377. doi:10.1073/pnas.0508947102

Silva, G. M., Finley, D., & Vogel, C. (2015). K63 polyubiquitination is a new modulator of the oxidative stress response. *Nat Struct Mol Biol, 22*(2), 116-123. doi:10.1038/nsmb.2955

Smit, J. J., & Sixma, T. K. (2014). RBR E3-ligases at work. *EMBO Rep, 15*(2), 142-154. doi:10.1002/embr.201338166

Somasekharan, S. P., El-Naggar, A., Leprivier, G., Cheng, H., Hajee, S., Grunewald, T. G., . . . Sorensen, P. H. (2015). YB-1 regulates stress granule formation and tumor progression by translationally activating G3BP1. *J Cell Biol, 208*(7), 913-929. doi:10.1083/jcb.201411047

Sowa, M. E., Bennett, E. J., Gygi, S. P., & Harper, J. W. (2009). Defining the human deubiquitinating enzyme interaction landscape. *Cell, 138*(2), 389-403. doi:10.1016/j.cell.2009.04.042

Spence, J., Gali, R. R., Dittmar, G., Sherman, F., Karin, M., & Finley, D. (2000). Cell cycle-regulated modification of the ribosome by a variant multiubiquitin chain. *Cell, 102*(1), 67-76.

Sreedharan, J., Blair, I. P., Tripathi, V. B., Hu, X., Vance, C., Rogelj, B., . . . Shaw, C. E. (2008). TDP-43 mutations in familial and sporadic amyotrophic lateral sclerosis. *Science, 319*(5870), 1668-1672. doi:10.1126/science.1154584

Stewart, G. S., Panier, S., Townsend, K., Al-Hakim, A. K., Kolas, N. K., Miller, E. S., . . . Durocher, D. (2009). The RIDDLE syndrome protein mediates a ubiquitin-dependent signaling cascade at sites of DNA damage. *Cell, 136*(3), 420-434. doi:10.1016/j.cell.2008.12.042

Sudhakar, A., Ramachandran, A., Ghosh, S., Hasnain, S. E., Kaufman, R. J., & Ramaiah, K. V. (2000). Phosphorylation of serine 51 in initiation factor 2 alpha (eIF2 alpha) promotes complex formation between eIF2 alpha(P) and eIF2B and causes inhibition in the guanine nucleotide exchange activity of eIF2B. *Biochemistry, 39*(42), 12929-12938. doi:10.1021/bi0008682

Szaflarski, W., Fay, M. M., Kedersha, N., Zabel, M., Anderson, P., & Ivanov, P. (2016). Vinca alkaloid drugs promote stress-induced translational repression and stress granule formation. *Oncotarget, 7*(21), 30307-30322. doi:10.18632/oncotarget.8728

Takahashi, M., Higuchi, M., Matsuki, H., Yoshita, M., Ohsawa, T., Oie, M., & Fujii, M. (2013). Stress granules inhibit apoptosis by reducing reactive oxygen species production. *Mol Cell Biol, 33*(4), 815-829. doi:10.1128/MCB.00763-12

Tang, S. J., Meulemans, D., Vazquez, L., Colaco, N., & Schuman, E. (2001). A role for a rat homolog of staufen in the transport of RNA to neuronal dendrites. *Neuron, 32*(3), 463-475.

Thomas, M. G., Martinez Tosar, L. J., Desbats, M. A., Leishman, C. C., & Boccaccio, G. L. (2009). Mammalian Staufen 1 is recruited to stress granules and impairs their assembly. *J Cell Sci, 122*(Pt 4), 563-573. doi:10.1242/jcs.038208

Thomas, P. D., Campbell, M. J., Kejariwal, A., Mi, H., Karlak, B., Daverman, R., . . . Narechania, A. (2003). PANTHER: a library of protein families and subfamilies indexed by function. *Genome Res, 13*(9), 2129-2141. doi:10.1101/gr.772403

Todd, P. K., Mack, K. J., & Malter, J. S. (2003). The fragile X mental retardation protein is required for type-I metabotropic glutamate receptor-dependent translation of PSD-95. *Proc Natl Acad Sci U S A, 100*(24), 14374-14378. doi:10.1073/pnas.2336265100

Tourriere, H., Chebli, K., Zekri, L., Courselaud, B., Blanchard, J. M., Bertrand, E., & Tazi, J. (2003). The RasGAP-associated endoribonuclease G3BP assembles stress granules. *J Cell Biol, 160*(6), 823-831. doi:10.1083/jcb.200212128

Tse, W. K., Jiang, Y. J., & Wong, C. K. (2013). Zebrafish transforming growth factor-beta-stimulated clone 22 domain 3 (TSC22D3) plays critical roles in Bmp-dependent dorsoventral patterning via two deubiquitylating enzymes Usp15 and Otud4. *Biochim Biophys Acta, 1830*(10), 4584-4593. doi:10.1016/j.bbagen.2013.05.006

Tubing, F., Vendra, G., Mikl, M., Macchi, P., Thomas, S., & Kiebler, M. A. (2010). Dendritically localized transcripts are sorted into distinct ribonucleoprotein particles that display fast directional motility along dendrites of hippocampal neurons. *J Neurosci, 30*(11), 4160-4170. doi:10.1523/jneurosci.3537-09.2010

Turakhiya, A., Meyer, S. R., Marincola, G., Bohm, S., Vanselow, J. T., Schlosser, A., . . . Buchberger, A. (2018). ZFAND1 Recruits p97 and the 26S Proteasome to Promote the Clearance of Arsenite-Induced Stress Granules. *Mol Cell, 70*(5), 906-919 e907. doi:10.1016/j.molcel.2018.04.021

Urbe, S., Liu, H., Hayes, S. D., Heride, C., Rigden, D. J., & Clague, M. J. (2012). Systematic survey of deubiquitinase localization identifies USP21 as a regulator of centrosome- and microtubule-associated functions. *Mol Biol Cell, 23*(6), 1095-1103. doi:10.1091/mbc.E11-08-0668

Uversky, V. N., Oldfield, C. J., & Dunker, A. K. (2008). Intrinsically disordered proteins in human diseases: introducing the D2 concept. *Annu Rev Biophys, 37*, 215-246. doi:10.1146/annurev.biophys.37.032807.125924

Vacic, V., Markwick, P. R., Oldfield, C. J., Zhao, X., Haynes, C., Uversky, V. N., & Iakoucheva, L. M. (2012). Disease-associated mutations disrupt functionally important regions of intrinsic protein disorder. *PLoS Comput Biol, 8*(10), e1002709. doi:10.1371/journal.pcbi.1002709

Vance, C., Rogelj, B., Hortobagyi, T., De Vos, K. J., Nishimura, A. L., Sreedharan, J., . . . Shaw, C. E. (2009). Mutations in FUS, an RNA processing protein, cause familial amyotrophic lateral sclerosis type 6. *Science, 323*(5918), 1208-1211. doi:10.1126/science.1165942

Vanderweyde, T., Youmans, K., Liu-Yesucevitz, L., & Wolozin, B. (2013). Role of stress granules and RNA-binding proteins in neurodegeneration: a mini-review. *Gerontology, 59*(6), 524-533. doi:10.1159/000354170

Ventii, K. H., & Wilkinson, K. D. (2008). Protein partners of deubiquitinating enzymes. *Biochem J, 414*(2), 161-175. doi:10.1042/BJ20080798

Vessey, J. P., Vaccani, A., Xie, Y., Dahm, R., Karra, D., Kiebler, M. A., & Macchi, P. (2006). Dendritic localization of the translational repressor Pumilio 2 and its contribution to dendritic stress granules. *J Neurosci, 26*(24), 6496-6508. doi:10.1523/JNEUROSCI.0649-06.2006

Villace, P., Marion, R. M., & Ortin, J. (2004). The composition of Staufen-containing RNA granules from human cells indicates their role in the regulated transport and translation of messenger RNAs. *Nucleic Acids Res, 32*(8), 2411-2420. doi:10.1093/nar/gkh552

Wagner, S. A., Beli, P., Weinert, B. T., Nielsen, M. L., Cox, J., Mann, M., & Choudhary, C. (2011). A proteome-wide, quantitative survey of in vivo ubiquitylation sites reveals widespread regulatory roles. *Mol Cell Proteomics, 10*(10), M111 013284. doi:10.1074/mcp.M111.013284

Walters, R. W., Muhlrad, D., Garcia, J., & Parker, R. (2015). Differential effects of Ydj1 and Sis1 on Hsp70-mediated clearance of stress granules in Saccharomyces cerevisiae. *RNA, 21*(9), 1660-1671. doi:10.1261/rna.053116.115

Wang, C., Deng, L., Hong, M., Akkaraju, G. R., Inoue, J., & Chen, Z. J. (2001). TAK1 is a ubiquitin-dependent kinase of MKK and IKK. *Nature, 412*(6844), 346-351. doi:10.1038/35085597

Wang, D. O., Martin, K. C., & Zukin, R. S. (2010). Spatially restricting gene expression by local translation at synapses. *Trends Neurosci, 33*(4), 173-182. doi:10.1016/j.tins.2010.01.005

Wang, X., Mazurkiewicz, M., Hillert, E. K., Olofsson, M. H., Pierrou, S., Hillertz, P., . . . D'Arcy, P. (2016). The proteasome deubiquitinase inhibitor VLX1570 shows selectivity for ubiquitin-specific protease-14 and induces apoptosis of multiple myeloma cells. *Sci Rep, 6*, 26979. doi:10.1038/srep26979

Wang, Y., Sakano, H., Beebe, K., Brown, M. R., de Laat, R., Bothwell, M., . . . Rubel, E. W. (2014). Intense and specialized dendritic localization of the fragile X mental retardation protein in binaural brainstem neurons: a comparative study in the alligator, chicken, gerbil, and human. *J Comp Neurol, 522*(9), 2107-2128. doi:10.1002/cne.23520

Wek, R. C. (2018). Role of eIF2alpha Kinases in Translational Control and Adaptation to Cellular Stress. *Cold Spring Harb Perspect Biol, 10*(7). doi:10.1101/cshperspect.a032870

Wheeler, J. R., Matheny, T., Jain, S., Abrisch, R., & Parker, R. (2016). Distinct stages in stress granule assembly and disassembly. *Elife, 5*. doi:10.7554/eLife.18413

Wolozin, B. (2012). Regulated protein aggregation: stress granules and neurodegeneration. *Mol Neurodegener, 7*, 56. doi:10.1186/1750-1326-7-56

Wolozin, B. (2014). Physiological protein aggregation run amuck: stress granules and the genesis of neurodegenerative disease. *Discov Med, 17*(91), 47-52.

Wong, H. H., Lin, J. Q., Strohl, F., Roque, C. G., Cioni, J. M., Cagnetta, R., . . . Holt, C. E. (2017). RNA Docking and Local Translation Regulate Site-Specific Axon Remodeling In Vivo. *Neuron, 95*(4), 852-868 e858. doi:10.1016/j.neuron.2017.07.016

Wu, T., Merbl, Y., Huo, Y., Gallop, J. L., Tzur, A., & Kirschner, M. W. (2010). UBE2S drives elongation of K11-linked ubiquitin chains by the anaphase-promoting complex. *Proc Natl Acad Sci U S A, 107*(4), 1355-1360. doi:10.1073/pnas.0912802107

Xie, X., Matsumoto, S., Endo, A., Fukushima, T., Kawahara, H., Saeki, Y., & Komada, M. (2018). Deubiquitylases USP5 and USP13 are recruited to and regulate heat-induced stress granules through their deubiquitylating activities. *J Cell Sci, 131*(8). doi:10.1242/jcs.210856

Xu, P., Duong, D. M., Seyfried, N. T., Cheng, D., Xie, Y., Robert, J., . . . Peng, J. (2009). Quantitative proteomics reveals the function of unconventional ubiquitin chains in proteasomal degradation. *Cell, 137*(1), 133-145. doi:10.1016/j.cell.2009.01.041

Yang, X., Shen, Y., Garre, E., Hao, X., Krumlinde, D., Cvijovic, M., . . . Sunnerhagen, P. (2014). Stress granule-defective mutants deregulate stress responsive transcripts. *PLoS Genet, 10*(11), e1004763. doi:10.1371/journal.pgen.1004763

Yau, R., & Rape, M. (2016). The increasing complexity of the ubiquitin code. *Nat Cell Biol, 18*(6), 579-586. doi:10.1038/ncb3358

Yoon, Y. J., Wu, B., Buxbaum, A. R., Das, S., Tsai, A., English, B. P., . . . Singer, R. H. (2016). Glutamate-induced RNA localization and translation in neurons. *Proc Natl Acad Sci U S A, 113*(44), E6877-E6886. doi:10.1073/pnas.1614267113

Youn, J. Y., Dunham, W. H., Hong, S. J., Knight, J. D. R., Bashkurov, M., Chen, G. I., . . . Gingras, A. C. (2018). High-Density Proximity Mapping Reveals the Subcellular Organization of mRNA-Associated Granules and Bodies. *Mol Cell, 69*(3), 517-532 e511. doi:10.1016/j.molcel.2017.12.020

Zalfa, F., Achsel, T., & Bagni, C. (2006). mRNPs, polysomes or granules: FMRP in neuronal protein synthesis. *Curr Opin Neurobiol, 16*(3), 265-269. doi:10.1016/j.conb.2006.05.010

Zalfa, F., Giorgi, M., Primerano, B., Moro, A., Di Penta, A., Reis, S., . . . Bagni, C. (2003). The fragile X syndrome protein FMRP associates with BC1 RNA and regulates the translation of specific mRNAs at synapses. *Cell, 112*(3), 317-327.

Zhang, H., Xing, L., Rossoll, W., Wichterle, H., Singer, R. H., & Bassell, G. J. (2006). Multiprotein complexes of the survival of motor neuron protein SMN with Gemins traffic to neuronal processes and growth cones of motor neurons. *J Neurosci, 26*(33), 8622-8632. doi:10.1523/JNEUROSCI.3967-05.2006

Zhang, H. L., Eom, T., Oleynikov, Y., Shenoy, S. M., Liebelt, D. A., Dictenberg, J. B., . . . Bassell, G. J. (2001). Neurotrophin-induced transport of a beta-actin mRNP complex increases beta-actin levels and stimulates growth cone motility. *Neuron, 31*(2), 261-275.

Zhang, H. L., Pan, F., Hong, D., Shenoy, S. M., Singer, R. H., & Bassell, G. J. (2003). Active transport of the survival motor neuron protein and the role of exon-7 in cytoplasmic localization. *J Neurosci, 23*(16), 6627-6637.

Zhang, J., Okabe, K., Tani, T., & Funatsu, T. (2011). Dynamic association–dissociation and harboring of endogenous mRNAs in stress granules. *Journal of Cell Science, 124*(23), 4087-4095. doi:10.1242/jcs.090951

Zhang, K., Daigle, J. G., Cunningham, K. M., Coyne, A. N., Ruan, K., Grima, J. C., . . . Lloyd, T. E. (2018). Stress Granule Assembly Disrupts Nucleocytoplasmic Transport. *Cell, 173*(4), 958-971.e917. doi:10.1016/j.cell.2018.03.025

Zhao, Y., Majid, M. C., Soll, J. M., Brickner, J. R., Dango, S., & Mosammaparast, N. (2015). Noncanonical regulation of alkylation damage resistance by the OTUD4 deubiquitinase. *EMBO J, 34*(12), 1687-1703. doi:10.15252/embj.201490497

Zhao, Y., Mudge, M. C., Soll, J. M., Rodrigues, R. B., Byrum, A. K., Schwarzkopf, E. A., . . . Mosammaparast, N. (2018). OTUD4 Is a Phospho-Activated K63 Deubiquitinase that Regulates MyD88-Dependent Signaling. *Mol Cell, 69*(3), 505-516 e505. doi:10.1016/j.molcel.2018.01.009

Zivraj, K. H., Tung, Y. C., Piper, M., Gumy, L., Fawcett, J. W., Yeo, G. S., & Holt, C. E. (2010). Subcellular profiling reveals distinct and developmentally regulated repertoire of growth cone mRNAs. *J Neurosci, 30*(46), 15464-15478. doi:10.1523/jneurosci.1800-10.2010

Zou, T., Yang, X., Pan, D., Huang, J., Sahin, M., & Zhou, J. (2011). SMN deficiency reduces cellular ability to form stress granules, sensitizing cells to stress. *Cell Mol Neurobiol, 31*(4), 541-550. doi:10.1007/s10571-011-9647-8

Zurla, C., Lifland, A. W., & Santangelo, P. J. (2011). Characterizing mRNA interactions with RNA granules during translation initiation inhibition. *PLoS One, 6*(5), e19727. doi:10.1371/journal.pone.0019727

Appendix

	Fold enrichment	
Gene	**Cerebellum**	**Cortex**
Adar	4.4E+01	1.8E+07
Adarb1	5.6E+06	8.4E+06
Ago1	6.8E+06	8.0E+06
Ago3	4.0E+06	5.7E+06
Ago4	5.4E+06	3.7E+06
Aip	1.9E+06	5.6E+06
Alyref	4.8E+02	1.7E+02
Alyref2	4.1E+02	1.2E+02
Angel1	2.7E+06	3.4E+06
Ankrd17	3.5E+01	4.9E+01
Ascc1	1.3E+06	1.4E+06
Asph	3.1E+06	5.1E+06
Atxn2	8.9E+05	1.5E+06
Atxn2l	1.2E+07	3.1E+01
B3galt6	6.2E+05	9.1E+05
C1qbp	1.8E+02	1.9E+02
Caprin1	4.0E+01	1.2E+02
Ccar2	1.5E+06	5.3E+06
Chpf	1.0E+06	2.6E+06
Cmtr1	3.4E+05	1.1E+06
Cpeb3	2.8E+06	3.6E+06
Cpeb4	1.5E+06	9.3E+05
Ctu1	2.2E+06	1.6E+06
Dap3	2.8E+06	3.0E+06
Ddx20	2.9E+01	4.3E+01
Dhx36	4.3E+01	2.2E+02
Dis3l2	2.0E+06	3.7E+06
Dnajb1	1.6E+06	1.5E+06
Eif3h	5.7E+05	5.6E+01
Eif4a2	2.9E+06	4.3E+06
Eif4a3	5.5E+01	9.1E+01
Eif4e	3.1E+07	2.9E+02
Eif4g1	1.4E+02	1.2E+02
Elavl1	1.2E+02	4.4E+01
Elavl2	8.4E+01	5.0E+06
Elavl3	3.1E+01	1.3E+06

	Fold enrichment	
Gene	**Cerebellum**	**Cortex**
Ewsr1	4.9E+01	5.5E+01
FAM120A	2.8E+06	7.0E+06
Fam120c	9.9E+05	5.0E+06
Fam98a	1.1E+07	1.2E+07
Fbxo11	9.0E+05	1.0E+06
Fmr1	2.4E+02	6.0E+01
Fubp1	5.2E+06	1.9E+06
Fus	3.5E+01	3.8E+01
Fxr1	6.1E+02	6.0E+02
Fxr2	2.1E+02	3.1E+03
G3bp1	3.5E+07	2.5E+07
G3bp2	7.0E+01	8.3E+01
Gabrb3	3.5E+06	2.0E+06
Gle1	3.0E+06	5.2E+06
Hnrnpa0	5.0E+01	8.2E+07
Hnrnpa1	5.5E+01	9.5E+01
Hnrnpa2b1	4.7E+01	5.5E+01
Hnrnpd	6.7E+01	4.1E+07
Hnrnpdl	3.5E+07	8.6E+01
Hnrnph1	9.3E+06	1.4E+07
Hnrnph2	6.4E+06	3.0E+06
Hnrnpm	3.0E+01	5.1E+01
Hnrnpul1	4.4E+01	6.6E+01
Hspbp1	5.7E+05	3.5E+05
Igf2bp1	9.1E+01	8.3E+01
Igf2bp2	2.8E+07	3.6E+07
Igf2bp3	5.0E+07	6.4E+07
Ilf3	3.1E+01	4.5E+01
Ints1	2.1E+06	5.0E+06
Khdrbs1	1.1E+08	7.7E+06
Klhdc10	4.6E+06	1.2E+06
Krt24	3.1E+06	6.0E+06
Larp6	1.4E+06	3.6E+06
Matr3	4.6E+01	1.5E+02
Med12	5.8E+05	8.5E+05
Mov10	1.1E+08	1.7E+08

	Fold enrichment	
Gene	**Cerebellum**	**Cortex**
Mrpl44	2.1E+06	3.4E+06
Msi1	1.8E+07	1.6E+07
Msi2	2.3E+07	1.7E+07
Ncl	6.4E+01	6.4E+01
Ncoa5	2.9E+06	2.5E+06
Nufip2	3.2E+02	5.8E+01
Otud4	1.1E+03	7.1E+02
Pabpc1	1.1E+02	1.8E+02
Pabpn1	5.0E+06	8.2E+06
Pacs1	1.4E+06	4.4E+01
Pcbp3	2.3E+06	4.9E+06
Pclo	3.4E+05	9.6E+05
Ppp4c	2.4E+06	3.0E+06
Prkd1	2.5E+06	4.0E+06
Psmd14	1.3E+06	3.8E+06
Purb	5.1E+01	3.6E+01
Qki	2.2E+06	3.0E+06
Ralyl	1.2E+07	8.9E+06
Rbm10	2.3E+06	5.5E+06
Rbm4	5.1E+06	2.9E+06
Rbm4b	5.7E+06	3.0E+06
Rbmx	2.0E+06	2.2E+06
Rbmxl1	1.9E+06	1.6E+06
Rcor1	1.7E+06	1.0E+06
Rdh14	1.6E+06	2.4E+06
Rnf41	3.2E+06	3.0E+06
Rpf2	3.6E+06	4.2E+06
Rpl15	1.0E+02	3.1E+01
Rpl18a	2.9E+06	5.6E+05
Rpl4	3.3E+01	6.6E+01
Rpl7a	5.7E+01	4.6E+01

	Fold enrichment	
Gene	**Cerebellum**	**Cortex**
Rtraf	4.7E+01	3.1E+01
Samd4b	9.2E+05	2.0E+06
Sars	2.5E+06	1.9E+06
Smg5	4.7E+05	1.2E+06
Smn1	1.1E+07	7.7E+06
Soga1	5.7E+06	2.9E+06
Spop	3.2E+06	4.4E+06
Srsf1	8.1E+01	2.9E+02
Srsf2	3.6E+06	1.7E+02
Srsf4	3.8E+06	1.6E+06
Srsf5	1.3E+07	1.7E+02
Stub1	1.2E+06	3.1E+06
Sugp2	1.5E+06	2.8E+06
Tarbp2	5.3E+06	6.2E+06
Tarsl2	1.9E+06	6.9E+06
Tmlhe	4.3E+06	1.2E+06
Tnrc6a	3.0E+06	3.8E+06
Tnrc6b	2.8E+06	2.2E+06
Tra2a	1.1E+07	1.8E+07
Trim25	1.7E+06	2.4E+06
Tut4	1.1E+06	9.0E+05
Uck2	7.6E+06	7.9E+06
Unk	3.5E+06	3.7E+06
Upf1	2.3E+02	1.3E+02
Usp10	2.8E+07	1.3E+02
Ybx1	3.1E+07	2.7E+07
Ybx3	1.0E+07	4.1E+06
Ythdf1	1.5E+07	2.0E+07
Ythdf2	3.6E+01	5.7E+01
Znf326	6.3E+06	9.0E+06

Table 19. List of OTUD4 interactors from mouse brain lysate identified by MS. Interactors that were identified in both cerebellum and cortex lysate are shown here in alphabetical sequence. The list contains proteins with fold enrichment ≥30. Mean Peak area was used as a measure for abundance to calculate fold enrichment. The fold enrichment values were calculated by dividing the mean peak area of the tissues by the respective mean area of the controls. For cerebellum data set, mean peak area was generated from three replicates and for cortex data set, this was generated from two replicates.

List of Conferences and posters

New roles for the deubiquitinating enzyme OTUD4 in an RNA-protein network and RNA granules. Richa Das, Lukas Schwintzer, Stanislav Vinopal, Eva Aguado Roca, Ana-Maria Oprisoreanu, Susanne Schoch, Frank Bradke & Meike Brömer. Proteomics in Cell Biology and Disease Mechanisms (EMBL-Wellcome Genome Campus Conference), Heidelberg, Germany (2019)

A deubiquitinating enzyme as new stress granule component. Richa Das, Lukas Schwintzer and Meike Brömer. RNA Transport Meeting (FOR2333 Conference), Düsseldorf-Kaiserswerth, Germany (2018)

The deubiquitinating enzyme OTUD4 is a novel component of cytoplasmic stress granules. Richa Das, Lukas Schwintzer and Meike Brömer. RNA Transport and local translation (EMBO Conference), Barga, Italy (2017)

The deubiquitinating enzyme OTUD4 is a novel component of cytoplasmic stress granules. Richa Das, Lukas Schwintzer and Meike Brömer. Annual meeting of the Bonner Forum Biomedizin (BFB), Hennef, Germany (2017)

List of Publications

Das R, Schwintzer L, Vinopal S, Aguado Roca E, Sylvester M, Oprisoreanu AM, Schoch S, Bradke F, Broemer M. New roles for the de-ubiquitylating enzyme OTUD4 in an RNA-protein network and RNA granules (2019). Journal of Cell Science, 132(12). pii: jcs229252.

Acknowledgement

First of all, I would like to express my immense gratitude to Dr. Meike Brömer for giving the opportunity to perform my PhD thesis in her lab and to assign me this fascinating project to work on. Your enthusiasm, competence and positive energy have been a strong motivation for me throughout. Thank you for your relentless support and guidance!

I would like to thank Prof. Dr. Ina Vorberg and Prof. Dr. Waldemar Kolanus for being my first and second examiner and for taking time to review this thesis. I would like to acknowledge Prof. Dr. Sven Burgdorf and Prof. Dr. Anton Bovier for kindly agreeing to be part of the examination committee.

I am deeply grateful to Dr. Lukas Schwintzer for his tremendous supervision throughout this project, right from the day I started. Working together with you has only been a learning experience for me. Your organization, work ethics and integrity are skills I strive for. Thank you for all the helpful advice and support, both scientific and non-scientific. I would also like to thank you for taking time to critically read and correct my thesis. I am grateful to Eva Aguado Roca, for excellent organization of the lab, for patiently teaching me techniques in the initial years and for constant support with the experiments. And also for all the good humor and fun atmosphere in the lab!

I would like to express my gratitude to Prof. Dr. Susanne Schoch and Dr. Ana Maria Oprisoreanu for their collaboration on HA-affinity purification experiments to identify OTUD4 interactors from mouse brain. Thank you for giving me the possibility to perform these experiments in your lab and special thanks to Dr. Oprisoreanu who provided technical expertise and supervision for the preparation of mouse brain lysate and the pull-down experiments.

I would like to thank Prof. Dr. Frank Bradke for giving me the opportunity to conduct all the experiments using primary neuronal culture in his lab. Furthermore, I am indebted to Dr. Stanislav Vinopal for his extensive support and expertise with the live cell imaging experiments using primary neurons. I greatly benefited from his scientific curiosity and valuable insights towards this project. I would like to express my gratitude Liane Meyn and Blanca Randel for excellent technical assistance in the preparation of primary neuronal culture.

Besides, I would like to thank Manuel Schölling and Dr. Christoph Möhl for their support with all the quantification and statistical analysis. Many thanks to Dr. Marc Sylvester who provided excellent service for conducting mass spectrometry.

Lastly, I express my deepest gratitude to my parents, my younger brothers, Raja & Rinku and my aunts for their unceasing love & support throughout this journey. To Sanak, my husband, thank you for your unyielding love and support and always pushing me to be a better person. To Lipsa, my closest friend, I can take on the world with only you by my side! Thank you to all my friends for always being there. I dedicate this work to my mentor, my mother and father who have always encouraged me to dream big. Thank you, Maa!